

Marta Wróbel, MSc

**The role of ESCRT-I proteins in the regulation of lysosomal
function and lysosome-related signaling**

PhD thesis
completed in the Laboratory of Cell Biology
of the International Institute of Molecular and Cell Biology
in Warsaw

SUPERVISOR:
Prof. dr hab. Marta Międzyńska

AUXILIARY SUPERVISOR:
Dr Jarosław Cendrowski

Warsaw, 2023



The research leading to these results has received funding from the TEAM programme (POIR.04.04.00-00-20CE/16-00) of the Foundation for Polish Science co-financed by the European Union under the European Regional Development Fund.

Acknowledgements

First, I would like to express my sincere gratitude to my supervisor Professor Marta Miączyńska for giving me the opportunity to perform a PhD project in the Laboratory of Cell Biology. I am thankful for the support and guidance that I received throughout my studies. In addition, I would like to thank for the critical review of this thesis.

I would like to acknowledge my auxiliary supervisor Dr Jarosław Cendrowski for introducing me into the world of endocytosis, mentoring me and for time spent on scientific discussions during this challenging period of my life. I would like to also thank for the critical reading of this thesis.

I would like to thank members of my Thesis Advisory Committee, Dr Ewelina Szymańska from the Laboratory of Cell Biology and Professor Michał Mikula from the Maria Skłodowska-Curie National Research Institute of Oncology for their thoughtful and invaluable pieces of advice.

I would like to acknowledge Dr Noga Budick-Harmelin, who guided me through experiments when I entered the lab and joined the ESCRT project. Many thanks to Dr Krzysztof Kolmus for performing GO analysis, as well as to Malwina Grębowicz-Maciukiewicz and Michał Mazur for their involvement in the experimental part of our publication.

I would like to thank Professor Jacek Jaworski's group for sharing reagents and helpful suggestions.

Additionally, I would like to thank all present and past members of the Laboratory of Cell Biology that I had the pleasure to work with, namely: Magdalena Banach-Orłowska, Marta Chwałek, Patrycja Daszczuk, Purevsuren Erdenebat, Kamil Jastrzębski, Julia Kirylczuk, Katarzyna Kuźmich-Kowalska, Małgorzata Maksymowicz, Agnieszka Mamińska, Monika Matuszczyk, Ranjana Maurya, Paulina Nowak, Agata Poświata, Karolina Romaniuk, Blair Stewig, Patryk Ślusarczyk, Małgorzata Świątek, Karolina Wojciechowska, Lidia Wolińska-Nizioł, Renata Wszyńska and Daria Zdżalik-Bielecka for their willingness to help and a friendly atmosphere in the lab.

Finally, I acknowledge my husband for his support and endless words of encouragement throughout this journey.

Table of contents

Abbreviations	7
Abstract	9
Streszczenie	11
1. Introduction.....	13
1.1. Endolysosomal transport	13
1.1.1. Endocytosis and endocytic trafficking to lysosomes.....	13
1.1.2. Markers of organelles involved in endolysosomal trafficking.....	15
1.2. Lysosomes as degradative organelles.....	16
1.2.1. Lysosomes as sites of efflux of LDL-derived cholesterol	17
1.3. Lysosomes as Ca ²⁺ storage organelles.....	18
1.3.1. Ca ²⁺ in activation of calcineurin signaling.....	19
1.3.2. Regulation of lysosomal Ca ²⁺ release via MCOLN1 channel.....	19
1.4. Lysosomes as platforms for the regulation of mTORC1-dependent signaling	20
1.4.1. Composition of mTORC1	20
1.4.2. Functions of mTORC1	21
1.4.3. Regulation of mTORC1 signaling	22
1.4.3.1. Regulation of Rag GTPase complex activity.....	23
1.4.3.2. Regulation of Rheb	24
1.4.4. Transcriptional responses related to lysosomal function	24
1.4.4.1. MiT-TFE transcription factor family	25
1.4.4.2. Intracellular roles of MiT-TFE factors	25
1.4.4.3. Regulation of subcellular localization of MiT-TFE transcription factors	26
1.5. Role of ESCRT machinery in delivering cargo for lysosomal degradation	27
1.6. Involvement of ESCRT in controlling signaling from endosomes	29
1.7. Role of ESCRT components in maintaining lysosomal homeostasis	30
1.8. Other roles of ESCRT components	31
1.9. Diseases caused by mutations or abnormal expression of genes encoding ESCRT proteins	31
1.10. Targeting lysosomal function in diseases including cancer.....	33
2. Aims of the study	35

3.	Materials and methods	36
3.1.	Materials	36
3.1.1.	Cell lines	36
3.1.2.	Cell culture media and supplements	36
3.1.3.	Primary antibodies	37
3.1.4.	Secondary antibodies	38
3.1.5.	Plasmids.....	38
3.1.6.	Bacterial strains	38
3.1.7.	Bacterial culture reagents	39
3.1.8.	Chelator and inhibitors	39
3.1.9.	Small interfering RNA oligonucleotides (siRNA).....	39
3.1.10.	Transfection reagents.....	40
3.1.11.	Primers.....	40
3.1.12.	Commonly used buffers and solutions	40
3.1.13.	Commercial assay kits	41
3.1.14.	Other reagents	41
3.2.	Methods	43
3.2.1.	Cell culture	43
3.2.2.	Cell treatment.....	43
3.2.3.	Cell transfection with siRNA using Lipofectamine RNAiMAX	43
3.2.4.	Cell transfection with plasmids	45
3.2.5.	Preparation of chemically competent bacteria	45
3.2.6.	Bacteria transformation	45
3.2.7.	Generation of GFP-MCOLN1 RKO cell line by lentiviral transduction	46
3.2.7.1.	Generation of a plasmid encoding GFP-MCOLN1 for lentiviral transduction using the SLIC method.....	46
3.2.7.2.	Production of lentiviruses and infection of RKO cells	48
3.2.8.	Western blotting (WB)	48
3.2.9.	Cell fractionation	49
3.2.10.	Immunofluorescence and imaging	50
3.2.10.1.	Lysosomal imaging.....	50

3.2.10.2.	Immunofluorescence staining (IF).....	50
3.2.10.3.	Imaging using Opera Phenix automated confocal microscope.....	51
3.2.10.4.	Quantitative image analysis using Harmony software.....	51
3.2.11.	Quantitative real time PCR (RT-qPCR).....	52
3.2.12.	Analysis of transcriptome by RNA sequencing.....	52
3.2.13.	Statistical analysis.....	53
4.	Results.....	55
4.1.	Characterization of lysosomal morphology upon ESCRT-I depletion.....	55
4.2.	The role of ESCRT-I in degradation of lysosomal membrane proteins.....	61
4.3.	The identification of lysosome-related signaling pathways activated upon ESCRT-I depletion.....	65
4.4.	The effect of impaired cholesterol efflux from lysosomes on the activation of MiT-TFE signaling upon ESCRT-I depletion.....	72
4.5.	The involvement of Ca ²⁺ mediated signaling in the MiT-TFE activation upon ESCRT-I depletion.....	75
4.6.	The status of mTORC1 activation upon ESCRT-I depletion and its contribution to the MiT-TFE activation.....	79
4.7.	The contribution of Rag GTPase complex to the activation of MiT-TFE signaling upon ESCRT-I depletion.....	84
5.	Discussion.....	87
5.1.	ESCRT-I maintains lysosomal membrane protein turnover potentially thereby restricting size of lysosomes.....	88
5.2.	Delivery of luminal cargo to lysosomes, such as cathepsin D, seems to be not impaired upon ESCRT-I depletion.....	90
5.3.	ESCRT-I depletion evokes a cholesterol starvation response due to the inhibited efflux of luminal cholesterol from enlarged lysosomes.....	91
5.4.	Activation of TFEB and TFE3 factors by Rag GTPase inhibition is likely a hallmark of lysosomal nutrient starvation due to lack of ESCRT-I.....	92
5.5.	A potential mechanism underlying regulation of substrate-specific Rag GTPase-dependent mTORC1 signaling may involve several proteins.....	93
5.6.	Altered calcineurin activity or cholesterol-induced lysosomal stress are not causative factors of TFEB and TFE3 activation upon lysosomal nutrient starvation.....	95
5.7.	Regulation of basal MiT-TFE signalling in cancer cells relies on Rag GTPase activity and availability of exogenous lipids.....	97

6. Future prospects	99
7. Summary and conclusions.....	101
8. Literature	102
9. Publications by Marta Wróbel	127
10. Supplementary materials	128

Abbreviations

ALIX	ALG-2 interacting protein X
BafA1	bafilomycin A1
CaM	calmodulin
CaN	calcineurin
CHMP	charged multivesicular body protein
CnA	catalytic subunit calcineurin A
CnB	Ca ²⁺ -binding regulatory subunit calcineurin B
CRC	colorectal cancer
CRISPR	clustered regularly-interspaced short palindromic repeats
CsA	cyclosporin A
DAPI	4',6-diamidino-2-phenylindole dihydrochloride
DMEM	Dulbecco's Modified Eagle's Medium
DMSO	dimethyl sulfoxide
EEA1	early endosome antigen 1
ER	endoplasmic reticulum
ERK	extracellular signal-regulated kinase
EMEM	Eagle's Minimum Essential Medium
ESCRT	endosomal sorting complex required for transport
FBS	fetal bovine serum
FLCN	folliculin
GAP	GTPase-activating protein
HOPS	homotypic fusion and vacuole protein sorting complex
HRS	hepatocyte growth factor-regulated tyrosine kinase substrate
ILV	intraluminal vesicle
LAMP1/2	lysosomal associated membrane protein 1/2
LDL	low-density lipoprotein
LDLR	low-density lipoprotein receptor
LSD	lysosomal storage disease
M6P	mannose-6-phosphate
M6PR	mannose-6-phosphate receptor

MCOLN	mucolipin
MiTF	microphthalmia-associated transcription factor
mTORC1/2	mechanistic target of rapamycin complex 1/2
MVB	multivesicular body
NF- κ B	nuclear factor kappa-light-chain-enhancer of activated B cells
NPC1/2	Niemann–Pick C1/2
PCR	polymerase chain reaction
PI3K	phosphoinositide-3-kinase
PI3P	phosphatidylinositol-3-phosphate
PM	plasma membrane
Rab5	Ras-associated GTP-binding protein 5
RT-qPCR	quantitative real-time polymerase chain reaction
siRNA	small interfering RNA
SLIC	sequence- and ligation-independent cloning
TFE3	transcription factor E3
TFEB	transcription factor EB
TFEC	transcription factor EC
TSC	tuberous sclerosis complex
Tsg101	tumor susceptibility 101
UBAP1	ubiquitin-associated protein 1
Vps28	vacuolar protein sorting 28 homolog
Vps4	vacuolar protein sorting 4
WB	western blot
WT	wild type

Abstract

Endocytosis is a process of internalizing molecules from the extracellular milieu or the cell surface and delivering them to membrane-bound organelles called endosomes, which facilitate further transport of internalized cargoes. Proteins present on endosomal membranes are recognized by the endosomal sorting complexes required for transport (ESCRT), which consist of ESCRT-0, -I, -II and -III. ESCRT mediate remodeling of the limiting membrane of endosomes and formation of intraluminal vesicles (ILVs) inside endosomes. The content of ILVs can be secreted outside the cell or transported via the endolysosomal pathway to lysosomes for degradation. In addition, lysosomes regulate Ca^{2+} -dependent signaling and constitute platforms to sense nutrient availability.

Despite a well-characterized function of ESCRT-I in regulating endosomal size and sorting, its involvement in maintaining lysosomal homeostasis remains poorly investigated. The general aim of this thesis was to characterize the role of ESCRT-I in maintaining lysosomal homeostasis and investigate the consequences of ESCRT-I depletion for lysosomal function and lysosome-related signaling.

First, lysosomal morphology was characterized in colorectal cancer cell lines, RKO and DLD-1, upon siRNA-mediated depletion of ESCRT-I components, namely Tsg101 or Vps28. Quantitative microscopic analysis of lysosomal markers revealed that lack of ESCRT-I led to enlargement of lysosomes but did not impair lysosomal integrity, maintenance of acidic pH or content of degradative enzymes. The increased lysosomal size was likely due to an impaired degradation of resident membrane proteins that was observed in cells lacking ESCRT-I. This included MCOLN1, a lysosomal Ca^{2+} channel, whose lysosomal degradation was studied using a GFP-MCOLN1-expressing reporter cell line.

To verify whether the lack of ESCRT-I induced transcriptional responses characteristic for altered lysosomal function, RNA sequencing analysis was performed. It revealed that depletion of ESCRT-I upregulated expression of genes related to autophagy and/or lysosomal biogenesis. Activation of transcription factors from the MiT-TFE family, namely TFEB and TFE3, predicted to be responsible for induced expression of these genes, was confirmed in nuclear fractions of ESCRT-I-depleted cells.

Next, a mechanism involved in the activation of MiT-TFE signaling upon ESCRT-I depletion was investigated. Quantitative analysis of microscopic images revealed that in cells

lacking ESCRT-I, activation of TFEB and TFE3 required Ca^{2+} -dependent signaling and mTORC1 inhibition, but was not due to calcineurin-dependent dephosphorylation of these transcription factors. Moreover, biochemical analyses indicated that the lack of ESCRT-I inhibited mammalian target of rapamycin complex 1 (mTORC1) kinase activity specific towards TFEB and TFE3 but it did not affect canonical mTORC1 substrates. Therefore, it was verified whether the MiT-TFE activation upon ESCRT-I depletion occurred due to the reduced activity of the Rag GTPase complex, known to control the TFEB- and TFE3-specific lysosomal mTORC1 signaling. Overexpression of constitutive active RagC mutant prevented nuclear translocation of TFEB and TFE3 in Tsg101-depleted cells. Hence, the activation of MiT-TFE factors in cells lacking ESCRT-I occurred due to the inhibition of Rag GTPase-dependent mTORC1 pathway.

The results presented in this thesis characterize new roles of ESCRT-I in the turnover of lysosomal membrane proteins and maintaining lysosome-related Rag GTPase-dependent, non-canonical mTORC1 signaling. Lack of ESCRT-I leads to a homeostatic response, involving inhibition of the non-canonical mTORC1 signaling and, as a consequence, activation TFEB and TFE3 factors, in an attempt to counteract lysosomal nutrient starvation.

Streszczenie

Endocytoza to proces pobierania cząsteczek ze środowiska zewnątrzkomórkowego lub powierzchni komórki i dostarczania ich do organelli zwanych endosomami, które pośredniczą w transporcie ładunku wewnątrz komórki. Białka obecne na błonach endosomalnych są rozpoznawane przez endosomalne kompleksy sortujące ESCRT (ang. endosomal sorting complexes required for transport), tworzone przez kompleksy ESCRT-0, -I, -II i -III. Umożliwiają one deformację zewnętrznej błony endosomalnej prowadząc do utworzenia pęcherzyków wewnętrznych w świetle endosomów, tzw. ILVs (ang. intraluminal vesicles). Zawartość ILVs może być wydzielana na zewnątrz komórki lub transportowana szlakiem endolizosomalnym do lizosomów. Dzięki aktywności hydrolaz, lizosomy dostarczają komórce składników odżywczych pochodzących z degradacji makrocząsteczek. Dodatkowo lizosomy regulują sygnalizację zależną od Ca^{2+} , a także stanowią platformę umożliwiającą wykrywanie dostępności składników odżywczych.

Mimo dobrze scharakteryzowanej roli ESCRT-I w funkcjonowaniu endosomów, udział tego kompleksu w utrzymaniu homeostazy lizosomów pozostaje słabo zbadany. Celem rozprawy doktorskiej było scharakteryzowanie roli ESCRT-I w utrzymaniu homeostazy lizosomów, a także zbadanie konsekwencji braku ESCRT-I dla prawidłowego funkcjonowania lizosomów i sygnalizacji związanej z lizosomami.

Realizując wyznaczony cel, w pierwszej kolejności scharakteryzowano morfologię lizosomów po usunięciu białek kompleksu ESCRT-I (Tsg101 i Vps28) za pośrednictwem siRNA (ang. small interfering RNA) w modelowych liniach komórkowych raka jelita grubego RKO i DLD-1. Analiza mikroskopowa znaczników lizosomalnych wykazała, że brak ESCRT-I prowadził do powstawania powiększonych lizosomów, ale nie zaburzał ich integralności, utrzymania niskiego pH i zawartości hydrolaz. Powiększenie lizosomów po usunięciu ESCRT-I mogło być spowodowane zaburzoną degradacją białek błonowych obecnych na lizosomach, m. in. kanału wapniowego MCOLN1, którego degradacja została zbadana przy użyciu linii reporterowej RKO-GFP-MCOLN1.

W celu weryfikacji czy brak podjednostek ESCRT-I prowadzi do aktywacji odpowiedzi transkrypcyjnej charakterystycznej dla zaburzonej funkcji lizosomów, przeprowadzono analizę sekwencjonowania RNA. Wykazano, że brak ESCRT-I indukował ekspresję genów związanych z autofagią i/lub biogenezą lizosomów. Analiza frakcji jądrowych komórek pozbawionych ESCRT-

I potwierdziła aktywację czynników transkrypcyjnych z rodziny MiT-TFE, takich jak TFEB i TFE3, potencjalnie zaangażowanych w indukcję ekspresji tych genów.

Następnie zbadano mechanizm związany z aktywacją czynników MiT-TFE po usunięciu ESCRT-I. Analiza mikroskopowa wykazała, że w komórkach pozbawionych ESCRT-I aktywacja czynników TFEB i TFE3 wymagała sygnalizacji zależnej od Ca^{2+} i hamowania aktywności kinazy mTORC1, ale nie była spowodowana ich defosforylacją zależną od kalcyneuryny. Dodatkowo, analiza biochemiczna pokazała, że brak ESCRT-I hamował aktywność mTORC1 specyficzną względem TFEB i TFE3, lecz nie wpływał na kanoniczne substraty mTORC1. Dlatego sprawdzono czy aktywacja MiT-TFE po usunięciu ESCRT-I nastąpiła z powodu zmniejszonej aktywności kompleksu GTPazy Rag, o którym wiadomo, że kontroluje aktywność mTORC1 specyficzną dla TFEB i TFE3. Nadekspresja stale aktywowanego mutantu RagC zapobiegła translokacji TFEB i TFE3 do jądra komórkowego w komórkach pozbawionych ESCRT-I, wskazując iż aktywacja czynników MiT-TFE zachodziła w wyniku hamowania szlaku mTORC1 zależnego od GTPazy Rag.

Wyniki przedstawione w niniejszej rozprawie opisują nowe funkcje kompleksu ESCRT-I w degradacji lizosomalnych białek błonowych i utrzymaniu niekanonicznej sygnalizacji mTORC1. Brak ESCRT-I prowadzi do odpowiedzi homeostatycznej, polegającej na hamowaniu niekanonicznej sygnalizacji mTORC1, a w konsekwencji aktywację czynników TFEB i TFE3, by przeciwdziałać niedoborom składników odżywczych pochodzących z degradacji lizosomalnej.

1. Introduction

1.1. Endolysosomal transport

1.1.1. Endocytosis and endocytic trafficking to lysosomes

Endocytosis is a cellular process, which enables internalization of nutrients and macromolecules from the cell exterior or from the plasma membrane (PM) and their subsequent transport (trafficking) to various cellular destinations [1]. This includes trafficking of membrane proteins including signaling receptors and channels. Endosomes are specialized membrane-bound vesicles that facilitate the intracellular trafficking of internalized cargo. Among them, early endosomes, recycling endosomes and multivesicular bodies (MVBs)/late endosomes can be distinguished (Fig. 1.1) [2]. The initial destination of cargoes internalized at the PM are early endosomes that serve as sorting stations directing the cargo depending on whether it is destined for recycling back to the PM or for further endocytic trafficking towards degradation [3]. Recycling can occur rapidly, directly from early endosomes, or may involve additional step of transporting the cargo from early endosomes to recycling endosomes [3]. Macromolecules that instead of recycling should undergo degradation are inserted into the lumen of endosomes by invagination of their limiting membrane and subsequent scission of smaller internal vesicles called intraluminal vesicles (ILVs) [4]. Formation of ILVs is coupled with maturation of early endosomes into late endosomes which, when contain many ILVs, are called multivesicular bodies (MVBs) [2]. The macromolecules present in ILVs can be either removed from the cell upon fusion of MVBs with the PM (resulting in exosomal secretion) or they can be degraded by hydrolases provided by degradative organelles called lysosomes [1].

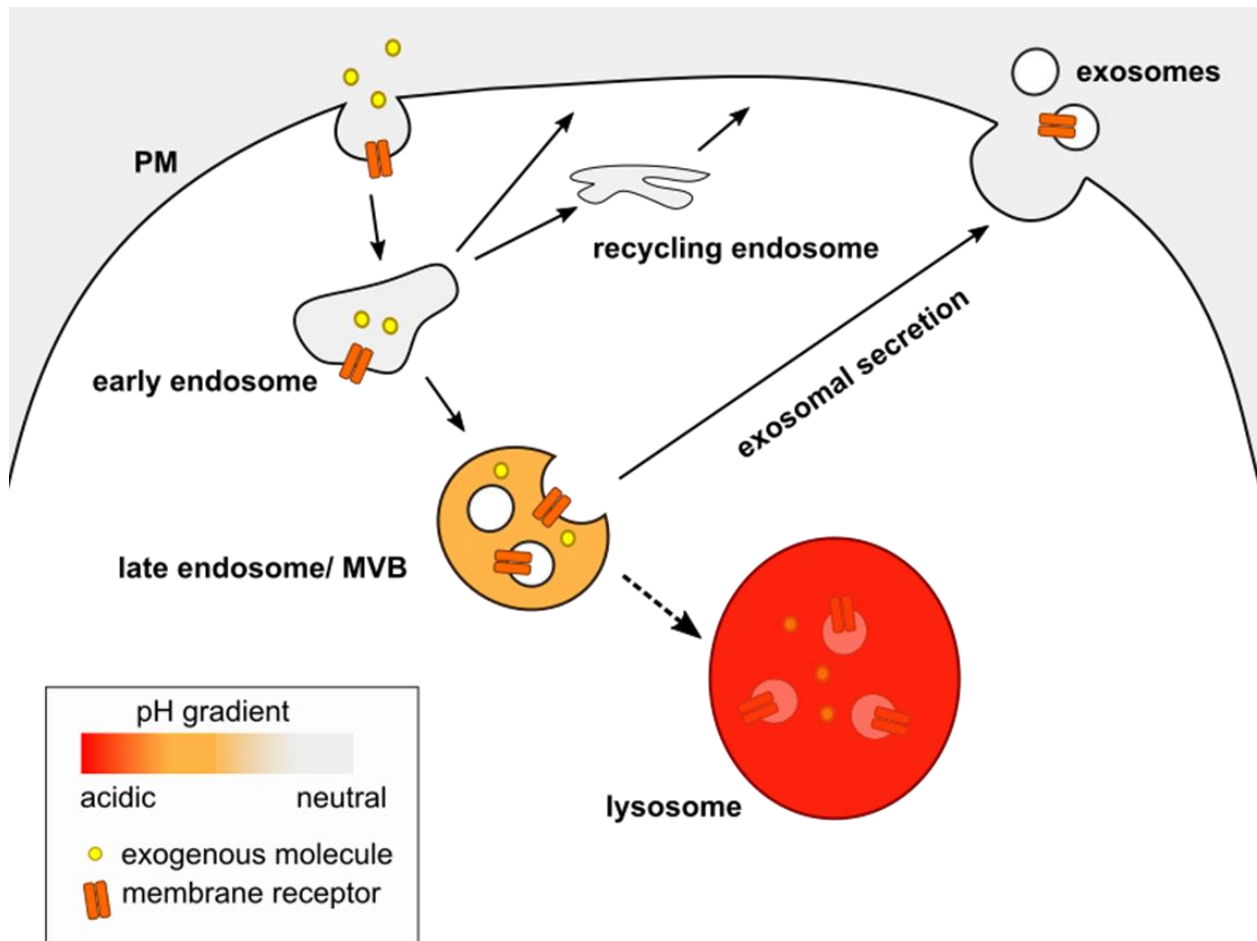


Figure 1.1. Schematic representation of endocytic trafficking. Upon internalization, exogenous molecules and membrane receptors reach early endosomes, which sort the endocytosed cargo for further degradative trafficking or recycling back to the PM. The content of late endosomes undergoes lysosomal degradation or is secreted as exosomes. Along the transport towards degradative compartments, the luminal pH of endocytic compartments decreases. Dashed line indicates a still unclear mechanism of cargo delivery to lysosomes. PM, plasma membrane; MVB, multivesicular body.

How endocytic cargoes are trafficked from late endosomes to lysosomes is still debated (Fig. 1.2) [5, 6]. One of the theories suggests that late endosomes progressively mature to become lysosomes [5, 6]. The second model proposes the involvement of transport of vesicles carrying cargo from late endosomes/MVBs to preexisting lysosomes [5, 6]. The third model involves the kiss-and-run events, which encompass the formation of transient contact sites to transfer cargo between late endosomes and lysosomes, followed by organelle dissociation [5, 6]. Finally, the fourth theory assumes direct fusion of late endosomes and lysosomes resulting in the formation of hybrid degradative organelles (endolysosomes) [5, 6]. Of note, to maintain the size of lysosomes

and their steady-state number, the formation of hybrid organelles has to be balanced by the lysosomal reformation and fission events [7].

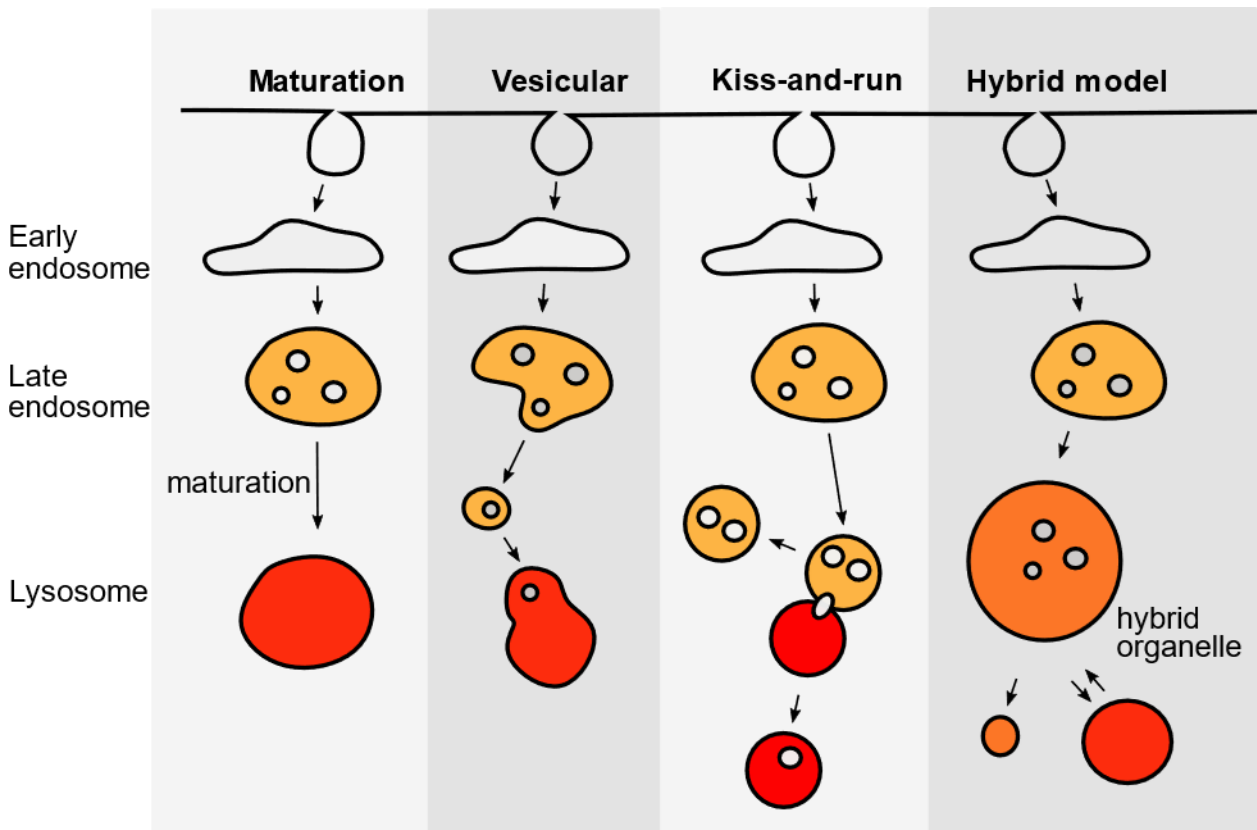


Figure 1.2. Hypothetical models of delivery of endocytosed cargoes from late endosomes to lysosomes. The model of maturation assumes progressive addition of lysosomal components and removal of late endosomal elements from a given, maturing compartment. The vesicular model suggests that cargo-loaded vesicles bud from the late endosomes and deliver their contents to the lysosome. The kiss-and-run model proposes formation of transient contact sites, allowing for the content exchange between late endosomes and lysosomes without complete fusion of the two compartments. The hybrid model posits formation of fused hybrid organelles containing components of late endosomes and lysosomes, followed by the retrieval of late endosome and lysosome components. Modified from Luzio et al. [5].

1.1.2. Markers of organelles involved in endolysosomal trafficking

To fulfill their function in endolysosomal trafficking, endosomes and lysosomes have unique features, which can be used as markers. They include particular proteins and lipids as well as specific properties, such as low pH. The first station in cargo trafficking, early endosomes, are characterized by the presence of Ras-associated GTP-binding protein 5 (Rab5) molecules, which associate with the endosomal surface and recruit a number of effectors, including early endosome

antigen 1 (EEA1) [8]. EEA1 mediates the fusion of endocytic vesicles with early endosomes [9] and is considered as one of the most specific markers of this compartment [10]. Rab5 recruits also phosphoinositide-3-kinase (PI3K), which promotes the synthesis of endosome-specific lipid, phosphatidylinositol-3-phosphate (PI3P) [11]. Gradually, early endosomes mature into MVBs/late endosomes. This process involves a removal of Rab5 that is substituted by another peripheral membrane protein, Rab7 [12] and progressive acidification from pH ~6.5 to pH ~5.5 [13] (Fig. 1.1). Moreover, endosomal maturation includes also a conversion of PI3P into phosphatidylinositol-3,5-diphosphate (PI(3,5)P₂) [14].

In addition to the presence of PI(3,5)P₂, late endosomes and lysosomes are highly enriched in transmembrane glycoproteins such as lysosomal associated membrane protein 1 and 2 (LAMP1, LAMP2) [2]. The presence of the same glycoproteins (and several other markers) in late endosomes and lysosomes is consistent with the model of progressive maturation of endosomes into lysosomes. However, it also fits the model of late endosome-lysosome fusion, according to which late endosomal membranes must be prepared to meet the degradative lysosomal environment [5, 6].

As compared to other cellular compartments, lysosomes are the most acidic organelles in the cell (pH ~5, Fig. 1.1), that ensures optimal conditions for the activity of lysosomal hydrolases [6]. Thus, detecting low pH and the presence of active luminal hydrolases in LAMP-positive vesicular structures can be applied to identify functional lysosomes [15], distinguishing them from late endosomes.

1.2. Lysosomes as degradative organelles

Due to the activity of resident hydrolytic enzymes, lysosomes degrade macromolecules, which are delivered not only from the endolysosomal pathway but also upon fusion of autophagosomes with lysosomes (forming hybrid organelles termed autolysosomes) in a process called macroautophagy, hereafter referred to as autophagy [16]. To perform all their degradative duties, lysosomes contain more than 60 acidic hydrolytic enzymes, including proteases and peptidases [17].

Newly synthesized lysosomal enzymes are transported as inactive precursors from the endoplasmic reticulum (ER) to the Golgi complex where mannose-6-phosphate (M6P) residues are added. Modified enzymes are recognized by mannose-6-phosphate receptors (M6PRs) in the *trans*-Golgi network and transported to endosomes, from where they are further delivered to

lysosomes [6]. In the mildly acidic pH of late endosomes, M6PR dissociates from a precursor enzyme and returns to the Golgi apparatus to participate in the next round of transport of M6P-tagged enzymes [18]. When enzymes reach the lysosomal lumen, its more acidic pH allows for their proteolytic processing, hence maturation into active enzymes [19].

The best characterized group of lysosomal enzymes is the family of cathepsin proteases. Most of them are endopeptidases and hence preferably hydrolyze the peptide bonds inside a polypeptide chain. Depending on the amino acid found in the active site, cathepsins are classified into three distinct groups: serine (cathepsins A and G), cysteine (cathepsins B, C, F, H, K, L, O, S, V, W, and X) and aspartic (cathepsins D and E) proteases [20]. Amino acids obtained from lysosomal hydrolysis of peptide bonds are exported from the lysosomal lumen by transporters. Up to date, only a few transporters were characterized at the molecular level, including cystinosin [21], LAAT-1/PQLC2 [22], LYAAT-1/SLC36A1 [23], SLC38A9 [24] and SNAT7/SLC38A7 [25].

Targeting of membrane proteins to lysosomes can occur via direct delivery from the *trans*-Golgi network or via an indirect route, which encompasses secretory transport from the Golgi to the PM and endocytic trafficking to lysosomes [18, 26-29]. The lysosomal membrane proteins are crucial for the function of lysosomes. For instance, low lysosomal pH required for maturation and activity of lysosomal hydrolases is generated by the V-type ATPase proton pump [30, 31], whose pharmacological inhibition using bafilomycin A1 (BafA1) is a commonly used approach for studying lysosomal function [32]. Moreover, the presence of heavily glycosylated membrane proteins, including LAMP1 and LAMP2, on the inner face of lysosomal membranes protects these membranes from degradation by the luminal hydrolases and therefore ensures lysosomal integrity [33].

1.2.1. Lysosomes as sites of efflux of LDL-derived cholesterol

Cholesterol constitutes an essential component of cell membranes [34] and lysosomes play an important role in cholesterol homeostasis. Although cells may produce cholesterol by *de novo* synthesis, they often acquire it from the extracellular milieu by endocytic uptake of low-density lipoproteins (LDL) that bind to LDL receptors [35]. Upon internalization, receptor-bound LDL particles are transported through endolysosomal compartments, where low pH promotes LDL dissociation from the receptors [35]. Whereas the receptors are recycled back to the PM, LDL particles undergo lysosomal degradation [35]. In contrast to a wide variety of characterized lysosomal proteases, only one lysosomal acid lipase (LAL) is known to hydrolyze LDL-derived

cholesteryl esters to free cholesterol and fatty acid molecules [36]. In addition to endocytic transport, cholesterol can be delivered to lysosomes from cellular membranes through autophagy [37].

The efflux of free cholesterol from the lysosomal lumen is regulated by an orchestrated action of two lysosomal proteins: Niemann–Pick C1 (NPC1) and Niemann–Pick C2 [38]. NPC2 acts in the lysosomal lumen where it binds free cholesterol released from LDL particles and transfers it onto NPC1. NPC1 is a transmembrane protein that transports cholesterol across lysosomal membranes [38]. Genetic mutations in genes encoding NPC1/2 proteins lead to the development of Niemann–Pick type C disease characterized by massive accumulation of cholesterol and other lipids within enlarged lysosomes [38]. In recent years, other lysosomal proteins, i.e. lysosomal integral membrane protein 2 (LIMP-2) and LAMP1/2, were also reported to participate in cholesterol export [39, 40]. Once it reaches the outer side of lysosomal membrane, cholesterol is distributed among membrane-bound organelles. A growing body of evidence shows that major mechanisms of this transport encompass the involvement of sterol-binding proteins and protein-mediated membrane contact sites [41]. Perturbed transport of cholesterol or LDL deficiency affects sensing of cholesterol levels in the ER, leading to the activation of sterol regulatory element binding protein (SREBP) transcription factor, which increases expression of genes involved in cholesterol biosynthesis and transport [42].

1.3. Lysosomes as Ca²⁺ storage organelles

Besides their role in degradation of macromolecules, lysosomes constitute a reservoir of the intracellular pool of calcium ions (Ca²⁺) and support the function of the ER, the main store of intracellular Ca²⁺ [43]. Under resting conditions, cytoplasmic Ca²⁺ concentration is low (~100 nM), whereas its lysosomal concentration is almost 3-4 orders of magnitude higher [43, 44]. Hence, there is a Ca²⁺ gradient between the lysosomal compartment and the cytoplasm. Upon activation of Ca²⁺-permeable channels or damage of lysosomal membranes, lysosomal Ca²⁺ is released to the cytosol, leading to the activation of Ca²⁺-modulated proteins, such as calmodulin (CaM) [45]. In turn, Ca²⁺-bound CaM activates its effector proteins, which regulate a broad range of processes, including lysosomal biogenesis [46], phagophore formation [47], lysosomal positioning and tubulation [48], lysosomal repair [49], fusion events with late endosomes [50] and the PM [51]. Of note, the generation of a Ca²⁺ gradient between lysosomes and the cytoplasm is

driven by pH-dependent activity of $\text{Ca}^{2+}/\text{H}^{+}$ (CAX) exchangers or ER-mediated refilling mechanism [44, 52].

1.3.1. Ca^{2+} in activation of calcineurin signaling

An important CaM target in signal transmission is serine/threonine phosphatase calcineurin (CaN), which regulates many processes, including gene expression, cytoskeletal reorganization and apoptosis [53]. For instance, CaN-mediated dephosphorylation of nuclear factors of activated T-cells (NFAT), myocyte-specific enhancer factor 2 (MEF2), forkhead transcription factors (FOXO) or transcription factor EB (TFEB), promotes nuclear translocation of these factors and expression of their target genes [53]. Noteworthy, starvation, ER stress or elevated levels of reactive oxygen species activate the expression of target genes of TFEB and transcription factor E3 (TFE3) in a CaN-dependent manner. These genes are involved in lysosomal biogenesis and autophagy (described in chapter 1.4.4.) [46, 54-56].

Structurally, CaN is a heterodimer consisting of a catalytic subunit, calcineurin A (CnA) and a Ca^{2+} -binding regulatory subunit, calcineurin B (CnB). A complete activation of CaN requires Ca^{2+} and Ca^{2+} -loaded CaM binding to the CnB, that leads to conformational changes and removal of an autoinhibitory domain from the active site of CnA [53]. To explore biological functions of CaN, immunosuppressive drugs, cyclosporin A (CsA) and FK506, are widely used to inhibit CaN activity [57]. In the cytoplasm, CsA and FK506 form complexes with cyclophilin and FK506-binding protein, respectively, which in turn inhibit CaN phosphatase activity [57].

1.3.2. Regulation of lysosomal Ca^{2+} release via MCOLN1 channel

Lysosomal Ca^{2+} signaling can be regulated by modulation of the activity of Ca^{2+} channels, including mucolipins (MCOLN1-3), two-pore channels (TPC1-2) and purinergic receptor P2X4 (P2X4) [6]. Mucolipin1 (MCOLN1), also known as transient receptor potential mucolipin 1 (TRPML1), is considered as a major protein that releases Ca^{2+} from the lumen of late endosomes and lysosomes to the cytoplasm [58].

In addition to Ca^{2+} , MCOLN1 can also transport Fe^{2+} and Zn^{2+} ions and therefore regulate their homeostasis [59, 60]. Impaired MCOLN1 function affects lysosome-related membrane trafficking, including lysosomal exocytosis [61-63], fusion of lysosomes with autophagosomes [47, 64, 65] and trafficking from lysosomes to the *trans*-Golgi network [27, 66, 67]. Moreover,

loss-of-function mutations in human MCOLN1 result in the development of lysosomal storage disease (LSD) known as Mucopolidosis type IV (MLIV) [68-70].

The activity of MCOLN1 to maintain lysosomal functions is regulated by lipid composition of late endosomal or lysosomal membranes. It can be promoted by phosphatidylinositol-3,5-bisphosphate (PI(3,5)P₂) [71], and blocked by phosphatidylinositol-4,5-bisphosphate (PI(4,5)P₂) [72] or sphingomyelin [67]. In recent years, several pharmacological activators of MCOLN channels were identified [67, 73-76]. However, till now, only two inhibitors are commonly used: ML-SI1 and ML-SI3, which strongly affect MCOLN1 activity and to a lesser extent MCOLN2 [77].

1.4. Lysosomes as platforms for the regulation of mTORC1-dependent signaling

In addition to degradation of macromolecules and regulation of Ca²⁺ signaling, lysosomes provide a physical platform to sense nutrient availability by the mechanistic target of rapamycin complex 1 (mTORC1) [78]. mTORC1 integrates information concerning energetic status of the cell, extracellular stimuli and stress-induced signals to regulate catabolic and anabolic processes of the cell [78].

1.4.1. Composition of mTORC1

mTOR is a serine/threonine protein kinase, which constitutes a catalytic center of two multiprotein complexes, mTORC1 and mTORC2. In addition to mTOR, the core of mTORC1 consists of regulatory-associated protein of mTOR (RAPTOR), involved in the recruitment of mTOR substrates [79] and mammalian lethal with SEC13 protein 8 (mLST8), which stabilizes the complex and promotes mTOR activity (Fig. 1.3) [80]. The two other components of mTORC1, proline-rich AKT substrate 40 kDa (PRAS40) and DEP-domain-containing mTOR-interacting protein (DEPTOR), act as inhibitors of mTOR activity [81, 82]. Additionally, mTORC1 activity can be blocked by the recruitment of FK506-binding proteins, that is stimulated by rapamycin compound [83]. Hence, rapamycin inhibits the activity of mTOR kinase in the mTORC1 complex [84]. In last decades, the second generation of mTOR inhibitors, such as INK128 or AZD8055 drugs, were developed to effectively target both mTORC1 and rapamycin-insensitive mTORC2 [85].

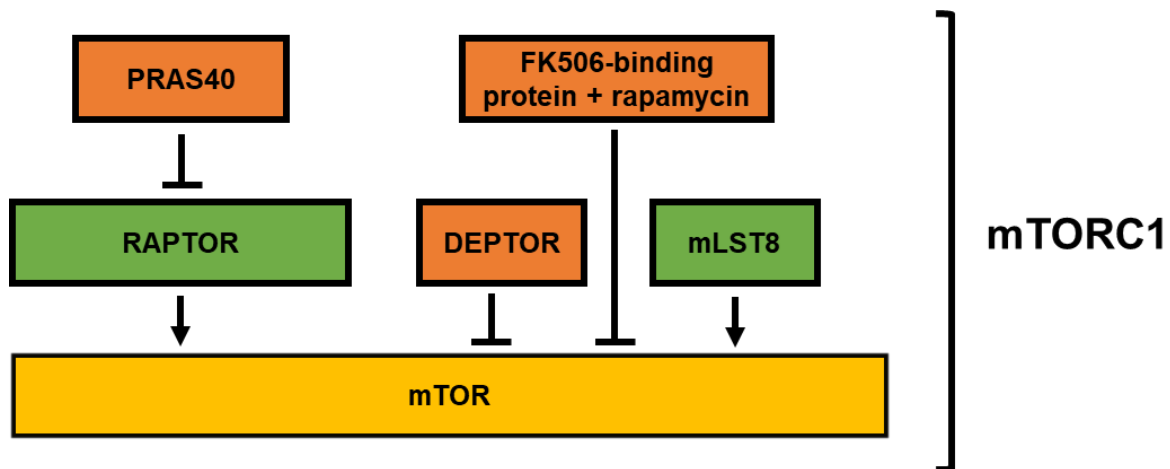


Figure 1.3. Schematic representation of components of mTORC1. Together with mTOR (yellow), RAPTOR and mLST8 form a core of mTORC1, leading to complex stabilization and activation (green). PRAS40, DEPTOR and rapamycin-bound FK506-binding protein inhibit mTORC1 activity (orange). Modified from Sabatini [86].

1.4.2. Functions of mTORC1

To ensure cell growth and proliferation, mTORC1 supports anabolic processes, such as protein synthesis and lipid biogenesis, whereas it limits degradation of cellular components [78].

To promote protein synthesis, mTORC1 phosphorylates the eukaryotic initiation factor 4E-binding proteins (4E-BPs) and p70 S6 kinase 1 (S6K1). In the dephosphorylated state, 4E-BPs bind and sequester eukaryotic translation initiation factor 4E (eIF4E), hence inhibiting its interaction with the mRNA 5' cap structure [87]. mTORC1-mediated phosphorylations of 4E-BP1 at its threonine residues 37 and 46 prevent eIF4E sequestration and thus promote protein synthesis [87]. Moreover, mTORC1 phosphorylation of S6K1 at threonine 389 induces activation of its downstream targets, including ribosomal protein S6, which controls the translation of a subset of mRNAs encoding ribosomal components [88, 89] and eukaryotic translation initiation factor 4B (eIF4B), which promotes initiation of translation by potentiating the eIF4A RNA helicase activity [90, 91].

Furthermore, mTORC1 activity controls lipid metabolism, promoting lipogenesis and inhibiting lipolysis and fatty acid β -oxidation [92]. mTORC1 promotes lipid synthesis via activation of SREBP transcription factor which induces expression of genes involved in synthesis of cholesterol, fatty acids, phospholipids and triglycerides [42]. Moreover, mTORC1 phosphorylation of lipin-1 leads to nuclear export of this transcriptional repressor and enables SREBP binding to its target genes [93]. mTORC1 activates also another transcription factor,

peroxisome proliferator-activated receptor- γ (PPAR γ), which regulates expression of genes encoding proteins involved in fatty acid esterification, lipid storage and triglyceride synthesis [92]. Additionally, mTORC1 may downregulate expression of genes involved in β -oxidation of fatty acids via promoting nuclear translocation of nuclear receptor corepressor 1 (NCoR1) [92].

mTORC1 regulates also glucose metabolism via S6K1- and 4E-BP1-dependent synthesis of hypoxia inducible factor 1 α (HIF1 α) protein, which induces expression of genes encoding glycolytic enzymes [94, 95]. To keep up with energetic demands for ATP production required in anabolic processes, mTORC1 promotes mitochondria fission and translation of nucleus-encoded mitochondrial proteins via activation of yin–yang 1 (YY1) and PPAR γ coactivator 1 α (PGC1 α) transcription factors [96].

To avoid undesirable degradation of newly synthesized macromolecules, mTORC1 suppresses the initiation of autophagy. To this end, mTORC1 phosphorylates unc-51-like autophagy-activating kinase 1 (Ulk1) at serine 757 and ATG13 at serine 258, leading to the inhibition of autophagosome formation [97, 98]. Upon starvation, inactivation of mTORC1 shifts the cellular metabolic balance in favour of catabolism, resuming formation of autophagosomes and hence autophagic degradation [99]. Additionally, reduced mTORC1 activity promotes nuclear accumulation of mTORC1 downstream targets, TFEB and TFE3 transcription factors, and expression of lysosomal and autophagic genes (described in chapter 1.4.4.) [46, 54, 55]. Newly formed lysosomes supply the cell with nutrients derived from endolysosomal and autolysosomal degradation and restore cellular pools of amino acids, lipids and glucose. This feedback loop ensures reactivation of mTORC1 activity after starvation, once new nutrients are provided [78].

1.4.3. Regulation of mTORC1 signaling

To adapt its activity to cellular needs, mTORC1 monitors, collects and integrates upstream inputs, such as the levels of nutrients, ATP, growth factors or stressors. Activation of mTORC1 by many of these inputs requires its association with the surfaces of lysosomes, where this complex may interact with its regulators, such as guanine nucleotide-binding proteins, Ras-related GTP-binding (Rag) GTPases and Ras homolog enriched in brain (Rheb) [78].

1.4.3.1. Regulation of Rag GTPase complex activity

Rag GTPase is a heterodimer complex formed by RagA or RagB bound to RagC or RagD proteins. It plays an important role in sensing the levels of amino acids [100]. Depending on whether RagA/B or C/D bind GDP or GTP, this complex exists either in an active state (RagA/B^{GTP} and RagC/D^{GDP}) or an inactive state (RagA/B^{GDP} and RagC/D^{GTP}, Fig. 1.4) [100]. Rag proteins are unable to directly interact with the lysosomal membrane. Instead, they are scaffolded to lysosomes via interaction with the Ragulator complex (also known as LAMTOR) [101, 102]. Moreover, Ragulator exhibits a GTP exchange factor (GEF) activity toward RagA/B^{GDP} and promotes their conversion into RagA/B^{GTP} [101]. Only in their active state, Rag GTPases recruit mTOR to the lysosomal surface, enabling mTORC1 activation [103, 104]. Otherwise, mTORC1 remains inactive in the cytoplasm [103, 104].

Under amino acid-depleted conditions, a GTPase-activating protein (GAP) activity of the GATOR1 complex promotes RagA/B^{GTP} hydrolysis to RagA/B^{GDP}, thus inactivating mTORC1 [105, 106]. In turn, the folliculin (FLCN)–folliculin-interacting protein (FNIP) complex activates Rag GTPases by promoting RagC/D^{GTP} hydrolysis to RagC/D^{GDP} that supports mTORC1 recruitment to lysosomes [107, 108]. Leucyl-tRNA synthetase (LRS), a sensor of intracellular leucine concentration, also exhibits a GAP function for RagC/D^{GTP} activating the Rag GTPase complex (Fig. 1.4) [109]. Additionally, in the presence of amino acids, the conversion of RagA/B^{GDP} into the RagA/B^{GTP} active state is supported by lysosomal transmembrane proteins, SLC38A9 and V-type ATPase [110-113].

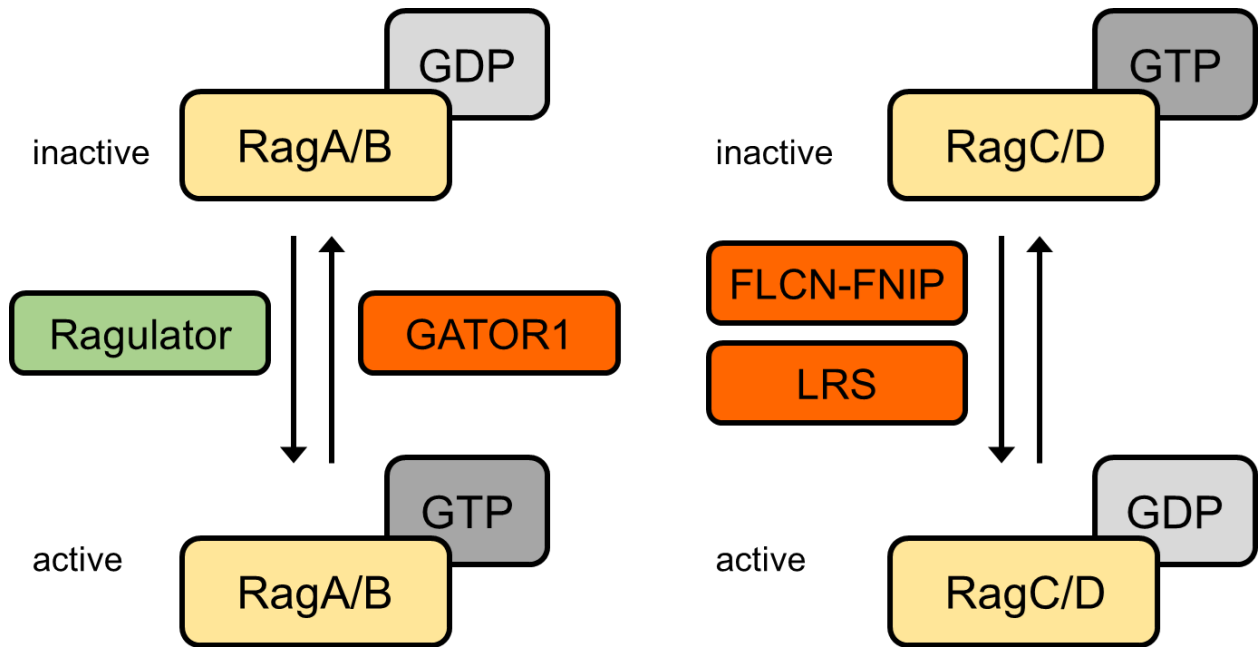


Figure 1.4. Schematic representation of the regulation of Rag GTPase activity by GEF (Ragulator, green) and GAPs (GATOR1, FLCN-FNIP, LSR, orange). Ragulator or FLCN-FNIP and LSR promote activation of Rag GTPase complex under nutrient-rich conditions via conversion of $\text{RagA/B}^{\text{GDP}}$ into $\text{RagA/B}^{\text{GTP}}$ or hydrolysis of $\text{RagC/D}^{\text{GTP}}$ into $\text{RagC/D}^{\text{GDP}}$, respectively. In turn, upon shortage of amino acids GATOR1 converts $\text{RagA/B}^{\text{GTP}}$ into $\text{RagA/B}^{\text{GDP}}$, inactivating the Rag GTPase complex.

1.4.3.2. Regulation of Rheb

Upon tethering at the lysosomal surface via active Rag GTPase complex, mTORC1 is directly activated by GTP-bound Rheb GTPase [114]. The best known modulator of Rheb activity is tuberous sclerosis (TSC) complex, which mediates conversion of active Rheb^{GTP} into inactive Rheb^{GDP} [114]. Upon growth factor-induced signaling, phosphorylation of TSC suppresses its GAP activity towards Rheb and enables mTORC1 activation [115, 116]. Regulation of TSC activity occurs via multiple signaling pathways, including PI3K–Akt [117], extracellular signal-regulated kinase (ERK) [118], Wnt [119] and AMP-activated protein kinase (AMPK) [120] pathways.

1.4.4. Transcriptional responses related to lysosomal function

Since recently, lysosomes are recognized also as regulators of transcriptional responses induced upon impairment of intracellular transport, nutrient shortage or lysosomal dysfunction

[121, 122]. To date, the best characterized transcriptional response related to lysosomal function is orchestrated by transcription factors from the MiT-TFE family.

1.4.4.1. MiT-TFE transcription factor family

Transcription factors from the MiT-TFE family constitute a group of proteins that are evolutionary conserved from lower metazoans to mammals and contain basic helix-loop-helix leucine zipper (bHLH-ZIP) [123]. In vertebrates, the family comprises four members: transcription factor EB (TFEB), transcription factor E3 (TFE3), microphthalmia-associated transcription factor (MITF) and transcription factor EC (TFEC) [123]. Of note, TFEC is the only member that lacks a transcriptional activation domain, and therefore may exhibit an inhibitory role in the regulation of target gene expression [124]. Upon formation of homo- or heterodimers, MiT-TFE factors recognize and bind to palindromic DNA fragments containing the GTCACGTGAC sequence, known as the CLEAR motif [125, 126]. Although functions of MiT-TFE factors overlap to a large extent, their expression levels vary substantially in different tissues [127].

1.4.4.2. Intracellular roles of MiT-TFE factors

TFEB and TFE3 factors are master regulators of lysosomal function as they induce expression of genes encoding lysosomal and autophagic proteins [125, 128, 129]. Overexpression of TFEB increases the number of lysosomes and activity of lysosomal enzymes [125], as well as it promotes autophagic degradation of proteins [128], lipid droplets [130] and damaged mitochondria [131]. Additionally, activation of TFEB and TFE3 factors promotes clearance of non-degraded substances in models of LSD [63, 129, 132-134] and neurodegenerative diseases [135-139]. Moreover, TFEB is implicated in the regulation of lipid metabolism. Upon starvation, TFEB upregulates expression of PGC1 α , which induces expression of genes involved in free fatty acid oxidation in mitochondria and peroxisomes [130]. Interestingly, mammalian TFEB, TFE3 and their ortholog HLH-30 in *Caenorhabditis elegans* were also implicated in transcriptional activation of an inflammatory response upon pathogen infection or lipopolysaccharide treatment, pointing to an evolutionary conserved function of MiT-TFE members [140, 141].

The role of the MITF factor was primarily characterized in melanocyte development [142]. MITF amplification was established as oncogenic in melanocyte-derived tumors and was associated with melanoma progression [143]. MITF loss-of-function mutation leads to

development of Waardenburg syndrome type IIA, manifested by deafness and pigmentation defects in eye, hair and skin [144].

1.4.4.3. Regulation of subcellular localization of MiT-TFE transcription factors

In order to regulate transcription of target genes and adjust cellular metabolism, MiT-TFE factors exploit the phosphorylation-mediated mechanism and protein-protein interactions to shuttle from the cytoplasm to the nucleus [127]. Phosphoproteomic studies revealed that TFEB can be phosphorylated at more than 20 sites [145-147]. However, the most widely described mechanism of its regulation in the presence of nutrients relies on the phosphorylation of serine residues at 122 (S122), at 142 (S142) and at 211 (S211) positions, leading to TFEB cytoplasmic retention. Phosphorylation at S122 and S211 positions is regulated by mTORC1 [148-151], whereas phosphorylation of S142 can be controlled by ERK2 and/or mTORC1 [128, 148] (Fig. 1.5). Historically, the first identified mTORC1-dependent phosphorylation of TFEB was the S211 phosphorylation that was described in the same year in three independent studies by groups of Ballabio, Ferguson and Puertollano [148-150]. Generation of a constitutively active TFEB variant carrying the serine to alanine mutation at S142 or S211 positions resulted in its accumulation in the nucleus under nutrient-rich conditions [128, 149, 150]. A few years later, results concerning phosphorylation of S122 were provided by the Brugarolas group [151], showing that a phosphomimetic substitution of serine into aspartic acid at this site prevented nuclear accumulation of TFEB despite mTORC1 inhibition [151]. Moreover, in a series of experiments exploring ERK2-mediated regulation, phosphorylation of TFEB on S142 and TFEB cytoplasmic retention was abolished upon treatment with ERK pathway inhibitors or depletion of ERK proteins with siRNA [128].

The phosphorylation of TFEB by mTORC1 occurs at the lysosomal surface. Under nutrient-rich conditions, active Rag GTPases mediate lysosomal recruitment of both TFEB and mTORC1, thereby promoting mTORC1-dependent TFEB phosphorylation [152]. Phosphorylation of TFEB via mTORC1 enables binding of this transcription factor by a chaperone-like adaptor molecule 14-3-3 that masks the TFEB nuclear localization signal leading to its sequestration in the cytosol [149-151]. Consistent with this mechanism, MiTF and TFE3 can also be retained in the cytoplasm via interaction with 14-3-3 protein [153, 154]. TFEB cytoplasmic sequestration is also promoted through its phosphorylations by GSK3 β (on S134 and S138), Akt (on S467) kinases [155, 156] and FLCN (on S109, S114, S122 and S211) [107, 157] (Fig. 1.5).

Whereas cytoplasmic retention of MiT-TFE factors occurs upon their phosphorylation, their nuclear localization requires their dephosphorylation by phosphatases [46]. A high-content screen of putative phosphatases involved in TFEB activation upon nutrient shortage revealed the role of Ca²⁺-regulated CaN in the dephosphorylation of TFEB at both S142 and S211 residues, followed by its nuclear translocation [46]. Both siRNA-mediated depletion of CnA and treatment with CaN inhibitors, CsA or FK506, prevent nuclear accumulation of TFEB upon starvation [46]. Similarly, activation of TFE3 due to ER stress can be hampered by CaN inhibition or depletion [55]. Moreover, TFEB and TFE3 nuclear translocation in response to oxidative stress can be promoted by dephosphorylation of TFEB at S109, S114, S122, and S211 residues and TFE3 at S321 residue by the protein phosphatase 2A (PP2A) [158, 159].

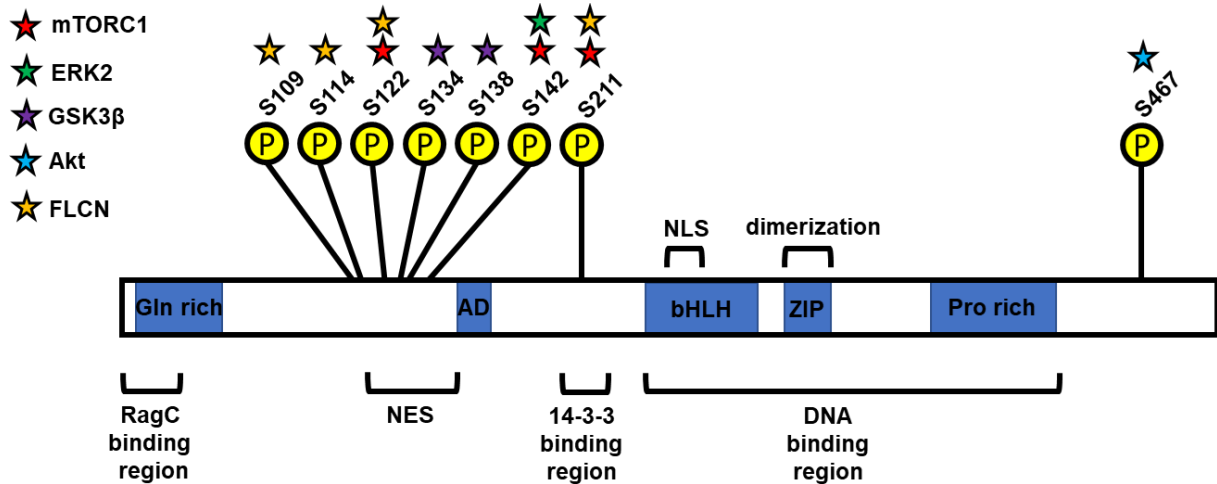


Figure 1.5. Schematic representation of domains, functional regions and phosphorylation sites of TFEB protein. Modified from Astanina et al. [160]. Gln rich, glycine rich region; NES, nuclear export signal; AD, transcriptional activation domain; NLS, nuclear localization signal; bHLH, basic helix-loop-helix; ZIP, leucine zipper domain; Pro rich, proline rich region. Different star colors indicate kinases involved in phosphorylation of relevant serine residues.

1.5. Role of ESCRT machinery in delivering cargo for lysosomal degradation

Endosomal sorting complexes required for transport (ESCRT) are a group of protein complexes that are involved in various membrane remodeling processes in cells. ESCRT machinery consists of four complexes (0-III) and additional accessory proteins that assemble in a coordinated manner to enable membrane invagination and scission [161].

The best characterized function of ESCRT machinery is the formation of ILVs during endocytic sorting of proteins destined for lysosomal degradation (Fig. 1.6). In this process, subunits of ESCRT-0, hepatocyte growth factor-regulated tyrosine kinase substrate (Hrs) and

signal-transducing adaptor molecule (STAM) recognize and bind endocytosed membrane proteins marked for degradation by ubiquitin [162-165]. Then, a heterotetrameric ESCRT-I complex binds to ESCRT-0 [166, 167]. ESCRT-I encompasses the following subunits: tumor susceptibility 101 (Tsg101), vacuolar protein sorting-associated protein 28 homolog (Vps28), vacuolar protein sorting-associated protein 37 (one out of four known Vps37A-D isoforms), and multivesicular body subunit 12 (MVB12A or MVB12B isoform) or ubiquitin associated protein 1 (UBAP1) [166]. Apart from binding to ESCRT-0, some ESCRT-I components (specifically Tsg101, UBAP1 or MVB12) also recognize ubiquitinated proteins with their ubiquitin binding domains [166]. The Vps28 subunit of ESCRT-I interacts directly with ELL-associated protein of 45 kDa (EAP45) [168], which together with EAP30 and two subunits of EAP20 forms the ESCRT-II complex [169]. After their recruitment to the endosomal membrane, the ESCRT0-II complexes initiate inward membrane budding [170]. In the next step, EAP20 proteins support the assembly of the ESCRT-III complex by binding to its component, charged multivesicular body protein 6 (CHMP6) [171]. In addition to CHMP6, ESCRT-III consists of other core proteins, such as CHMP4A-C, CHMP3, CHMP2A-B, and several accessory proteins, which regulate the polymerization of ESCRT-III subunits [161]. In contrast to ESCRT0-II complexes, which form stable complexes, ESCRT-III subunits reside in the cytoplasm as monomers. Upon recruitment to endosomal membrane, ESCRT-III forms membrane-bending spirals that facilitate membrane deformation to generate ILVs. Specifically, polymerization of ESCRT-III spirals leads to membrane invagination into the endosomal lumen and constriction of this invagination near the endosomal limiting membrane [161]. As a final step in ILV formation, an accessory ATPase protein that cooperates with ESCRT-III, vacuolar protein sorting 4 (Vps4), provides energy for further constriction and scission of the vesicle forming in the endosomal lumen [172-174]. At the same time ESCRT-III subunits are disassembled and may be recycled to form the next ILVs [175, 176]. As a result of the coordinated action of ESCRT machinery, endosomes transform into MVBs containing numerous internal vesicles that can be delivered for lysosomal degradation [20]. Alternatively, instead of being directed to lysosomal degradation, the content of MVBs can be targeted to the cell surface. Upon fusion of MVBs with the plasma membrane, ILVs loaded with cargo are released into the extracellular environment as extracellular vesicles (exosomes), in a process called exosome secretion [177]. Given their role in MVB formation, deficiency of ESCRT components leads to intracellular accumulation of enlarged endosomes largely devoid of ILVs [178-180].

Another intracellular process that delivers cargo for lysosomal degradation and is controlled by ESCRT machinery is autophagy. Upon induction of autophagy, the intracellular content is engulfed by a double-membrane structure, a phagophore, which after its closure forms an autophagosome that subsequently fuses with the lysosome [181]. Depletion of ESCRT components (ESCRT-I, -II, -III or Vps4) disrupts autophagic flux resulting in a massive accumulation of autophagosomes and protein aggregates [182, 183]. Additionally, a genome-wide CRISPR screen revealed that ESCRT proteins are required for phagophore closure [184, 185].

Hence, due to the involvement of ESCRT machinery in endosomal sorting and autophagy, they mediate transport of cargo destined for lysosomal degradation.

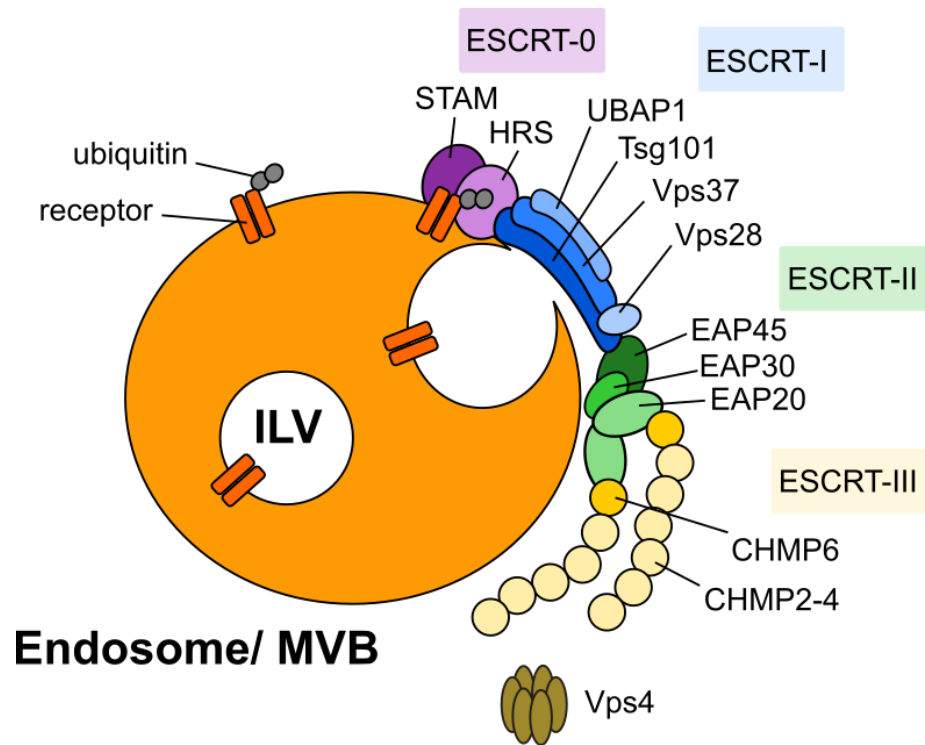


Figure 1.6. Schematic representation of ESCRT assembly and function in MVB biogenesis. Upon binding to ubiquitinated receptors on the endosomal membrane, a coordinated action of ESCRT-0, -I, -II, -III and Vps4 enables constriction of ILV neck and receptor sorting into the MVB lumen. Modified from Vietri et al. [186].

1.6. Involvement of ESCRT in controlling signaling from endosomes

ESCRT machinery plays an important role in controlling signal transduction. Because signaling receptors are among membrane proteins that are sorted into the interior of MVBs, ESCRT components (i) regulate the intracellular pool of receptors by delivering them for

lysosomal degradation, and (ii) disconnect receptors from their cytoplasmic effectors, thus attenuating receptor signaling [187, 188].

ESCRT proteins negatively regulate signalling from a broad range of receptors, including receptor tyrosine kinases (RTKs) and cytokine receptors [189-194]. One of the model receptor commonly used to study endocytosis is a member of the RTK family, epidermal growth factor receptor (EGFR). Depletion of Hrs, Tsg101 or Vps4A leads to EGFR accumulation on enlarged endosomes as well as increased activation of its downstream effectors, including ERK1/2 [180]. Moreover, some cytokine receptors, such as lymphotoxin β receptor (LT β R) and tumor necrosis factor receptor 1 (TNFR1), undergo constitutive ESCRT-mediated downregulation. Lack of Tsg101, Vps28, UBAP1 or CHMP4B results in abnormal accumulation of these receptors on enlarged endosomes and activation of TNFR-associated factor 2/3 (TRAF2/3) effectors, inducing an inflammatory NF- κ B response [193, 194].

1.7. Role of ESCRT components in maintaining lysosomal homeostasis

ESCRT proteins are also implicated in the repair of lysosomal membranes. Many factors including lysosomotropic drugs, mineral crystals, β -amyloid or pathogen infection may disrupt lysosomal membrane integrity [195]. Unintended release of hydrolases from the lysosomal lumen to the cytosol can lead to digestion of essential proteins and eventually kill the cell in a process termed lysosomal cell death [196, 197]. To limit this hazardous effect, cells utilize a quality control mechanism which exploits the affinity of cytosolic galectins to glycoproteins present on the luminal lysosomal surface. Galectins binding to damage-exposed glycoproteins initiate selective autophagy to remove damaged lysosomes, so called lysophagy [195]. Unlike lysophagy, which is defined as a slow process of removal of the whole organelle [186], ESCRT components are rapidly recruited to the perforation site to restore lysosomal membrane integrity [49, 198, 199]. siRNA-mediated depletion of several ESCRT subunits impairs lysosomal membrane repair upon treatment with lysoosmotic agents, silica crystals and bacterial infection [49, 198].

Furthermore, ESCRT components are implicated in turnover of vacuolar membrane proteins in yeast. Similar to ESCRT-mediated endosomal sorting, ubiquitinated vacuolar membrane proteins, like vacuolar lysine transporter Ypq1, zinc importer Zrc1 or cobalt uptake protein Cot1, are recognized and internalized into the vacuolar lumen by the ESCRT machinery [200-203]. Despite the functional analogy of yeast vacuoles with mammalian lysosomes [204], so far only one very recent study showed the involvement of mammalian ESCRT-III and Vps4 protein in the

turnover of lysosomal membrane proteins, namely lysosomal-associated transmembrane protein 4A (LAPTM4A) and E3 ubiquitin-protein ligase RNF152 ([205], the study published when the experimental part of this thesis was finished). Nevertheless, the role of ESCRT proteins in the degradation of lysosomal membrane proteins still remains poorly defined.

1.8. Other roles of ESCRT components

In addition to their role in the endolysosomal pathway, ESCRT proteins are involved in the regulation of many other cellular processes, including cytokinesis, viral budding, PM or nuclear envelope repair [186]. During cell abscission, centrosomal protein CEP55 mediates accumulation of Tsg101 and ALIX at the midbody ring followed by engagement of other subunits of ESCRT-II, -III and Vps4 [206]. Next, ESCRT components bind spastin, an AAA-ATPase, which mediates removal of remaining microtubules and splitting of the intercellular bridge [207]. The ESCRT properties in membrane remodeling can be usurped by viruses, such as HIV-1 or Ebola, for their maturation and budding [208]. To enable virus release from infected cells, different short peptide motifs within the viral proteins recognize and bind to particular ESCRT subunits [208]. Moreover, ESCRT proteins mediate the sealing and repairing of damaged cellular membranes. In addition to the restoration of lysosomal membrane integrity upon damage, they act at the site of PM injury [209]. Massive Ca^{2+} influx through the membrane wound facilitates the formation of the calcium-binding protein-apoptosis-linked gene (ALG)-2-ALIX complex, followed by the recruitment of Tsg101 and late-acting ESCRT components [210, 211]. Inhibition of ESCRT function, particularly depletion of ESCRT-III, promotes activation of inflammatory caspases and pyroptotic cell death upon PM lesions [212]. Moreover, ESCRT machinery was implicated in the sealing of nuclear envelope upon mechanical stress [213, 214] or chromosomal separation during mitotic exit [215].

Collectively, the diversity of sites of action and numerous functions performed by ESCRT components underlie their unique role in membrane trafficking, regulation of signaling cascades and maintaining organelle integrity.

1.9. Diseases caused by mutations or abnormal expression of genes encoding ESCRT proteins

Given the diversity of ESCRT-driven processes, the impairment of ESCRT functions lead to the development of severe pathologies [216]. Point mutations, abnormal protein levels or loss of ESCRT components are associated with several types of cancers [216]. For instance, genes

encoding ESCRT-I proteins, Tsg101 and Vps37, were reported as often deleted or mutated in cancer and may act as tumor suppressors [217-219]. Aberrant expression of the gene encoding Tsg101 is observed in many cancer types, including cervical carcinomas [220], head and neck squamous cell carcinoma, stomach adenocarcinoma and kidney renal clear cell carcinoma [221]. Additionally, transcription of another ESCRT-I, Vps37A, is downregulated in hepatocellular carcinomas [218], breast cancer [222], ovarian cancer [223], renal cell carcinoma [224] and colorectal adenocarcinoma [221, 225]. Additionally, deficiency of Vps37A is associated with increased proliferation and migration of cancer cells [226-229]. However, some studies indicated ESCRT-I overexpression rather as a prognostic marker, which correlates with poor patient prognosis and increased metastasis [230-233].

The late-acting components of ESCRT machinery, ESCRT-III and Vps4, are also associated with tumor development, however whether they promote or inhibit carcinogenesis is still debated. A subunit of ESCRT-III, CHMP1A, was found to be downregulated in pancreatic cancer cells [234], renal cell carcinomas [235] and colorectal adenocarcinoma [221]. Additionally, downregulation of Vps4B was observed in different types of cancer, notably in colorectal cancer [236]. On the other hand, components of ESCRT-III (CHMP4B and CHMP4C) and Vps4A appeared as pro-oncogenic and their elevated levels improved resistance to anticancer treatment [237-240]. Recent studies revealed also that ESCRT-mediated membrane repair can help tumor cells to resist immune attack [241]. Interestingly, targeting Vps4A function was proposed as a new therapeutic strategy for personalized treatment of cancer with low expression of gene encoding Vps4B [236].

Dysregulated ESCRT functions were also observed in many diseases related to neurodegeneration. Lack of a functional ESCRT-I subunit, UBAP1, was recently described in hereditary spastic paraplegia [242-245]. Mutations within the ESCRT-III subunit, CHMP2B, were reported in patients with a rare form of frontotemporal dementia [246] and amyotrophic lateral sclerosis [247, 248]. Moreover, ESCRT components are involved in endosomal sorting of β -amyloid and α -synuclein, proteins contributing to the development of Alzheimer's disease and Parkinson's disease, respectively [249, 250]. As a consequence of ineffective ESCRT-mediated endolysosomal and autolysosomal degradation, accumulated ubiquitin and/or p62 protein aggregates promote progressive neurodegeneration [251]. Thus, activation of ESCRT-mediated

processes or a genetic correction of impaired trafficking proteins may be a beneficial approach to support clearance of toxic aggregates.

Recently, Vps4A was shown as a critical factor in reticulocyte maturation. Mutations in the gene encoding Vps4A were reported among patients with congenital dyserythropoietic anemia and contributed to defects in erythropoiesis and neurodevelopment [252]. Similarly, *de novo* missense mutations in the gene encoding Vps4 were identified among individuals suffering from a severe neurodevelopmental delay, brain abnormalities and anemia [253].

1.10. Targeting lysosomal function in diseases including cancer

A possible strategy to target lysosomal function under pathological conditions depends on the etiology of lysosomal impairment. Generally, there are two opposite therapeutic strategies relying on the induction or inhibition of lysosomal function depending on the cellular context [254].

The improvement or induction of lysosomal function is a desired approach in treatment of LSDs and neurodegenerative diseases [254]. In this case, dysfunction of lysosomal enzymes or non-enzymatic proteins impairs processes of cellular clearance, leading to the accumulation of potentially toxic products, dysregulation of cellular signaling and inflammation [255-257]. Up to date, substantial progress was made in treatment of LSDs using enzyme replacement therapy, chemical chaperone therapy or substrate reduction therapy [258]. Moreover, targeting autophagy upstream of lysosomes is gaining more interest in treatment of neurodegenerative diseases [181, 259]. A particular example of such treatment is a pharmacological or genetic activation of TFEB, which partially restores degradation of protein aggregates in Alzheimer's disease [137, 138, 260], Parkinson's disease [135, 136, 261] and Huntington's disease [262].

The second therapeutic approach aims to alleviate excessive lysosomal activity in treatment of cancer and autoimmune diseases [254]. Lysosomes are important regulators of macromolecule recycling to support cancer cell growth and proliferation. Due to their exocytosis, lysosomes can also acidify and degrade extracellular matrix, promoting cell migration and metastasis [263]. Excessive lysosomal function can contribute to development of the multidrug resistance phenotype via sequestration of chemotherapeutics in lysosomes, which results in impaired delivery of these drugs to intracellular targets [264]. An example of such mechanism is treatment of cancer cells with hydrophobic weak-base drugs, e.g. doxorubicin, which was associated with TFEB activation, lysosomal biogenesis and increased lysosomal enzyme activity [264]. Moreover, overexpression of genes encoding MiT-TFE factors or increased nuclear translocation of these proteins were

reported in many types of cancer cells, including melanoma [265], pancreatic adenocarcinoma [266], renal cell carcinoma [267], non-small cell lung cancer [268] and colorectal cancer [269]. Because cancer cells greatly rely on lysosomal functions, targeting lysosomal acidification, lysosomal cathepsins, lysosomal membrane integrity, lysosomal Ca^{2+} signaling, mTORC1 signaling or TFEB may serve as a therapeutic window to make cancer cells more vulnerable to death [270]. However, the greatest limitation of this strategy is the lack of drugs with high efficiency and specificity towards lysosomal compartment of cancer cells [254, 270].

2. Aims of the study

Recently, ESCRT components, including ESCRT-I, were shown to mediate degradation of ubiquitinated vacuole membrane proteins in yeast by facilitating their sorting into the vacuolar lumen [200, 202, 203, 271]. However, whether mammalian ESCRT proteins act also at lysosomes has been poorly studied. Initially, the only known role of mammalian ESCRT components, including ESCRT-I, at lysosomes was their contribution to repairing the lysosomal membrane upon damage [49, 198, 272]. Only at the final stages of the study presented in this thesis, another publication reported the involvement of some ESCRT components in the turnover of lysosomal membrane proteins [205]. Nevertheless, the role of ESCRT proteins in lysosomal homeostasis was not fully unraveled.

The general aim of this project was to characterize the role of ESCRT-I in the regulation of lysosomal morphology, function and signaling, as well as to identify molecular mechanisms that activate MiT-TFE signaling from lysosomes upon ESCRT-I depletion. The specific aims of this thesis were to:

1. Characterize morphology and degradative capacity of lysosomes upon ESCRT-I depletion.
2. Determine the role of ESCRT-I in degradation of lysosomal membrane proteins.
3. Identify transcription factors activated upon ESCRT-I depletion and involved in signaling from lysosomes.
4. Verify the effect of impaired cholesterol efflux from lysosomes on the activation of MiT-TFE signaling upon ESCRT-I depletion.
5. Examine the involvement of Ca^{2+} mediated signaling on the activation of MiT-TFE transcription factors upon ESCRT-I depletion.
6. Investigate the status of mTORC1 activation upon ESCRT-I depletion and its contribution to MiT-TFE activation.
7. Study the contribution of Rag GTPase complex to the activation of MiT-TFE signaling upon ESCRT-I depletion.

3. Materials and methods

3.1. Materials

3.1.1. Cell lines

Table 3.1.1. List of cell lines used in the PhD project

Cell line	Culture medium	Description	Source
DLD-1	DMEM	Human colon carcinoma cells	ATCC
HEK293T	DMEM	Human embryonic kidney 293T cells	ATCC
RKO	EMEM	Human colon carcinoma cells	ATCC
RKO-GFP-MCOLN1	EMEM	RKO cells with stable expression of GFP-MCOLN1	Generated in this thesis

3.1.2. Cell culture media and supplements

Table 3.1.2. List of cell culture reagents used in the PhD project

Name	Source	Cat. No.	Application
Eagle's Minimum Essential Medium (EMEM)	LGC Standards-ATCC	30-2003	Cell culture of RKO
Dulbecco's Modified Eagle's Medium (DMEM)	Sigma-Aldrich	M2279	Cell culture of DLD-1, HEK293T
Fetal bovine serum (FBS)	Sigma-Aldrich	F7524	DMEM and EMEM media supplement
Delipidated FBS	Biowest	S181L	EMEM medium supplement
L-glutamine	Sigma-Aldrich	G7513	DMEM medium supplement
Earle's balanced salt solution (EBSS)	Sigma-Aldrich	E2888	Starvation medium
Trypsin	VWR	MDTC25-052-CV	Cell detachment
Puromycin	ABO	P001	Cell selection

3.1.3. Primary antibodies

Table 3.1.3. List of primary antibodies used in the PhD project. WB, western blot; IF, immunofluorescence

Antigen	Origin	Source	Cat. No.	Application, dilution
EEA1	Mouse	BD Biosciences	610457	IF 1:200
GAPDH	Rabbit	Santa Cruz Biotechnology	sc-25778	WB 1:1000
GFP	Goat	R&D Systems	AF4240	WB 1:1000
H3	Rabbit	Sigma-Aldrich	H0164	WB 1:10000
HA	Mouse	Cell Signaling Technology	2367	WB 1:1000, IF 1:100
Hrs	Rabbit	Abcam	Ab155539	WB 1:1000
LAMP1	Mouse	DSHB	H4A3	IF 1:400
LAMP1	Rabbit	Sigma-Aldrich	L-1418	IF 1:200
mTOR	Rabbit	Cell Signaling Technology	2983	IF 1:100
P-4E-BP1 Thr37/46	Rabbit	Cell Signaling Technology	2855	WB 1:1000
P-S6K1 Thr389	Rabbit	Cell Signaling Technology	9234	WB 1:1000
P-TFEB S122	Rabbit	Cell Signaling Technology	86843	WB 1:1000
P-Ulk1 S757	Rabbit	Cell Signaling Technology	6888	WB 1:1000
TFE3	Rabbit	Cell Signaling Technology	14779S	WB 1:1000, IF 1:100
TFEB	Rabbit	Cell Signaling Technology	4240S	WB 1:1000, IF 1:100
Tsg101	Mouse	Abcam	ab83	WB 1:1000
Ubiquitin (FK2)	Mouse	Enzo Life Sciences	BML-PW8810	IF 1:400
Vinculin	Mouse	Sigma-Aldrich	V9131	WB 1:1000
Vps28	Rabbit	Abcam	ab167172	WB 1:1000

3.1.4. Secondary antibodies

Table 3.1.4. List of secondary antibodies used in the PhD project. WB, western blot; IF, immunofluorescence

Antigen	Origin	Source	Cat. No.	Application,dilution
Alexa Fluor 488–conjugated donkey anti-mouse	Donkey	Thermo Fisher Scientific	A-21202	IF 1:500
Alexa Fluor 555–conjugated donkey anti-mouse	Donkey	Thermo Fisher Scientific	A-31570	IF 1:500
Alexa Fluor 647–conjugated donkey anti-rabbit	Donkey	Thermo Fisher Scientific	A-31573	IF 1:500
Horseradish peroxidase (HRP)-conjugated anti-goat	Bovine	Jackson ImmunoResearch Labs	805-035-180	WB 1:10000
Horseradish peroxidase (HRP)-conjugated anti-mouse	Goat	Jackson ImmunoResearch Labs	115-035-062	WB 1:10000
Horseradish peroxidase (HRP)-conjugated anti-rabbit	Goat	Jackson ImmunoResearch Labs	111-035-144	WB 1:10000

3.1.5. Plasmids

Table 3.1.5. List of plasmids used in the PhD project

Name	Source	Cat. No.
pLenti-CMV-MCS-GFP-SV	Addgene	73582
pMD2.G	Addgene	12259
psPAX2	Addgene	12260
mucolipin1-pEGFP C3	Addgene	62960
pRK5-HA GST RagC WT	Addgene	19304
pRK5-HA GST RagC 75L	Addgene	19305

3.1.6. Bacterial strains

Table 3.1.6. Bacterial strain used in the PhD project

Strain	Source	Genotype
Stbl3 (<i>Escherichia coli</i>)	Thermo Fisher Scientific	F-mcrB mrrhsdS20(rB-, mB-) recA13 supE44 ara-14 galK2 lacY1 proA2 rpsL20(StrR) xyl-5 λ-leumtl-1

3.1.7. Bacterial culture reagents

Table 3.1.7. List of reagents used for bacteria culture in the PhD project

Name	Source	Cat. No.
LB Broth Lennox	Bio Shop	LBL405.1
LB Agar Lennox	Bio Shop	LBL406.1
Ampicilin (antibiotic)	Sigma-Aldrich	A9518

3.1.8. Chelator and inhibitors

Table 3.1.8. List of chelator and inhibitors used in PhD project

Name	Source	Cat. No.	Final concentration/ time of treatment	Application
Bafilomycin A1 (BafA1)	Sigma-Aldrich	B1793	50 nM, 18 h	V-ATPase inhibitor of lysosomal acidification
BAPTA-AM (BAPTA)	Santa Cruz	sc-202488	10 μ M, 2 h	Intracellular Ca ²⁺ chelator
Cyclosporin A (CsA)	Santa Cruz	sc-3503	25 μ M, 2 h	Calcineurin inhibitor
INK128	Selleckchem	S2811	1 μ M, 2 h	mTORC1/2 inhibitor
ML-SI1	Cayman Chemical	GW 405833	25 μ M, 2 h	MCOLN1 inhibitor

3.1.9. Small interfering RNA oligonucleotides (siRNA)

Table 3.1.9. Ambion Silencer Select small interfering RNA (siRNA) from Thermo Fisher Scientific used in the PhD project

Name	Target gene/protein	Cat. No.	Sequence 5'-3'
siCtrl#1	Non-targeting control no. 1	4390843	Sequence not provided by the manufacturer
Ctrl#2	Non-targeting control no. 2	4390846	Sequence not provided by the manufacturer
siTsg101#1	<i>TSG101</i> /Tsg101	s14439	GAAAAAGGGUCACCAGAAAtt
siTsg101#2	<i>TSG101</i> /Tsg101	s14440	CUGUAAUGUUAUUACUCUtt
siVps28#1	<i>VPS28</i> /Vps28	s27577	AAUCAGCUCUAUUGACGAAAtt
siVps28#2	<i>VPS28</i> /Vps28	s27579	GAAGUGAAGUUGUACAAGAtt

siTFEB#1	<i>TFEB/TFEB</i>	s15495	ACAUCAAUCCUGAAAUGCAtt
siTFEB#2	<i>TFEB/TFEB</i>	s15496	AGGAGACGAAGGUUCAACATT
siTFEB#3	<i>TFEB/TFEB</i>	s15497	AGACGAAGGUUCAACAUCAtt
siTFE3#1	<i>TFE3/TFE3</i>	s14030	GCAGCUCCGAAUUCAGGAAtt
siTFE3#2	<i>TFE3/TFE3</i>	s14031	GGCGAUUCAACAUAACGAtt
siTFE3#3	<i>TFE3/TFE3</i>	s14032	AGCUUCUACGAGCUCAAAAtt

3.1.10. Transfection reagents

Table 3.1.10. List of transfection reagents used in the PhD project

Name	Source	Cat. No.
Lipofectamine RNAiMAX	Thermo Fisher Scientific	13778150
Lipofectamine 2000	Thermo Fisher Scientific	11668019

3.1.11. Primers

Table 3.1.11. List of RT-qPCR primers used in the PhD project

Name of gene	Forward primer	Reverse primer
<i>GAPDH</i>	CATGTTCGTCATGGGTGTGAACCA	GTGATGGCATGGACTGTGGTCAT
<i>MCOLN1</i>	GAGTGGGTGCGACAAGTTTC	TGTTCCTCTCCCGGAATGTC
<i>NPC1</i>	GGGCAGCTCCGTGTTTCAG	ACTTTTGGCTTTATTTACTGATGGC
<i>TFE3</i>	TGTTTCGTGCTGTTGGAGGAG	TCCTGGAGCCCCCTTGAG
<i>TFEB</i>	GCAACAGTGCTCCCAATAG	TCAGGATTGATGTAGCCAAG
<i>TSG101</i>	CCTCCCAATCCCAGTGGTTACCCA	GGTGTCTCTCGCTGATTGTGCCA
<i>VPS28</i>	AGCCGTCCAGGTCTCAGTGC	AGCCGTCCAGGTCTCAGTGC

3.1.12. Commonly used buffers and solutions

Table 3.1.12. List of buffers and solution used in the PhD project

Name	Composition
Phosphate buffered saline (PBS)	0.13 M NaCl, 2.7 mM KCl, 4.2 mM Na ₂ HPO ₄ , 1.4 mM KH ₂ PO ₄ , pH 7.4
PBST	0.1% Tween-20 in PBS
Laemmli buffer	50 mM Tris pH 6.8, 100 mM DTT, 2% SDS, 10% glycerol, 0.05% bromophenol blue
RIPA lysis buffer	1% Triton X-100, 0.5% sodium deoxycholate, 0.1% SDS, 50 mM Tris (pH 8), 150 mM NaCl, 0.5 mM EDTA
CLAAP	0.6 µg/ml chymostatin, 0.5 µg/ml leupeptin, 10 µg/ml antipain, 2 µg/ml aprotinin, 0.7 µg/ml pepstatin, 10 µg/ml APMSF

Running buffer	25 mM Tris pH 8.5, 0.19 M glycine, 1% SDS
Transfer buffer	20 mM Tris pH 8.3, 0.15 M glycine, 10% methanol
Ponceau S solution	0.1% Ponceau S, 1% acetic acid
Blocking buffer	5% non-fat dry milk in washing buffer
Paraformaldehyde (PFA)	3.6% paraformaldehyde, 0.12 mM CaCl ₂ , 0.12 mM MgCl ₂ in PBS
Saponin solution I	0.1% saponin, 0.2% gelatin, 5 mg/ml BSA in PBS
Saponin solution II	0.01% saponin, 0.2% gelatin in PBS
TAE buffer	40 mM Tris, 20 mM acetic acid, 1 mM EDTA
2x HBS buffer	280 mM NaCl, 50 mM HEPES, 1.5 mM Na ₂ HPO ₄ , 10 mM KCl, 12 mM sucrose, pH 7.5
TF1	10 mM MES pH 5.8, 45 mM MnCl ₂ , 10 mM CaCl ₂ , 100 mM RbCl
TF2	10 mM PIPES pH 6.5, 50 mM CaCl ₂ , 10 mM RbCl, 15% glycerol

3.1.13. Commercial assay kits

Table 3.1.13. List of commercial assay kits used in the PhD project

Name	Source	Cat. No.
Clarity Western ECL Substrate	Bio-Rad	1705061
Gel Extraction Kit NucleoBond Xtra Midi EF	Mecherey-Nagel	740422.50
High Pure RNA Isolation Kit	Roche Diagnostics	11828665001
KAPA SYBR FAST qPCR Master Mix (2X) Universal Kit	KapaBiosystem	KK4618
Pierce BCA Protein Assay	Thermo Fisher Scientific	23225
QIAquick Gel Extraction Kit	Syngen	SY103000

3.1.14. Other reagents

Table 3.1.14. List of other reagents used in the PhD project

Name	Source	Cat. No.
Bovine serum albumin (BSA)	BioShop	ALB001
DAPI	Sigma-Aldrich	D9542
Dimethyl sulfoxide (DMSO)	BioShop	DMS666.100
dNTP mix	Thermo Fisher Scientific	R0193
DRAQ7	Thermo Fisher Scientific	D15106
Filipin III from <i>Streptomyces filipinensis</i> (Filipin)	Sigma-Aldrich	F4767
Hoechst 33342 (Hoechst)	Thermo Fisher Scientific	62249

LysoTracker Red DND-99 (LysoTracker)	Thermo Fisher Scientific	L7528
M-MLV Reverse Transcriptase	Sigma-Aldrich	M1302
NEBuffer™ 2.1	NEB	B7202
Oligo(dT) ₂₃ , Anchored	Sigma-Aldrich	O4387
Opti-MEM	Sigma-Aldrich	11058021
PageRuler Prestained Protein Ladder	Thermo Fisher Scientific	26617
Pepstatin A conjugated to BODIPY FL	Thermo Fisher Scientific	P12271
Phosphatase inhibitor cocktail 2 (PIC2)	Sigma-Aldrich	P5726
Phosphatase inhibitor cocktail 3 (PIC3)	Sigma-Aldrich	P0044
Phusion™ High-Fidelity DNA Polymerase	Thermo Fisher Scientific	F530L
Phusion HF reaction buffer	Thermo Fisher Scientific	F518L
R buffer	Thermo Fisher Scientific	BR5
Random Nonamers	Sigma-Aldrich	R7647
Restriction enzyme BamHI	Thermo Fisher Scientific	ER0051
Restriction enzyme MluI	Thermo Fisher Scientific	ER0561
Restriction enzyme XbaI	Thermo Fisher Scientific	ER0681
Restriction enzyme XhoI	Thermo Fisher Scientific	ER0691
T4 DNA polymerase	NEB	M0203S
Tango buffer	Thermo Fisher Scientific	BY5
Trypan blue	NanoEntek	EVS-050

3.2. Methods

3.2.1. Cell culture

RKO and RKO-GFP-MCOLN1 cells were maintained in EMEM medium supplemented with 10% FBS (full medium), whereas DLD-1 and HEK293T were maintained in DMEM medium supplemented with 10% FBS and 2 mM L-glutamine. All cell lines were cultured in P100 dishes in an incubator with 5% CO₂ at 37°C. At 70-80% confluency, cells were washed with PBS, detached from the dish surface by incubation with trypsin, diluted 1:8 or 1:16 and plated in a new dish. Cells were not passaged more than 10 times.

For freezing, cells were trypsinized and suspended in culture medium. Upon centrifugation at 200 g for 5 minutes, cell pellet was resuspended in culture medium supplemented with 10% dimethyl sulfoxide (DMSO) and 40% of fetal bovine serum (FBS), and transferred to cryotubes. After slow freezing at -80°C, the cryotubes were stored in liquid nitrogen.

To thaw a new batch, cells were quickly thawed in a water bath and transferred to a pre-warmed culture medium. In order to remove DMSO from the medium, cell suspension was centrifuged at 200 g for 5 minutes. Cell pellet was resuspended in fresh medium and plated in a new dish.

3.2.2. Cell treatment

LysoTracker dye was used for 30 minutes to stain lysosomes in RKO and DLD-1 cells at 50 nM concentration for live cell imaging or 500 nM concentration for fixed cell imaging. To chelate the intracellular pool of Ca²⁺, RKO cells were treated with 10 μM BAPTA-AM (BAPTA) for 2 h. In order to inhibit the activity of calcineurin (CaN) or MCOLN1 in RKO cells, Cyclosporin A (CsA) or ML-SI1 were applied, respectively, for 2 h, both at 25 μM concentration. To inhibit lysosomal function, RKO cells were treated with 50 nM bafilomycin A1 (BafA1) for 18 h. To deprive RKO cells of exogenous lipids, cells were incubated in EMEM medium supplemented with delipidated FBS for 40 h. EBSS medium was used for 2 h to deplete RKO cells of nutrients.

3.2.3. Cell transfection with siRNA using Lipofectamine RNAiMAX

Before transfection, cells were seeded at the concentrations indicated in Table 3.2.1. To this end, 12 μl of cell suspension was mixed with 12 μl of trypan blue. Cell density was analyzed using EVETM Automated Cell Counter (NanoEntek).

Table 3.2.1. Seeding concentrations of the indicated cell lines

Seeding concentrations		type of experiment; plate format
RKO, RKO-GFP-MCOLN1	DLD-1	
0.8×10^5 cells/well	0.8×10^5 cells/well	western blotting; 6-well plate
0.8×10^5 cells/well	-	quantitative real-time PCR; 6-well plate
0.9×10^6 cells/dish	0.9×10^6 cells/dish	cellular fractionation; P100 dish
0.25 or 0.4×10^3 cells/well	0.2×10^3 cells/well	immunofluorescence; 96-well Grainer Bio-One plate (additionally covered with 0.2% gelatin before seeding of RKO and RKO-GFP-MCOLN1 cells)

24 h after seeding, cells were transfected with siRNAs using Lipofectamine RNAiMAX transfection reagent according to the manufacturer's protocol. Ambion Silencer Select siRNAs (listed in Table 3.1.9) were used at the final concentration of 30 nM in experiments with single gene knockdowns. In experiments with simultaneous knockdown of three genes, each siRNA was used at a concentration of 20 nM and when necessary total siRNA concentration was adjusted to 60 nM with siCtrl#1. The siRNAs were diluted in Opti-MEM and mixed with Lipofectamine RNAiMAX diluted in Opti-MEM as described in Table 3.2.2. siRNAs and Lipofectamine RNAiMAX were incubated together for 20 minutes at room temperature to form complexes and added to cells. In each experiment, non-targeting siRNA (siCtrl #1 and/or #2) and/or mock (no siRNA in transfection mixture) controls were used. After 48 or 72 h cells were further analyzed.

Table 3.2.2. Transfection mixes with Lipofectamine RNAiMAX

Reagents per dish/well:	Plate format		
	P100 dish	6-well plate	96-well plate
30 nM siRNA	15 μ l	3 μ l	0.15 μ l/
20 nM siRNA	-	2 μ l	-
Opti-MEM for siRNA dilution	1000 μ l	200 μ l	10 μ l
Lipofectamine RNAiMAX	20 μ l	4 μ l	0.2 μ l
Opti-MEM for Lipofectamine RNAiMAX dilution	1000 μ l	200 μ l	10 μ l
Total volume added per dish/well	2000 μ l	400 μ l	20 μ l

3.2.4. Cell transfection with plasmids

24 h post transfection with siRNA (described in Table 3.2.2), RKO cells were transfected with plasmids using Lipofectamine 2000 transfection reagent according the manufacturer's protocol. First, HA-GST-RagC constructs were diluted in Opti-MEM and gently mixed with Lipofectamine 2000 diluted in Opti-MEM as described in the Table 3.2.3. After 5 minutes of incubation, transfection mixture was added to cells. To prevent a loss of cell viability due to Lipofectamine 2000 reagent, 5 h post transfection with plasmids, medium was exchanged into fresh EMEM medium.

Table 3.2.3. Transfection mixes with Lipofectamine 2000

Reagents per well:	Plate format	
	6-well plate	96-well plate
plasmid (stock: 1 µg/µl)	5 µl	0.1 µl
Opti-MEM for plasmid dilution	100 µl	4.9 µl
Lipofectamine 2000	20 µl	0.6 µl
Opti-MEM for Lipofectamine 2000 dilution	80 µl	4.4 µl
Total volume added per well	200 µl	10 µl

3.2.5. Preparation of chemically competent bacteria

Cells from a single colony of Stbl3 *E. coli* strain were transferred to 10 ml of LB medium using a 10 µl pipette tip. Bacteria were grown overnight at 37 °C at 180 rpm in STUART orbital incubator (SI500). The next day, the bacteria culture was added to 1000 ml of LB medium and grown until reaching the optical density between 0.3 and 0.5 (measured at 600 nm). Subsequently, bacteria were transferred on ice for 10 minutes and centrifuged at 1500 g for 10 minutes at 4 °C. The pellet was suspended in 100 ml of cold TF1 buffer and incubated on ice for 5 minutes. Then, bacteria were again pelleted by centrifugation as described above and resuspended in 20 ml of TF2 buffer. After 20 minute incubation on ice, competent bacteria were immediately frozen on dry ice as 50 µl aliquots and stored at -80 °C.

3.2.6. Bacteria transformation

Chemically competent Stbl3 bacteria were thawed on ice for 10 minutes. Next, 2 µl of SLIC reaction mixture (described in 3.2.7.1) was added to 50 µl of competent bacteria, gently mixed and incubated on ice for 20 minutes. Then, cells were transferred to 42 °C for 45 seconds (heat shock) and placed back on ice for 2 minutes. After that, 900 µl of warm LB medium was added and bacteria were grown for 1 h at 37 °C at 180 rpm in STUART orbital incubator (SI500). Finally,

bacteria were spread on agar plates with LB medium supplemented with 100 µg/ml ampicillin and incubated overnight at 37 °C.

3.2.7. Generation of GFP-MCOLN1 RKO cell line by lentiviral transduction

3.2.7.1. Generation of a plasmid encoding GFP-MCOLN1 for lentiviral transduction using the SLIC method

In order to generate a construct for the lentiviral transduction, the DNA sequence of human MCOLN1 was amplified by polymerase chain reaction (PCR). Reaction mix contained the following reagents (per reaction): 1 U of Phusion™ High-Fidelity DNA Polymerase, 10 µl of HF reaction buffer (5x concentrated), 200 µM of each dNTP, 10 ng of DNA template (mucolipin1-pEGFP C3), 0.5 µM of each primer (forward and reverse), and was filled with H₂O up to 50 µl. The primers were designed to have overhangs (red), which enabled subcloning of MCOLN1 sequence into XbaI and BamHI digestion sites of the pLenti-CMV-MCS-GFP-SV vector using the sequence- and ligation-independent cloning (SLIC) [273]. The primer sequences were:

Forward primer: 5'- **GACACCGACTCTAGA**ATGGTGAGCAAGGGCGAGGAGC -3'

Reverse primer: 5'- **AACTAGTCCGGATCCT**CAATTCACCAGCAGCGAATGC -3'

The pLenti-CMV-MCS-GFP-SV vector was digested with XbaI and BamHI restriction enzymes. The reaction mix contained 500 µg of pLenti-CMV-MCS-GFP-SV vector, 5 µl of Tango buffer (10x concentrated), 0.5 µl of XhoI, 0.5 µl of BamHI and H₂O (to final volume of 50 µl). The reaction was incubated for 1 h at 37 °C. Subsequently, the sizes of DNA fragment amplified by PCR and a linearized vector were assessed by DNA electrophoresis in 0.6% agarose gel. After electrophoresis, the insert and the vector were purified using Gel Extraction Kit according to the manufacturer's protocol.

For SLIC cloning (Fig. 3.1), the amplified DNA fragment and the linearized pLenti-CMV-MCS-GFP-SV vector were mixed in 2:1 molar ratio as recommended by Jeong et al. [273]. Next, NEBuffer 2.1 (10x concentrated), 0.2 µl of T4 DNA polymerase and H₂O were added (final volume of 10 µl per reaction). The reaction mix was incubated at room temperature for 2.5 minutes followed by 10 minute incubation on ice. Subsequently, chemically competent bacteria of the Stb13 *E. coli* strain were transformed with the reaction mix and seeded on LB agar plates supplemented with 100 µg/ml ampicillin (as described in 3.2.5). Plates were incubated overnight at 37 °C.

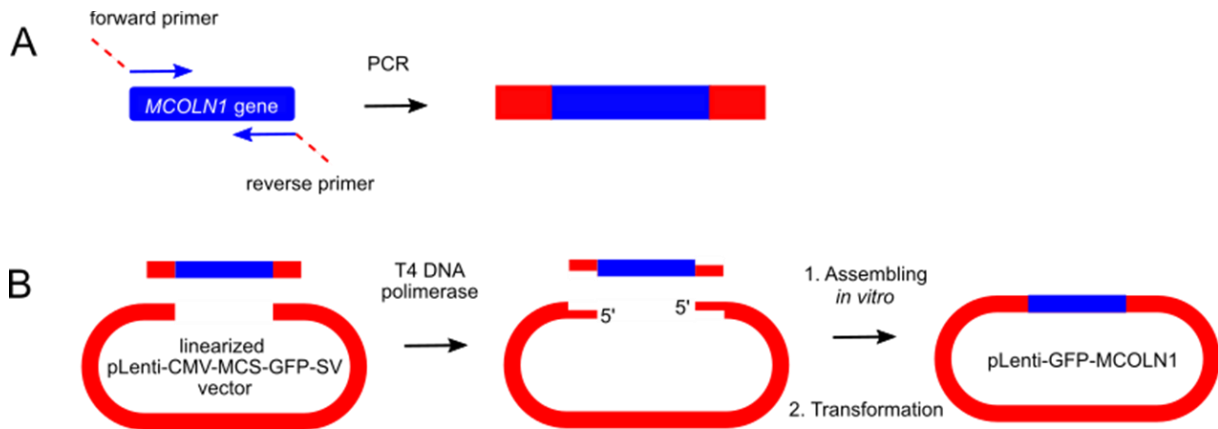


Figure 3.1. Schematic representation of the SLIC cloning method. (A) PCR using primers with overhangs (red) was applied to create an insert with ~15 bp of homology to the vector at each end. (B) Linearized vector and amplified DNA insert were incubated with T4 DNA polymerase to generate single-stranded DNA overhangs. Competent bacteria were transformed to produce the desired plasmid.

Next, bacteria from selected colonies were grown in 100 ml of LB supplemented with 100 $\mu\text{g/ml}$ ampicillin overnight at 37 $^{\circ}\text{C}$, at 180 rpm in STUART orbital incubator (SI500). Plasmid DNA was isolated with NucleoBond Xtra Midi EF kit and its concentration was measured using spectrophotometer (NanoDrop 8000, Thermo Fisher Scientific). To verify the efficiency of SLIC cloning, the isolated plasmids were double digested for 30 minutes at 37 $^{\circ}\text{C}$ with XhoI and MluI restriction enzymes, which recognize restriction sites in the MCOLN1 insert and pLenti-CMV-MCS-GFP-SV backbone, respectively. Reaction mix contained the following reagents (per reaction): 500 ng of pLenti-GFP-MCOLN1 plasmid, 3 μl R buffer (10x concentrated), 0.2 μl XhoI, 0.2 μl MluI and H₂O (final volume of 30 μl). Subcloning efficiency was assessed via DNA electrophoresis in agarose gel (Fig. 3.2). To this end, DNA constructs were mixed with 6x DNA Loading Dye (Thermo Fisher Scientific) and loaded onto 0.6% agarose gel with 2 $\mu\text{g/ml}$ ethidium bromide. DNA electrophoresis was performed at 80 V in TAE buffer and DNA bands were visualized using UV transilluminator. The presence of the cloned sequence was confirmed by DNA sequencing (Genomed Warsaw).

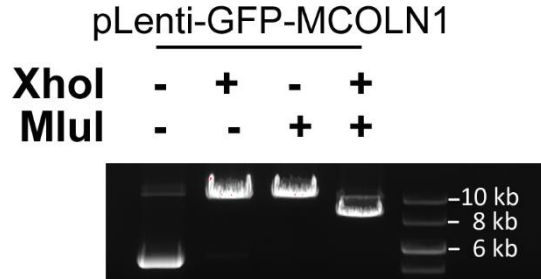


Figure 3.2. Image of 0.6% agarose gel showing DNA separation of pLenti-GFP-MCOLN1 plasmid (10.2 kb band) upon double digestion with XhoI and MluI enzymes that resulted in the formation of 8.4 kb and 1.8 kb digestion products (the latter not shown on the image).

3.2.7.2. Production of lentiviruses and infection of RKO cells

In order to produce lentiviral particles to transduce RKO cells, 1×10^6 HEK293T cells were seeded on P100 dish. The next day, 500 μ l mix of pLenti-GFP-MCOLN1 plasmid (20 μ g), pMD2G (5 μ g) and psPAX2 (15 μ g) packaging plasmids and CaCl₂ (250 mM) was added drop-wise to 500 μ l of 2x HBS. After 20 minute incubation at room temperature, 1000 μ l of mixture was added to HEK293T cells. The next day, medium was exchanged into 5.5 ml fresh EMEM medium to concentrate the virus. 48 h post transfection the medium containing the produced virus was collected, filtered through 0.45 μ m filters and used for infection of RKO cells.

The day before lentiviral infection, RKO cells were plated on P60 dish (3×10^5 cells/dish). For transduction, the medium was exchanged to 2.5 ml of EMEM and 2.5 ml of filtered virus-containing EMEM medium (total volume 5 ml). The following day, RKO cells were trypsinized and suspended in fresh EMEM medium supplemented with puromycin (final concentration 1 μ g/ml) for selection of infected cells and plated on P100 dish. After 48 h cells were split and expression of recombinant GFP-MCOLN1 protein was verified by western blotting and immunofluorescence staining.

3.2.8. Western blotting (WB)

For protein analysis, cells were transferred to ice, washed with cold PBS and lysed in RIPA buffer, supplemented with CLAAP (1:500) and PIC2 and 3 (1:100) for 20 minutes on ice. After that, lysates were centrifuged at 15000 g for 15 minutes at 4 °C and supernatants were collected. To determine protein concentration, Pierce BCA Protein Assay was performed according to the manufacturer's protocol. After adjusting protein concentration and adding 5x Laemmli buffer, samples were denatured by 10 minute incubation at 95 °C. Before protein separation, samples were

stored at -20 °C. Electrophoretic separation of proteins was conducted under denaturing conditions (SDS-PAGE). 15-25 µg of total protein per sample and PageRuler Prestained Protein Ladder (molecular weight marker) were loaded on 8-14% polyacrylamide gels and resolved in running buffer at 60 V using the BioRad system. After entering of samples into the resolving gel, the voltage was increased to 120 V. Subsequently, proteins were transferred onto nitrocellulose membrane (GE Healthcare) in transfer buffer at 250 mA for 1.5 h at 4 °C. The transfer quality was evaluated by staining of membranes with Ponceau S solution. Then, membranes were blocked in 5% milk in PBST for 1 h at room temperature. After three 5-minute washes in PBST, the membranes were incubated overnight at 4 °C with primary antibodies diluted in 5% bovine serum albumin (BSA) (as listed in 3.1.3). The following day, membranes were washed three times for 5 minutes in PBST and incubated with secondary HRP-conjugated antibodies diluted in 5% milk in PBST for 1 h at room temperature (as listed in 3.1.4). Then, membranes were washed three times for 5 minutes with PBST and incubated with Clarity Western ECL substrate for 5 minutes. To detect the proteins of interest, ChemiDoc Touch Imaging System (BioRad) was applied. The acquired images were assembled in Photoshop (Adobe) with only linear adjustments of brightness and contrast. Densitometric analysis of detected bands was performed using BioRad Image Lab Software. Vinculin, GAPDH and H3 bands were used as loading controls.

3.2.9. Cell fractionation

Cellular fractionation was carried out as described by Suzuki et al. [274]. First, cells were transferred to ice, washed with cold PBS and scrapped using cell scraper. Next, cells were collected in 1.5-ml Eppendorf tubes and centrifuged at 1.7×10^3 g for 10 seconds. Pellets were resuspended in 900 µl of cold 0.1% NP40 in PBS. After that, 300 µl samples of whole cell lysates (W) were collected in new tubes where they were mixed with 100 µl of 4x Laemmli sample buffer and kept for further analysis. The remaining lysates were centrifuged at 1.2×10^4 g for 10 seconds. The obtained pellets of cell nuclei were washed in 1000 µl of cold 0.1% NP40 in PBS and centrifuged at 1.2×10^4 g for 10 seconds. Pellets were collected as nuclear fraction (N) and resuspended in 180 µl of 1x Laemmli sample buffer. Both W and N samples were sonicated, boiled for 1 minute at 95°C and analyzed by western blotting.

3.2.10. Immunofluorescence and imaging

3.2.10.1. Lysosomal imaging

For live cell imaging, cells were incubated with 50 nM LysoTracker dye to visualize lysosomes [275] and Hoechst stain to mark cell nuclei. Cells were protected from light and kept in an incubator with 5% CO₂ at 37°C for 30 minutes. After this time, cells were washed with probe-free medium and imaged immediately using Opera Phenix microscope (as described in 3.2.10.3).

For fixed cell imaging, cells were incubated with 500 nM LysoTracker dye for 30 minutes in an incubator with 5% CO₂ at 37°C. Then, cells were washed twice with cold PBS and fixed with 3.6% paraformaldehyde followed by immunostaining (as described in 3.2.10.2). During the whole procedure, cells were protected from light.

3.2.10.2. Immunofluorescence staining (IF)

Cells seeded on 96-well plates (655-090; Grainer Bio-One) were washed twice with 100 µl/well cold PBS and fixed with 3.6% paraformaldehyde for 15 minutes at room temperature. After washing three times for 5 minutes with 100 µl/well PBS, cells were incubated for 10 minutes with 100 µl/well of saponin solution I to permeabilize the PM. Next, cells were incubated for 1.5 h with 30 µl/well of primary antibodies (listed in Table 3.1.3) diluted in saponin solution II. After washing two times for 5 minutes with 100 µl/well of saponin solution II, cells were incubated for 30 minutes with secondary antibodies (1:500; Table 3.1.4) and DAPI (1:1000) diluted in saponin solution II. Then, cells were washed three times for 5 minutes with 100 µl/well PBS and imaged using Opera Phenix microscope.

In order to visualize intracellular cholesterol, after fixation with 3.6% paraformaldehyde and washing with PBS (as described above), cells were incubated for 2 h at 37°C with 40 µl/well of 10% FBS containing 50 µg/ml filipin and primary antibodies (as listed in Table 3.1.3.). After washing two times for 5 minutes with 100 µl/well PBS, cells were incubated for 30 minutes at room temperature with 30 µl/well of 5% FBS with secondary antibodies (1:500; Table 3.1.4) and DRAQ7 dye (1:200). Then, cells were again washed three times for 5 minutes with 100 µl/well PBS and imaged using Opera Phenix microscope.

3.2.10.3. Imaging using Opera Phenix automated confocal microscope

Cells were imaged using automated Opera Phenix high-content screening confocal microscope (PerkinElmer). To scan the plates, 40 x 1.1 NA water immersion objective was applied. At least 10 microscopic fields were scanned per each experimental condition. Z-stacks were acquired with 1 μm interval.

3.2.10.4. Quantitative image analysis using Harmony software

For quantitative analysis of confocal images, Harmony 4.9 software was applied. Maximum intensity projection images from at least 10 microscopic fields were applied for statistical analysis per each experimental condition.

First, images were segmented into the nucleus and the cytoplasm, using the “find nuclei” and “find cytoplasm” building blocks. Background signal for each channel was removed by the “sliding parabola” function. Next, objects corresponding to late endosomes and/or lysosomes were detected based on detection of LAMP1 protein and/or fluorescent LysoTracker dye using the “find spot” building block. Afterwards, other objects were identified based on detection signals of additional proteins (cathepsin D, ubiquitin, GFP-MCOLN1, mTOR) or cholesterol. Then, parameters of the indicated objects, such as mean area of vesicular structures expressed in μm^2 , fluorescence intensity per structure expressed in arbitrary units or colocalization expressed as Pearson’s correlation coefficient were calculated.

To calculate percentage of cells with nuclear staining, images were segmented into the nucleus and the cytoplasm, and background signal was removed (as described above). Next, fluorescence intensity of TFEB or TFE3 detection in the nuclei mask was calculated. Using this parameter, cells were considered as positive or negative in terms of the nuclear presence of TFEB or TFE3 transcription factors. Fraction of positive cells among all cells in the analyzed populations was expressed as percentage.

In order to calculate percentage of cells with nuclear staining of cells overexpressing RagC (WT or S75L), images were segmented into the nucleus and the cytoplasm, and background signal was removed (as described above). Next, cells with the detected HA tag were chosen for further analysis using the “select population” building block. Only this subpopulation was used to calculate percentage of cells with nuclear staining (as described above).

Representative images from Harmony 4.9 software were exported as jpg files and assembled in ImageJ software and Photoshop (Adobe) with only linear adjustments of brightness and contrast.

3.2.11. Quantitative real time PCR (RT-qPCR)

To perform quantitative real time PCR (RT-qPCR), total RNA was isolated using High Pure RNA Isolation Kit according to the manufacturer's protocol. The concentration of RNA and purity of the samples were assessed using spectrophotometer (NanoDrop 8000, Thermo Fisher Scientific). For cDNA synthesis, 1 µg of isolated RNA was diluted in nuclease-free H₂O up to 10 µl and incubated with 1 µl of mix of random nonamers (50 µM), 1 µl of oligo(dT)23 (70 µM) and 1 µl of dNTPs (10 mM) for 10 minutes at 70°C. After denaturation, mixes were cooled down on ice and incubated with 2 µl of M-MLV reverse transcriptase buffer, 1 µl M-MLV reverse transcriptase and 4 µl of nuclease-free H₂O (final volume of 20 µl) for 10 minutes at room temperature, followed by 50 minute incubation at 37°C. The reaction of reverse transcription was stopped by 10 minute incubation at 90 °C. Samples were diluted five times in nuclease-free H₂O (final volume 100 µl).

cDNA sample amplification was performed with KAPA SYBR FAST qPCR Master Kit according to the manufacturer's protocol using a 7900HT fast real-time PCR thermocycler (Applied Biosystems). Each experimental condition was performed in two technical repeats. The primers used for RT-qPCR are listed in Table 3.1.11. The obtained data were quantified using Expression Suite v1.2 Software (Thermo Fisher Scientific). Expression of analyzed target genes was normalized to the expression level of *GAPDH* housekeeping gene and presented as a fold change.

3.2.12. Analysis of transcriptome by RNA sequencing

Sequencing of RNA was performed in Department of Genetics in Maria Skłodowska-Curie National Research Institute of Oncology, Warsaw. 72 h post transfection with siRNAs pellets of RKO cells were collected. Ion AmpliSeq Transcriptome Human Gene Expression Panel (Thermo Fisher Scientific) was applied to generate sequencing library. Ion PI Hi-Q Sequencing 200 Kit (Thermo Fisher Scientific) was used to sequence the samples using the Ion Proton instrument. Reads were aligned to the hg19 AmpliSeq transcriptome ERCC v1 using the Torrent Mapping Alignment Program (version 5.0.4; Thermo Fisher Scientific). Subsequently, the transcript quantification using HTseq-count (version 0.6.0) was performed. R package DESeq2 (version

1.18.1) [276] was applied to carry out analysis of differentially expressed genes whose expression exceeded more than 100 counts across conditions. The obtained counts were transformed to Z-scores using the transcript per million normalization method. Non-protein coding genes were excluded from the analysis. The gene expression levels were normalized against siCtrl#1-transfected patterns. The P-values were corrected for multiple testing using the Benjamini–Hochberg method, and genes with adjusted P-value < 0.05 and ≥ 1.5 -fold were considered significant. The list of differentially expressed genes (common for all on-target siRNAs) was subjected to Gene Ontology (GO) analysis of biological processes. The 0.6 cutoff function was applied to reduce the redundancy of GO terms. GO analysis and visualization was performed in R version 3.4.4 (<https://www.R-project.org>) by Dr. Krzysztof Kolmus (Laboratory of Cell Biology at IIMCB in Warsaw).

To identify any enrichment of transcription factor binding motifs among upregulated genes, the set of genes found as upregulated after Tsg101 or Vps28 depletion (≥ 1.5 -fold; adjusted P-value < 0.05) was subjected to RcisTarget analysis (Bioconductor) [277]. *Homo sapiens* parameter was set as the species of the input list of genes. The region of 5000 bp was selected to perform motif-based search upstream of the transcription start site. Only motifs with normalized enrichment score (NES) > 3 were considered as significant. The obtained transcription factor binding motifs were annotated to motifs recognized by transcription factors according to SwissRegulon database (<https://swissregulon.unibas.ch/sr/swissregulon>). RcisTarget analysis and visualization was performed in R version 4.0.3. (<https://www.R-project.org>).

RNA sequencing data are available in Gene Expression Omnibus under the accession number: GSE178665.

3.2.13. Statistical analysis

Each experiment was performed in at least three biological replicates (an exact number denoted as “n”), with the exception of experiments shown in Fig. 4.11 (n=1) and 4.12B (n=2). Statistical analysis was performed using the Prism 8.4.3 (GraphPad Software). Data were analyzed using the following tests: unpaired two-tailed *t* test (for qRT-PCR analysis, western blotting densitometry analysis and percentage of cells with nuclear staining based on confocal microscopy analysis) or paired two-tailed *t* test (for quantified parameters of confocal microscopy analysis such as mean structure area, fluorescence intensity and Pearson’s correlation coefficient). The significance of mean comparison is annotated as “ns”, non-significant ($P \geq 0.05$) or indicated with

exact P-value, *P < 0.05, **P < 0.01, ***P < 0.001, ****P < 0.0001. Results were considered as significant when P < 0.05.

4. Results

4.1. Characterization of lysosomal morphology upon ESCRT-I depletion

A recent study from the Laboratory of Cell Biology at IIMCB showed that ESCRT components are important for growth and intracellular signaling of colorectal cancer (CRC) cells [225], thus cell lines from this cancer type were chosen as a main experimental model applied for the purpose of this thesis. To address the involvement of ESCRT-I in lysosomal homeostasis, Tsg101 or Vps28 proteins were depleted in RKO or DLD-1 cells using two different siRNAs against each subunit. To obtain control cells, two different non-targeting siRNAs were used. Efficiency of Tsg101 or Vps28 depletion in RKO and DLD-1 cells was confirmed by western blotting (Fig. 4.1A-B). In both cell lines, depletion of one of the ESCRT-I core components, lead to reduced protein levels of the other component (Fig. 4.1A-B) which, according to previous studies, reflects destabilization of the whole complex [225, 278-280].

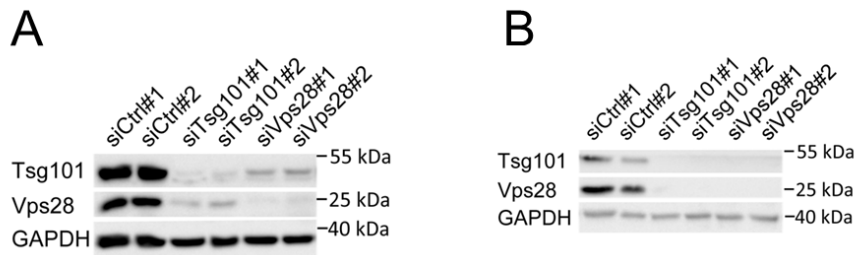


Figure 4.1. siRNA-mediated depletion of Tsg101 or Vps28 leads to deficiency of ESCRT-I in RKO and DLD-1 cells. Representative western blots showing depletion efficiencies of the indicated ESCRT-I subunits using two independent single siRNAs for each subunit, as compared to non-targeting control siRNAs (siCtrl#1 or #2) in RKO (A) or DLD-1 (B) cells 72 h post transfection. GAPDH was used as a loading control.

In order to test whether ESCRT-I deprivation could have any effect on lysosomal morphology, RKO cells were stained using antibodies recognizing LAMP1, a marker of late endosomes and lysosomes [2]. Intracellular distribution of LAMP1 upon ESCRT-I depletion was analyzed by confocal microscopy (Fig. 4.2A). Quantitative analysis of microscopy images revealed that depletion of Tsg101 or Vps28, in comparison to control cells, increased the area of LAMP1-positive structures (Fig. 4.2B), but did not affect their average fluorescence intensity (Fig. 4.2C). These results suggested that ESCRT-I deficiency affects the morphology of late endosomes and/or lysosomes.

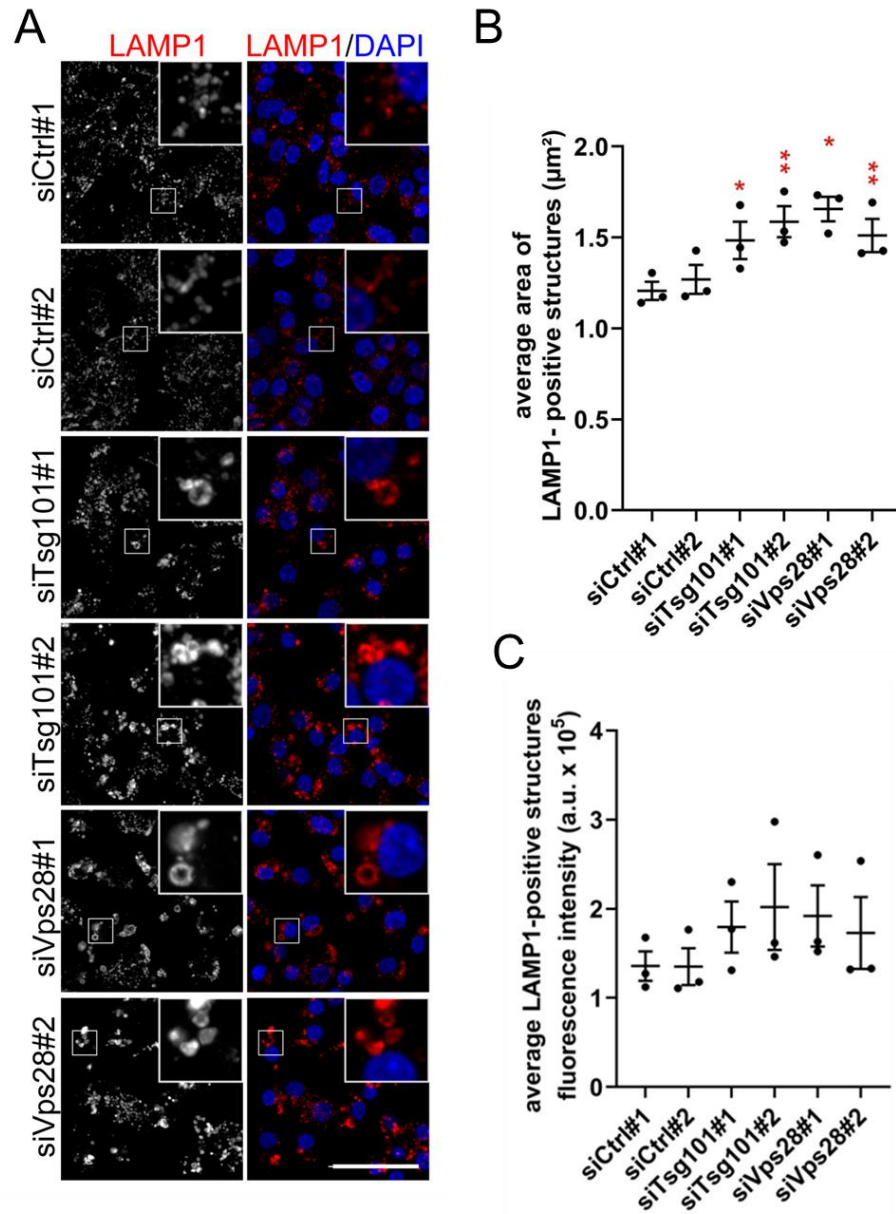


Figure 4.2. ESCRT-I depletion leads to enlargement of late endosomes and/or lysosomes in RKO cells. (A) Representative maximum intensity projection images from confocal microscopy of fixed cells showing the effect of ESCRT-I depletion on intracellular distribution of LAMP1 (red) 72 h post transfection. Two components of ESCRT-I, Tsg101 and Vps28 were depleted using two independent siRNAs each, siTsg101#1 or #2 and siVps28#1 or #2. Control cells were transfected with non-targeting siRNAs (siCtrl#1 or #2). Cell nuclei marked with DAPI stain (blue). Scale bar, 50 μm . (B-C) Quantitative analysis of microscopic images showing the average area (μm^2 in B) and average fluorescence intensity (arbitrary units, a.u. in C) of LAMP1-positive structures in control or ESCRT-I-depleted cells. Values derived from independent experiments (dots) and their means ($n=3 \pm$ SEM) are presented. Paired two-tailed t test to averaged values measured for siCtrl#1 and #2 cells was applied. * $P < 0.05$, ** $P < 0.01$.

To further elucidate the impact of ESCRT-I deficiency on the lysosomal compartment, the intracellular distribution of lysosomes was analyzed by confocal microscopy using LysoTracker (Fig. 4.3A). This cell-permeable fluorescent dye is commonly applied as a marker of non-damaged acidic lysosomes [198, 272, 281-284]. Observation of microscopic images and quantitative analysis of LysoTracker-positive structures revealed that knockdown of genes encoding Tsg101 or Vps28 led to enlargement of lysosomal area and increased LysoTracker fluorescence intensity per lysosome (Fig. 4.3A-C).

Next, to examine whether ESCRT-I-depletion affects lysosomal morphology also in another colorectal cancer cell line, the intracellular accumulation of LysoTracker dye was assessed in DLD-1 cells (Fig. 4.4A). Similarly as in the case of RKO cells, quantitative microscopic image analysis revealed that depletion of ESCRT-I subunits led to enlarged lysosomal area and LysoTracker fluorescence intensity per lysosome, as compared to control cells (Fig. 4.4B-C).

Because maintenance of low lysosomal pH observed as the strong LysoTracker incorporation upon depletion of ESCRT-I does not fully reflect lysosomal functionality, the lysosomal degradative capacity was tested. To this end, the intracellular distribution of a major lysosomal endopeptidase, cathepsin D, was analyzed by confocal microscopy using pepstatin A conjugated to BODIPY FL (Fig. 4.5A). Pepstatin A is an inhibitor of cathepsin D that binds to the active site of the enzyme and may be used to localize active cathepsin D in cells [285]. Using this tool, cathepsin D was detected in LAMP1-positive structures of both, control and ESCRT-I-depleted cells (Fig. 4.5A-B). The amount of lysosomal cathepsin D in cells lacking ESCRT-I was slightly increased (Fig. 4.5A-B), indicating that the delivery of this enzyme to the enlarged lysosomes was not impaired.

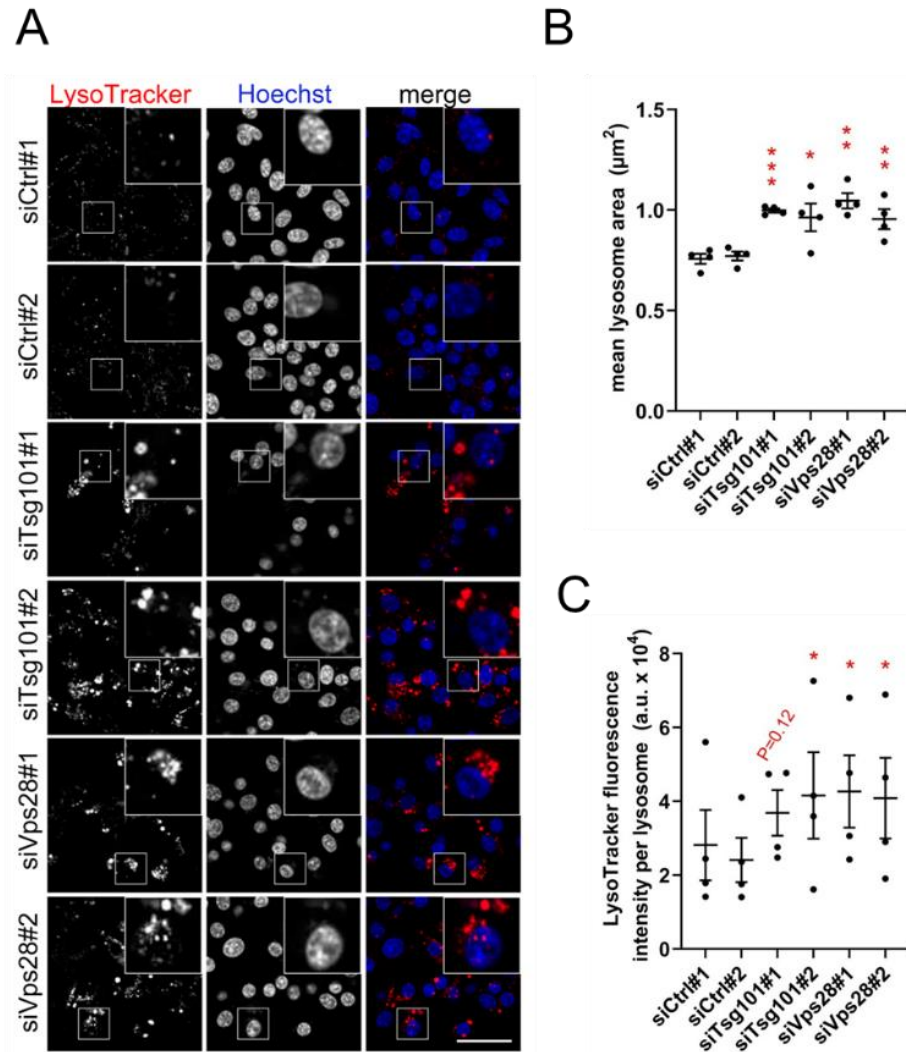


Figure 4.3. ESCRT-I depletion increases LysoTracker staining intensity and lysosomal area in RKO cells. (A) Representative maximum intensity projection images from confocal microscopy of live cells showing the effect of ESCRT-I depletion on intracellular distribution of lysosomes 72 h post transfection visualized upon 30 minute incubation with 50 nM LysoTracker dye (red). Two components of ESCRT-I, Tsg101 and Vps28 were depleted using two independent siRNAs each, siTsg101#1 or #2 and siVps28#1 or #2. Control cells were transfected with non-targeting siRNAs (siCtrl#1 or #2). Cell nuclei marked with Hoechst stain (blue). Scale bar, 50 μm . (B-C) Quantitative analysis of microscopic images showing the average area of detected lysosomal structures (μm^2 in B) and average fluorescence intensity of LysoTracker per lysosomal structure (arbitrary units, a.u. in C) in control or ESCRT-I-depleted cells. Values derived from independent experiments (dots) and their means ($n=4 \pm \text{SEM}$) are presented. Paired two-tailed t test to averaged values measured for control cells was applied. $P \geq 0.05$ was indicated with exact P -value, $*P < 0.05$, $**P < 0.01$, $***P < 0.001$.

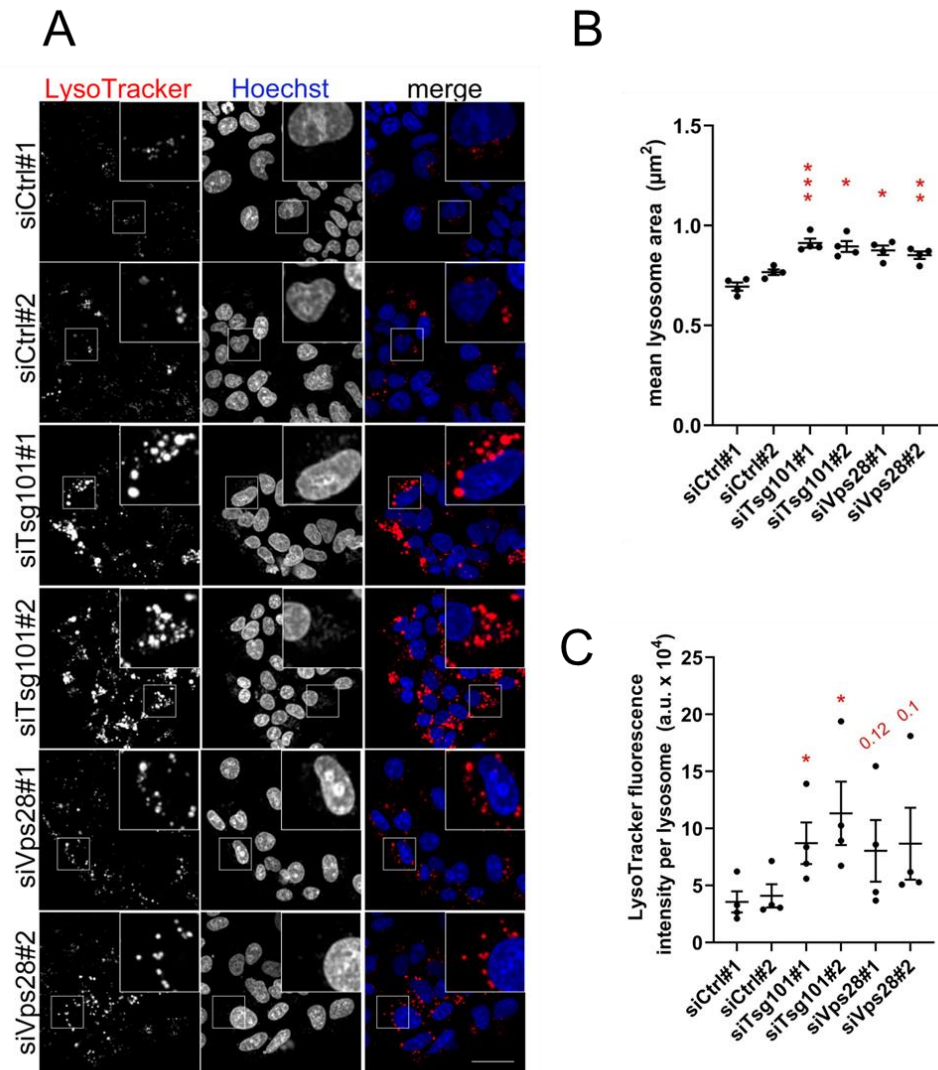


Figure 4.4. ESCRT-I depletion increases LysoTracker staining intensity and lysosomal area in DLD-1 cells. (A) Representative maximum intensity projection images from confocal microscopy of live cells showing the effect of ESCRT-I depletion on intracellular distribution of lysosomes 72 h post transfection visualized upon 30 minute incubation with 50 nM LysoTracker dye (red). Two components of ESCRT-I, Tsg101 and Vps28 were depleted using two independent siRNAs each, siTsg101#1 or #2 and siVps28#1 or #2. Control cells were transfected with non-targeting siRNAs (siCtrl#1 or #2). Cell nuclei marked with Hoechst stain (blue). Scale bar, 50 μm . (B-C) Quantitative analysis of microscopic images showing average area of detected lysosomal structures (μm^2 in B) and average fluorescence intensity of LysoTracker per lysosomal structure (arbitrary units, a.u. in C) in control or ESCRT-I-depleted cells. Values derived from independent experiments (dots) and their means ($n=4 \pm \text{SEM}$) are presented. Paired two-tailed t test to averaged values measured for control cells was applied. $P \geq 0.05$ was indicated with exact P -value, * $P < 0.05$, ** $P < 0.01$, *** $P < 0.001$.

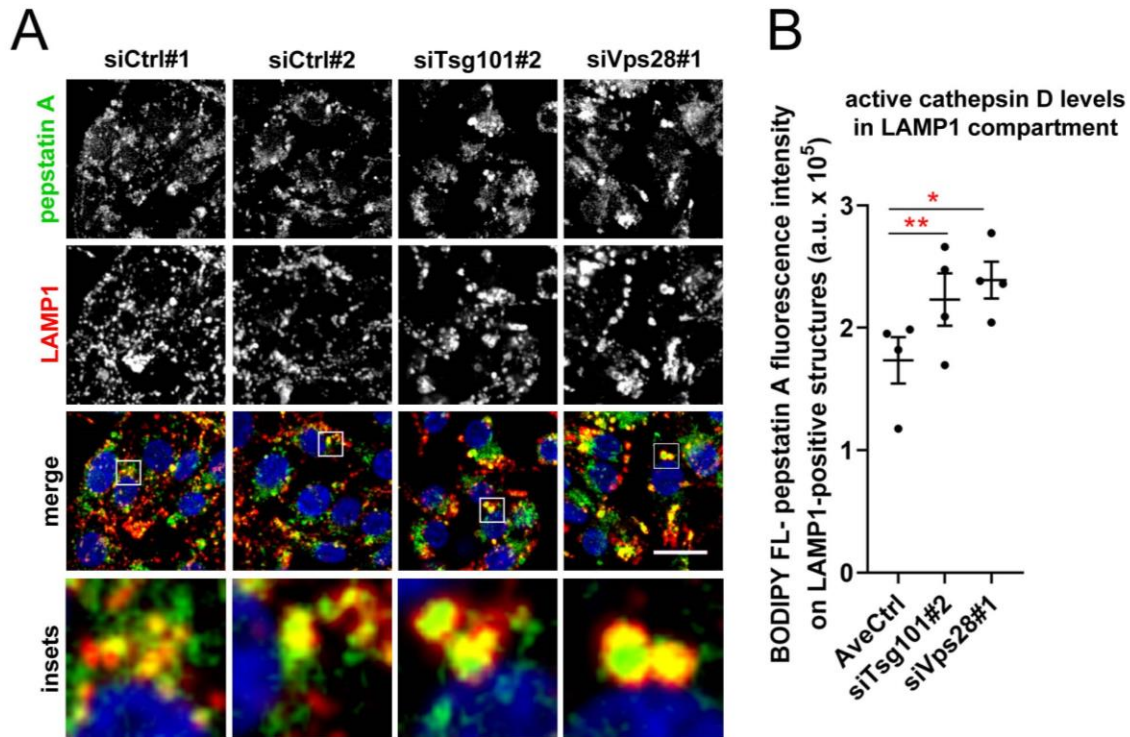


Figure 4.5. RKO cells lacking ESCRT-I contain high levels of cathepsin D in their late endosomes and/or lysosomes. (A) Representative maximum intensity projection images from confocal microscopy of fixed cells showing the effect of ESCRT-I depletion on intracellular distribution of cathepsin D detected using BODIPY FL-pepstatin A fluorescent probe (green) and LAMP1 (red) 72 h post transfection. Two components of ESCRT-I complex, Tsg101 and Vps28 were depleted using two independent siRNAs each, siTsg101#1 or #2 and siVps28#1 or #2. Control cells were transfected with non-targeting siRNAs (siCtrl#1 or #2). Cell nuclei marked with DAPI stain (blue). Scale bar, 20 μ m. (B) Quantitative analysis of microscopic images showing average fluorescence intensity of pepstatin A conjugated to BODIPY FL on LAMP1-positive structures (arbitrary units, a.u.) in control or ESCRT-I-depleted cells. Values derived from independent experiments (dots) and their means ($n=4 \pm$ SEM) are presented. Paired two-tailed t test to averaged values measured for control cells (AveCtrl) was applied. * $P < 0.05$, ** $P < 0.01$.

Cumulatively, the above presented results concerning the distribution of lysosomal markers confirmed that ESCRT-I restricts the size of lysosomes in CRC cell lines. They also showed that the lack of ESCRT-I does not impair the integrity, maintenance of low pH or degradative capacity of lysosomes, suggesting that lysosomes retain their functionality.

4.2. The role of ESCRT-I in degradation of lysosomal membrane proteins

Turnover of proteins present in lysosomal membranes relies on internalization of these proteins into the lysosomal lumen together with adjoining membrane parts [286]. To address whether enlargement of the lysosomal area in cells lacking ESCRT-I could be due to inhibited degradation of proteins from lysosomal surfaces, first, the amount of ubiquitinated proteins on lysosomes was analyzed by confocal microscopy. In control cells ubiquitinated proteins were barely detected on LysoTracker- and LAMP1-positive compartments, likely indicating their constitutive degradation, as described [200]. However, depletion of ESCRT-I led to massive accumulation of ubiquitinated proteins on lysosomal structures. The accumulated ubiquitin was particularly well observed at membranes of the enlarged lysosomes that were identified by LAMP1 detection (Fig. 4.6).

Next, to examine whether the lack of ESCRT-I inhibits degradation of lysosomal membrane proteins, a line of RKO cells stably expressing GFP-tagged MCOLN1 protein (GFP-MCOLN1) was generated. The presence of GFP-MCOLN1 in these cells was confirmed by western blotting (Fig. 4.7A). Depletion of Tsg101 or Vps28 proteins increased GFP-MCOLN1 protein levels as compared to control cells (Fig. 4.7A-B), suggesting that ESCRT-I mediates degradation of this lysosomal membrane protein.

To further study the involvement of ESCRT-I in turnover of lysosomal membrane proteins, the intracellular distribution of GFP-MCOLN1 was analyzed by confocal microscopy. In control cells, GFP-MCOLN1 was mainly observed on LAMP1-positive structures, both LysoTracker-negative (late endosomes) or LysoTracker-positive (lysosomes; Fig. 4.8A). Depletion of ESCRT-I subunits increased the intensity of GFP-MCOLN1 fluorescence on LAMP1-positive compartment (Fig. 4.8A) that was consistent with increased protein levels identified by western blotting (Fig. 4.7A-B). Noteworthy, GFP-MCOLN1 accumulation was observed on the enlarged lysosomal structures (Fig. 4.8A). Subsequently, to establish whether GFP-MCOLN1 accumulation occurred due to inhibited lysosomal degradation, the intracellular localization of this protein was analyzed in cells treated with bafilomycin A1 (BafA1) that inhibits function of lysosomes by raising their pH [32]. The efficacy of BafA1 treatment was manifested by the loss of LysoTracker staining (Fig. 4.8A). In control cells, BafA1 treatment increased the intensity of GFP-MCOLN1 fluorescence on LAMP1-positive structures to the levels comparable to those observed upon ESCRT-I knockdown only (Fig. 4.8A-B). Moreover, in BafA1-treated cells, depletion of ESCRT-

I did not significantly enhance the levels of GFP-MCOLN1 as compared to cells treated with control siRNAs (Fig. 4.8A-B). The above results showed that GFP-MCOLN1 undergoes constitutive lysosomal degradation that is mediated by ESCRT-I.

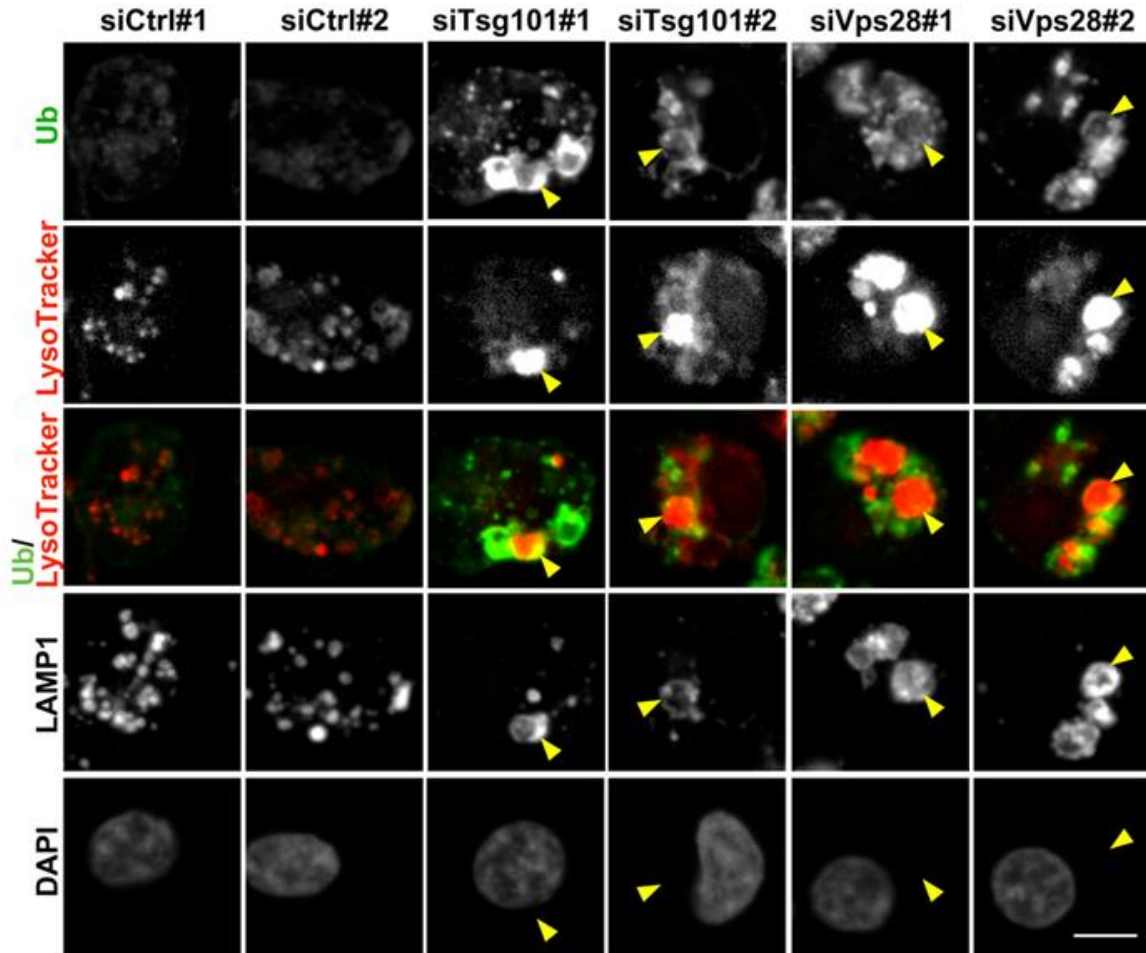


Figure 4.6. ESCRT-I depletion leads to intracellular accumulation of ubiquitin, observed also on lysosomes. Representative maximum intensity projection images from confocal microscopy of fixed RKO cells showing the effect of ESCRT-I depletion on intracellular distribution of mono- and polyubiquitinated protein conjugates (green), LAMP1 (gray) and LysoTracker dye (red) 72 h post transfection. Two components of ESCRT-I, Tsg101 and Vps28, were depleted using two independent siRNAs each, siTsg101#1 or #2 and siVps28#1 or #2. Control cells were transfected with non-targeting siRNAs (siCtrl#1 or #2). Enlarged LysoTracker-positive lysosomal structures enriched in ubiquitin and LAMP1 are indicated by arrowheads. Cell nuclei marked with DAPI stain (gray). Scale bar, 10 μ m.

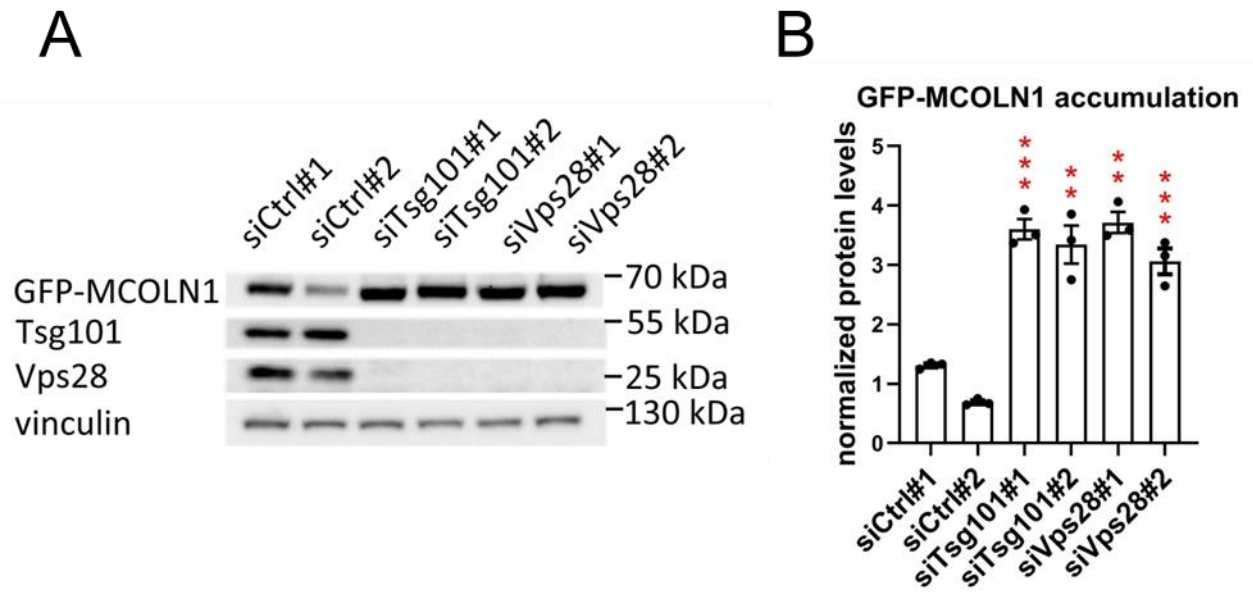


Figure 4.7. Depletion of ESCRT-I subunits leads to MCOLN1 protein accumulation. (A) Representative western blots showing the effect of ESCRT-I depletion on the levels of ectopically expressed GFP-tagged MCOLN1 protein in RKO cells with stable expression of this protein at 72 h post transfection with siRNAs. Two components of ESCRT-I, Tsg101 and Vps28, were depleted using two independent siRNAs each, siTsg101#1 or #2 and siVps28#1 or #2. Control cells were transfected with non-targeting siRNAs (siCtrl#1 or #2). Anti-GFP antibodies were used for immunoblotting of GFP-MCOLN1 protein. Vinculin was used as a loading control. (B) Densitometry analysis of western blotting bands showing the levels of ectopically expressed GFP-MCOLN1 protein in control or ESCRT-I-depleted cells presented as a fold change to averaged values measured for control cells. Dots indicate values derived from independent experiments. Bars represent the mean (n=3 +/- SEM). Unpaired two-tailed *t* test to siCtrl#1 was applied. **P<0.01, ***P<0.001.

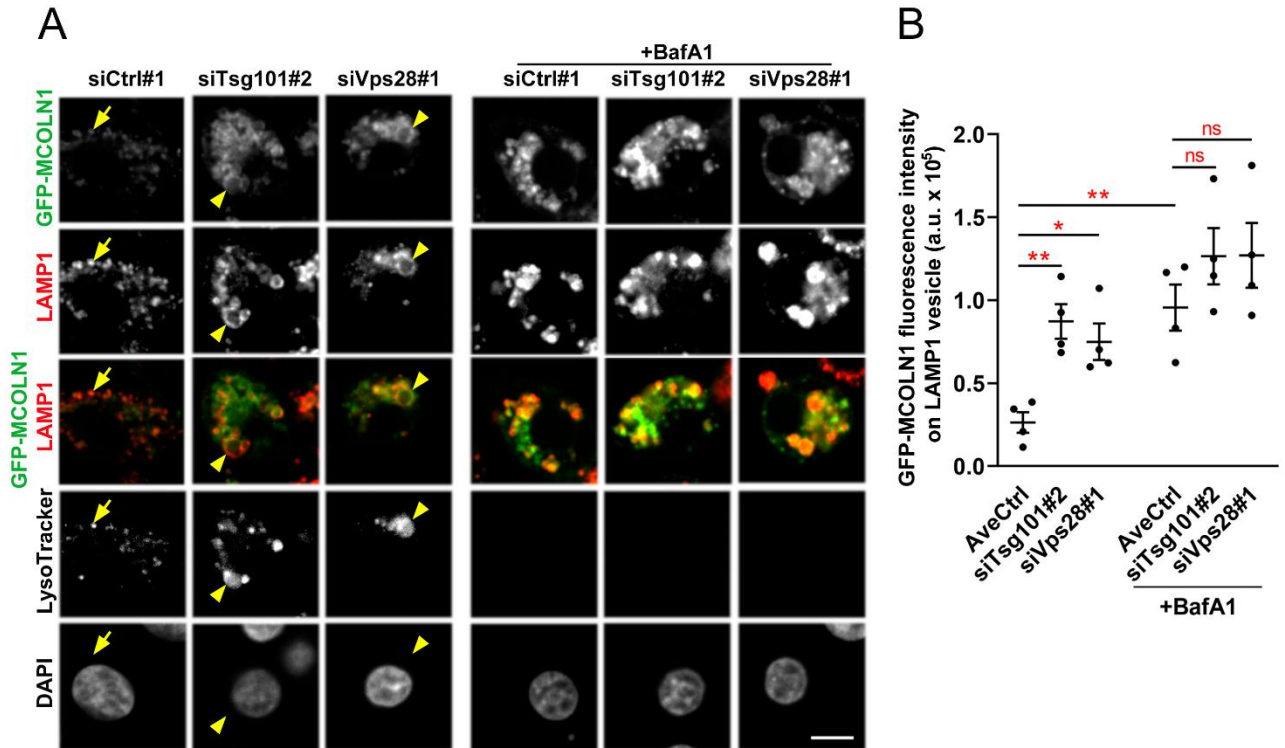


Figure 4.8. Depletion of ESCRT-I subunits leads to MCOLN1 protein accumulation on lysosomes due to its impaired lysosomal degradation. (A) Representative single plane images from confocal microscopy of fixed RKO cells showing the effect of ESCRT-I depletion and/or 18 h bafilomycin A1 treatment (BafA1) on intracellular distribution of ectopically expressed GFP-MCOLN1 (green), LAMP1 (red) and LysoTracker dye (gray) 72 h post transfection with siRNAs. Two components of ESCRT-I, Tsg101 and Vps28, were depleted with the indicated siRNAs. Control cells were transfected with non-targeting siRNA (siCtrl#1). GFP-MCOLN1 accumulation on LAMP1-positive structures indicated by arrows in control cells. In ESCRT-I-depleted cells, GFP-MCOLN1 accumulation on enlarged LAMP1-positive structures indicated by arrowheads. Cell nuclei marked with DAPI stain (gray). Scale bar, 10 μ m. (B) Quantitative analysis of microscopic images showing the fluorescence intensity of ectopically expressed GFP-MCOLN1 on LAMP1-positive vesicles (arbitrary units, a.u.) in control or ESCRT-I-depleted cells and/or upon 18 h BafA1 treatment. Values derived from independent experiments (dots) and their means (n=4 +/- SEM) are presented. Paired two-tailed *t* test to averaged values measured for siCtrl#1 and #2 cells (AveCtrl) was applied. $P \geq 0.05$ marked as “ns” - non-significant, * $P < 0.05$, ** $P < 0.01$.

Taken together, the results of analyzing lysosomal membrane protein degradation indicated that ESCRT-dependent turnover of lysosomal membrane proteins may prevent constitutive expansion of the limiting membranes and thus restrict the size of lysosomes.

4.3. The identification of lysosome-related signaling pathways activated upon ESCRT-I depletion

Lysosomal disorders often activate specific transcriptional responses to adjust cellular metabolism to the dysfunction of lysosomes [287, 288]. To test whether ESCRT-I deficiency induces responses characteristic of altered lysosomal function, RNA sequencing was performed in RKO cells lacking Tsg101 or Vps28. 1166 genes with upregulated expression upon Tsg101 depletion and 601 genes with upregulated expression upon Vps28 depletion were identified (listed in Table 1 in supplementary materials). 480 genes whose expression was upregulated under both conditions (listed in Table 2 in supplementary materials) were analyzed using gene ontology (GO) database. As expected, this analysis indicated increased expression of genes implicated in inflammatory response (Fig. 4.9), previously reported by the Laboratory of Cell Biology at IIMCB [193, 194, 225, 236]. Moreover, enhanced expression of genes encoding proteins involved in autophagy or cholesterol metabolism was identified (Fig. 4.9). Of note, their transcriptional activation may occur upon lysosomal dysfunction [34, 63, 125, 129, 148, 150, 156, 289] or nutrient starvation [128, 130, 148, 150, 152, 290].

To identify transcription factors potentially engaged in the activation of lysosome-related transcriptional response upon ESCRT-I depletion, promoter regions of the upregulated genes were investigated using RcisTarget packages (Bioconductor) and SwissRegulon database containing genome-wide annotations of transcription factor binding motifs. Among the overrepresented motifs, regulatory components from NF- κ B (NFKB1, REL, RELA) and AP-1 (FOS, FOSB, FOSL1, JUNB, JUND) signaling pathways were found (Fig. 4.10). This was consistent with the observed activation of inflammatory response upon ESCRT-I depletion (Fig. 4.9, [225]). The RcisTarget analysis also indicated that among genes upregulated in cells lacking Tsg101 or Vps28 there were known targets of transcription factors from the MiT-TFE (represented by TFEB factor) or SREBP (represented by SREBF1/2) families. This suggested that activation of MiT-TFE factors could be responsible for the induced expression of genes related to lysosomal biogenesis and autophagy, whereas SREBP factors could mediate the induced expression of cholesterol biosynthesis genes in ESCRT-I deficient cells.

GO Upregulated Biological Processes in RKO cells after Tsg101 or Vps28 silencing (480 genes)

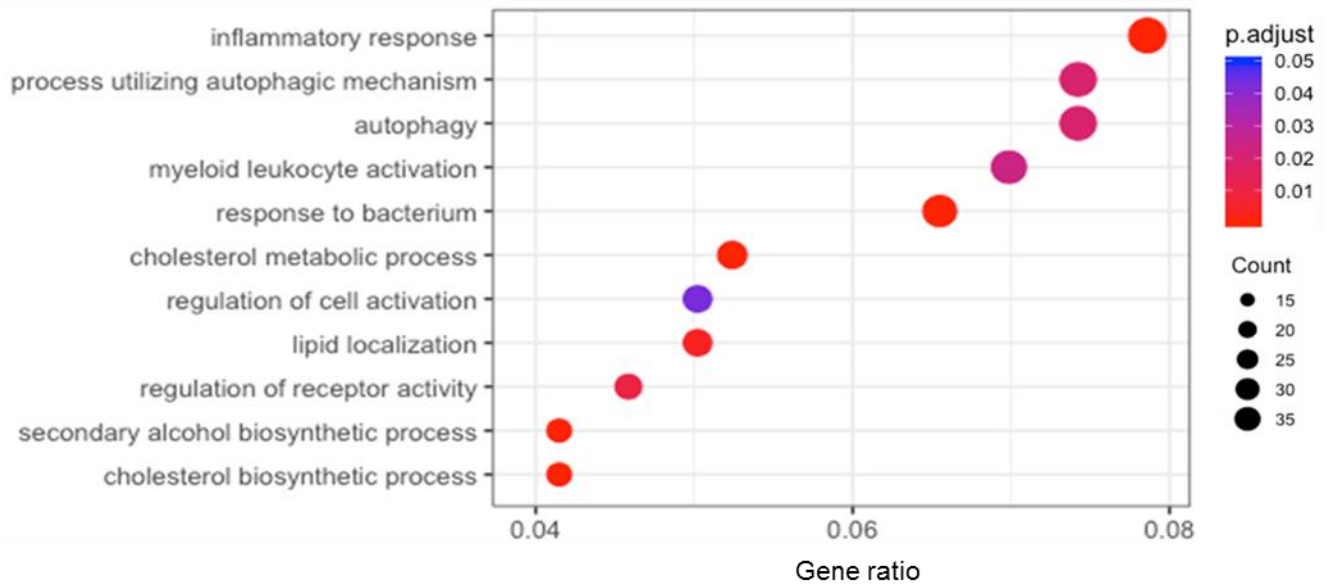


Figure 4.9. ESCRT-I depletion induces transcription of genes involved in inflammation, cholesterol biosynthesis and autophagy in RKO cells. Top biological processes from gene ontology (GO) enrichment analysis of commonly upregulated genes upon ESCRT-I depletion (≥ 1.5 -fold; adjusted P-value < 0.05). The list of genes upregulated upon Tsg101 or Vps28 depletion was derived from the RNA sequencing analysis in which the transcriptomes of cells transfected with siTsg101#2 and siVps28#1 or #2 siRNAs were compared to the transcriptome of control cells transfected with non-targeting siCtrl#1 or #2 siRNAs. Cells were collected 72 h post transfection. The size of each dot reflects the number (count) of upregulated genes annotated to the identified biological process. The color of each dot indicates the adjusted P-value. Gene ratio represents the ratio between the number of genes annotated to biological processes and the number of genes included in the GO analysis.

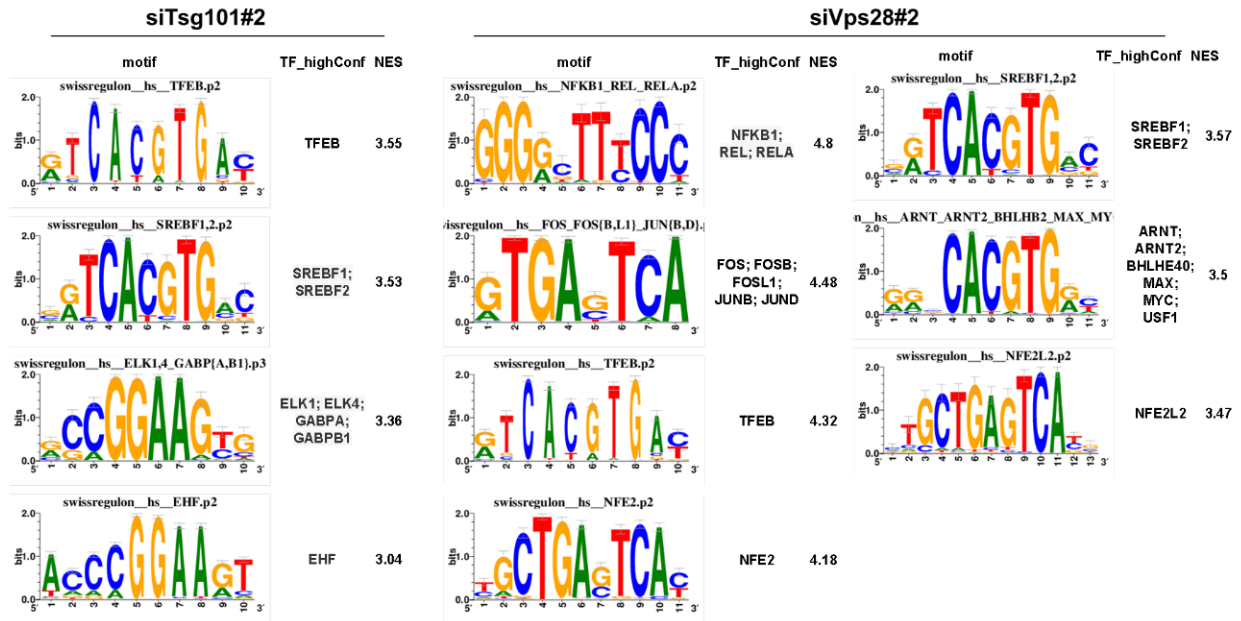


Figure 4.10. MiT-TFE and SREBP transcription factor binding motifs are overrepresented among promoter regions of genes transcriptionally upregulated upon ESCRT-I depletion. Transcription factor binding motifs overrepresented within the region of 5000 bp upstream of the transcription starting site of the genes upregulated upon ESCRT-I depletion (≥ 1.5 -fold; adjusted P-value < 0.05). The list of genes upregulated upon Tsg101 or Vps28 depletion was derived from the RNA sequencing analysis in which the transcriptomes of cells transfected with siTsg101#2 and siVps28#1 siRNAs for 72 h were compared to the transcriptome of control cells transfected with non-targeting siCtrl#1 siRNA. Established motifs from the *Homo sapiens* SwissRegulon database (<https://swissregulon.unibas.ch/sr/swissregulon>) are presented as schematic representations of motifs accompanied by the names of transcription factors annotated to these motifs (TF_highConf). NES (normalized enrichment score) > 3 was considered as significant.

To test whether MiT-TFE transcription factors were activated upon ESCRT-I depletion, the nucleocytoplasmic distributions of two members of this family, TFEB and TFE3 proteins, were analyzed by western blotting analysis of whole cell lysates and nuclear fractions of RKO and DLD-1 cells (Fig. 4.11A-B). In both cell lines, lack of Tsg101 or Vps28 subunits upregulated protein levels of TFEB and TFE3 factors in nuclear fractions (Fig. 4.11A-B), pointing to the activation of these transcription factors. Of note, their increased amounts were also observed upon ESCRT-I depletion in whole cell lysates (Fig. 4.11A-B).

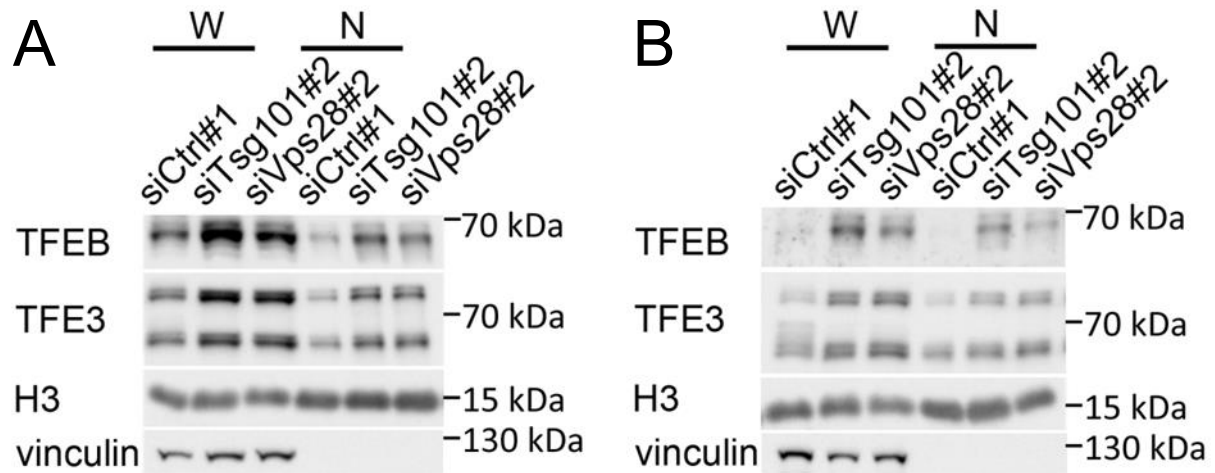


Figure 4.11. ESCRT-I depletion increases translocation of TFEB and TFE3 to the nucleus. Western blots showing the effect of ESCRT-I depletion on the intracellular and nuclear levels of TFEB and TFE3 transcription factors. Two components of ESCRT-I, Tsg101 and Vps28, were depleted using two independent siRNAs each, siTsg101#1 or #2 and siVps28#1 or #2. Control cells were transfected with non-targeting siRNAs (siCtrl#1 or #2). 72 h post transfection RKO (A) or DLD-1 (B) cells were collected to obtain their whole cell lysates (W) and nuclear fractions (N). The samples were immunoblotted with antibodies recognizing TFEB or TFE3. Histone H3 was used as a loading control. Vinculin was used as a cytosolic marker to examine the purity of nuclear fractions.

To confirm that the enhanced expression of genes related to lysosomal function occurred due to activation of MiT-TFE factors, TFEB and TFE3 proteins were co-depleted with Tsg101 or Vps28 subunits using siRNAs. First, the silencing efficiencies were assessed by western blotting to choose the best working siRNAs targeting these transcription factors (Fig. 4.12A). Although all three tested siRNAs targeting TFEB strongly reduced its protein level, one of them, siTFEB#1, was toxic for cells and thus excluded from further analysis. In case of depleting TFE3, siTFE3#2 was selected for further studies as the most effective siRNA. Given that TFEB and TFE3 transcription factors regulate similar sets of genes [129], concurrent depletion of TFEB (using siTFEB#2) and TFE3 (siTFE3#2) was applied. Silencing efficiencies of siRNAs targeting Tsg101, Vps28, TFEB and TFE3 were confirmed on mRNA levels (Fig. 4.12B). Simultaneous depletion of MiT-TFE factors in cells lacking ESCRT-I prevented the induction of MiT-TFE target genes, namely *NPC1* and *MCOLN1* (Fig. 4.12C). This showed that MiT-TFE factors were responsible for expression of genes encoding lysosomal and autophagosomal proteins that were upregulated upon ESCRT-I silencing.

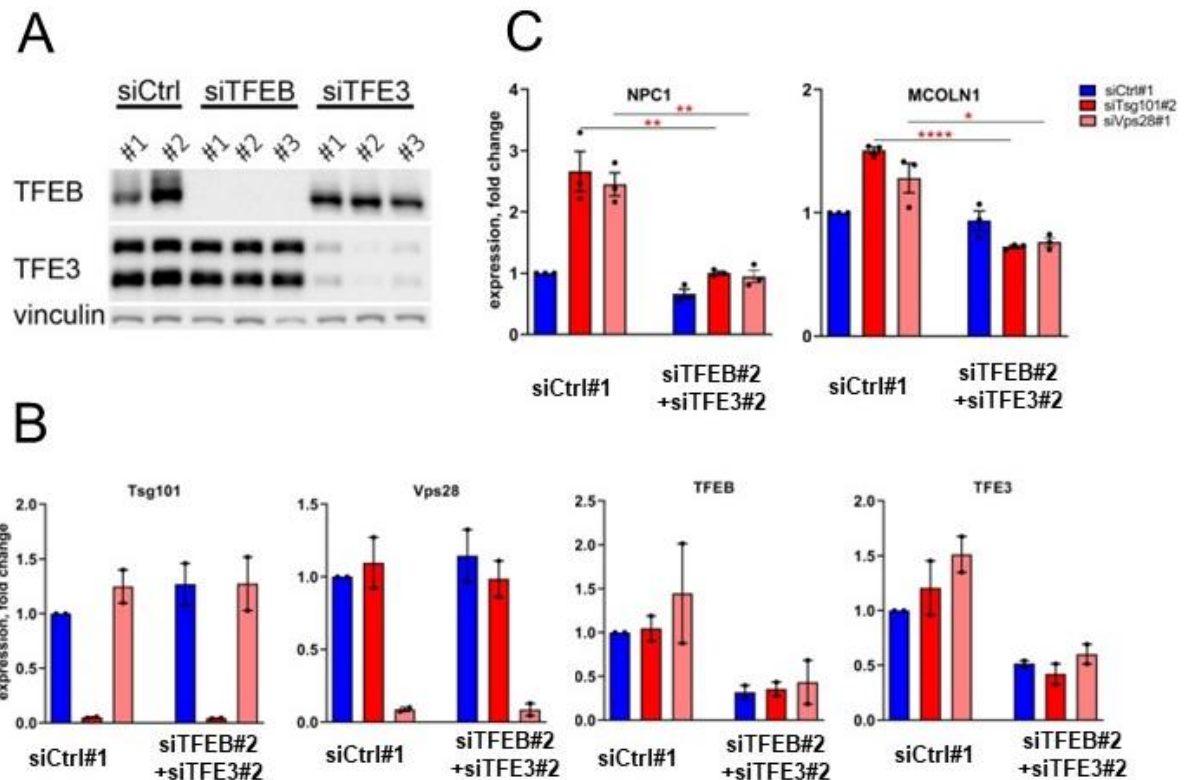


Figure 4.12. MiT-TFE transcription factors are required for upregulated expression of genes involved in lysosomal biogenesis upon ESCRT-I depletion. (A) Western blots showing depletion efficiency of TFEB and TFE3 proteins using three independent single siRNAs for each protein as compared to non-targeting control siRNAs (siCtrl#1 or #2). 72 h post transfection, cells were lysed and immunoblotted with antibodies recognizing TFEB or TFE3. Vinculin was used as a loading control. (B-C) mRNA levels of the indicated ESCRT-I subunits and MiT-TFE factors (in B) and of the indicated MiT-TFE target genes (in C) upon depletion of ESCRT-I (siTsg101#2 or siVps28#1) alone or together with TFEB and TFE3 (siTFEB#2 and TFE3#2) as analyzed by RT-qPCR. Control cells were transfected with non-targeting siRNAs (siCtrl#1). Values were normalized to mRNA levels of GAPDH housekeeping control and presented as a fold change to siCtrl#1 cells. Dots indicate values derived from independent experiments. Bars represent the mean (n=2 in B and n=3 in C +/- SEM). Unpaired two-tailed *t* test to siTsg101#2 or siVps28#1 conditions was applied (in C). *P<0.05, **P<0.01, ****P<0.0001.

The above data confirmed that ESCRT-I depletion activates MiT-TFE transcription factors to induce the expression of their target genes. However, although the upregulated expression of genes involved in lysosome or autophagosome biogenesis in the absence of ESCRT-I was observed at 72 h post siRNA transfection, it could be caused by a prolonged activation of

TFEB/TFE3 signaling that was initiated earlier. To verify the dynamics of activation of MiT-TFE factors upon depletion of ESCRT-I, their nuclear accumulation at 48 h and 72 h was assessed by immunofluorescence staining and confocal microscopy. In comparison to control cells, fluorescence signal detecting TFEB or TFE3 in confocal microscopy disappeared upon depletion of TFEB (Fig. 4.13A) or TFE3 (Fig. 4.13B), respectively, verifying the specificity of applied antibodies. Quantitative analysis of acquired images showed that at 48 h or 72 h post transfection around 10% of control cells were positive for TFEB or TFE3 staining (Fig. 4.13C-F). Depletion of Tsg101 increased the percentage of cells with nuclear accumulation of TFEB already at 48 h post transfection to 35%. This percentage remained at a similar level at 72 h post transfection (Fig. 4.13C, E). The percentage of cells with nuclear accumulation of TFE3 due to Tsg101 depletion was also elevated already at 48 h post transfection (around 18%), but increased in time (reaching the level of 30% at 72 h post transfection) (Fig. 4.13D, F). These results showed that activation of MiT-TFE factors occurs around 48 h post transfection with siRNA targeting siTsg101, hence this time point was chosen in experiments addressing the mechanisms underlying MiT-TFE activation due to ESCRT-I depletion.

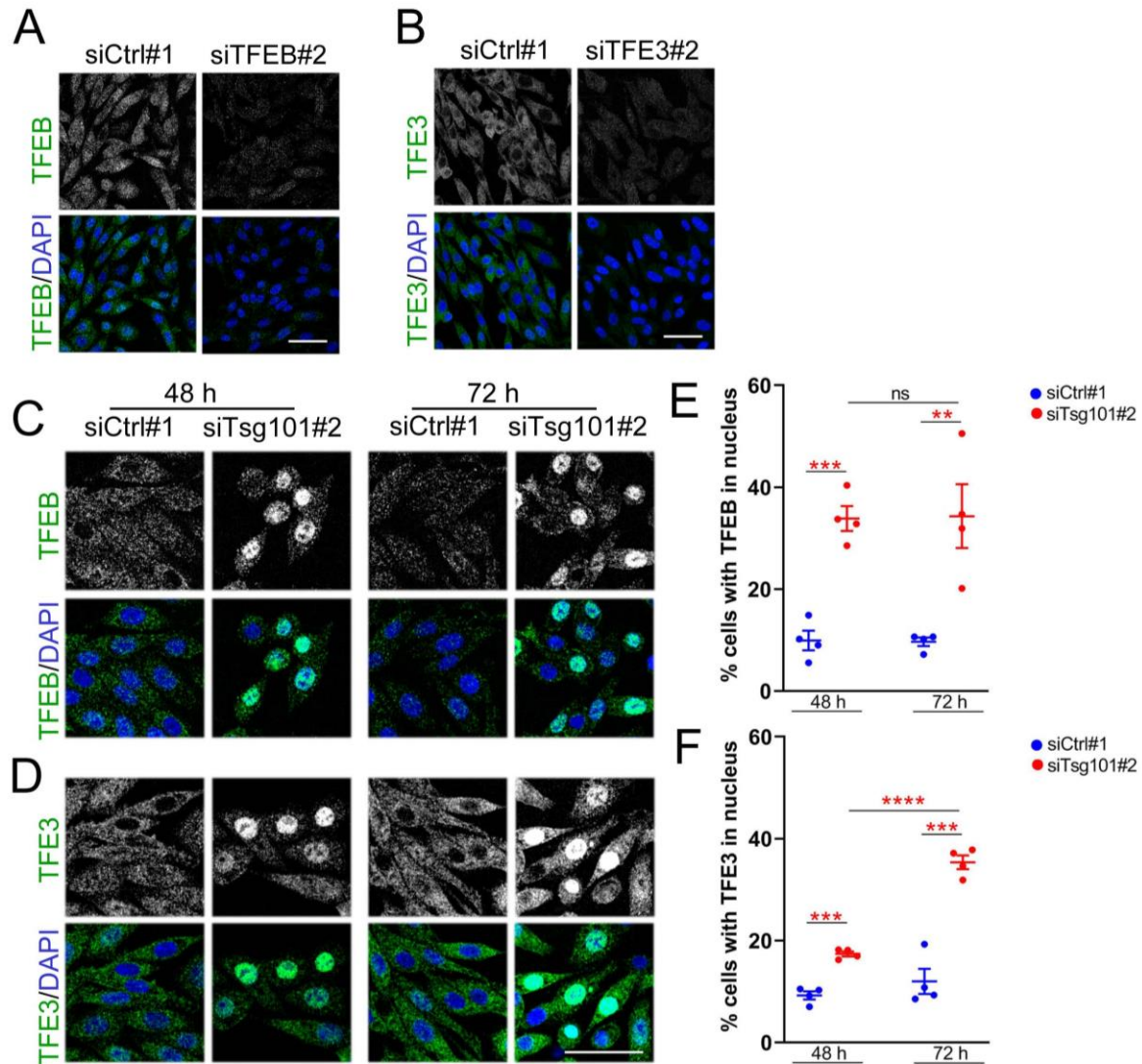


Figure 4.13. TFEB and TFE3 accumulate in the nucleus upon Tsg101 depletion at 48 and 72 h post transfection. (A-B) Representative maximum intensity projection images from confocal microscopy of fixed RKO cells showing the specificity of antibodies recognizing TFEB (green, in A) or TFE3 (green, in B) 72 h post transfection. TFEB or TFE3 were depleted using siTFEB#2 or siTFE3#2 siRNAs, respectively. Control cells were transfected with non-targeting siCtrl#1 siRNA. Cell nuclei marked with DAPI stain (blue). Scale bar, 50 μ m. (C-D) Representative maximum intensity projection confocal images of fixed RKO cells showing the effect of Tsg101 depletion on intracellular distribution of TFEB (green, in C) or TFE3 (green, in D) 48 h or 72 h post transfection. Control cells were transfected with non-targeting siCtrl#1 siRNA. Cell nuclei stained with DAPI (blue). Scale bar, 50 μ m. (E-F) Quantitative analysis of microscopic images showing the percentage of cells with TFEB (E) or TFE3 (F) in the nucleus 48 h or 72 h post transfection in control or Tsg101-depleted cells. Values derived from independent experiments (dots) and their means ($n=4 \pm$ SEM) are presented. Unpaired two-tailed *t* test was applied. $P \geq 0.05$ marked as “ns”- non-significant, ** $P < 0.01$, *** $P < 0.001$, **** $P < 0.0001$.

4.4. The effect of impaired cholesterol efflux from lysosomes on the activation of MiT-TFE signaling upon ESCRT-I depletion

Transcriptomic analysis of ESCRT-I-depleted RKO cells revealed an induced expression of genes related to cholesterol metabolism (Fig. 4.9). In line with this, analysis of promoter regions of differentially expressed genes identified SREBP as a transcription factor potentially involved in upregulated expression of these genes upon ESCRT-I knockdown (Fig. 4.10). To validate whether ESCRT-I depletion affected cholesterol homeostasis, the intracellular distribution of free cholesterol was assessed by confocal microscopy at 48 h post transfection of cells with siRNAs. Fluorescent polyene antibiotic, filipin, was used to detect free cholesterol [291]. As expected, in control cells, free cholesterol staining was observed predominantly in the PM and late endosomes/lysosomes. However, depletion of Tsg101 or Vps28 led to free cholesterol accumulation in enlarged LAMP1-positive structures (Fig. 14A-B), indicating impaired cholesterol trafficking upon ESCRT-I deficiency. To verify the source of accumulated cholesterol, cells were cultured in a delipidated medium, that lacks cholesterol and other lipids, thereby preventing endocytic uptake of exogenous cholesterol [292]. As shown in Fig. 14A-B, cholesterol accumulation in LAMP1-positive structures was reduced when cells were cultured in delipidated medium in comparison to cells grown in full medium. This showed that cholesterol accumulated upon ESCRT-I depletion originated from endocytic uptake. Of note, the data obtained by the Laboratory of Cell Biology at IIMCB revealed that in ESCRT-I-depleted RKO cells, supplementation with soluble form of cholesterol, which enters the cells bypassing the endolysosomal trafficking, prevented the induction of cholesterol biosynthesis genes [293].

Cumulatively, these results demonstrated that ESCRT-I depletion impaired the delivery of exogenously-derived cholesterol by endolysosomal trafficking to other intracellular compartments, inducing the expression of cholesterol biosynthesis genes in an attempt to restore cholesterol homeostasis.

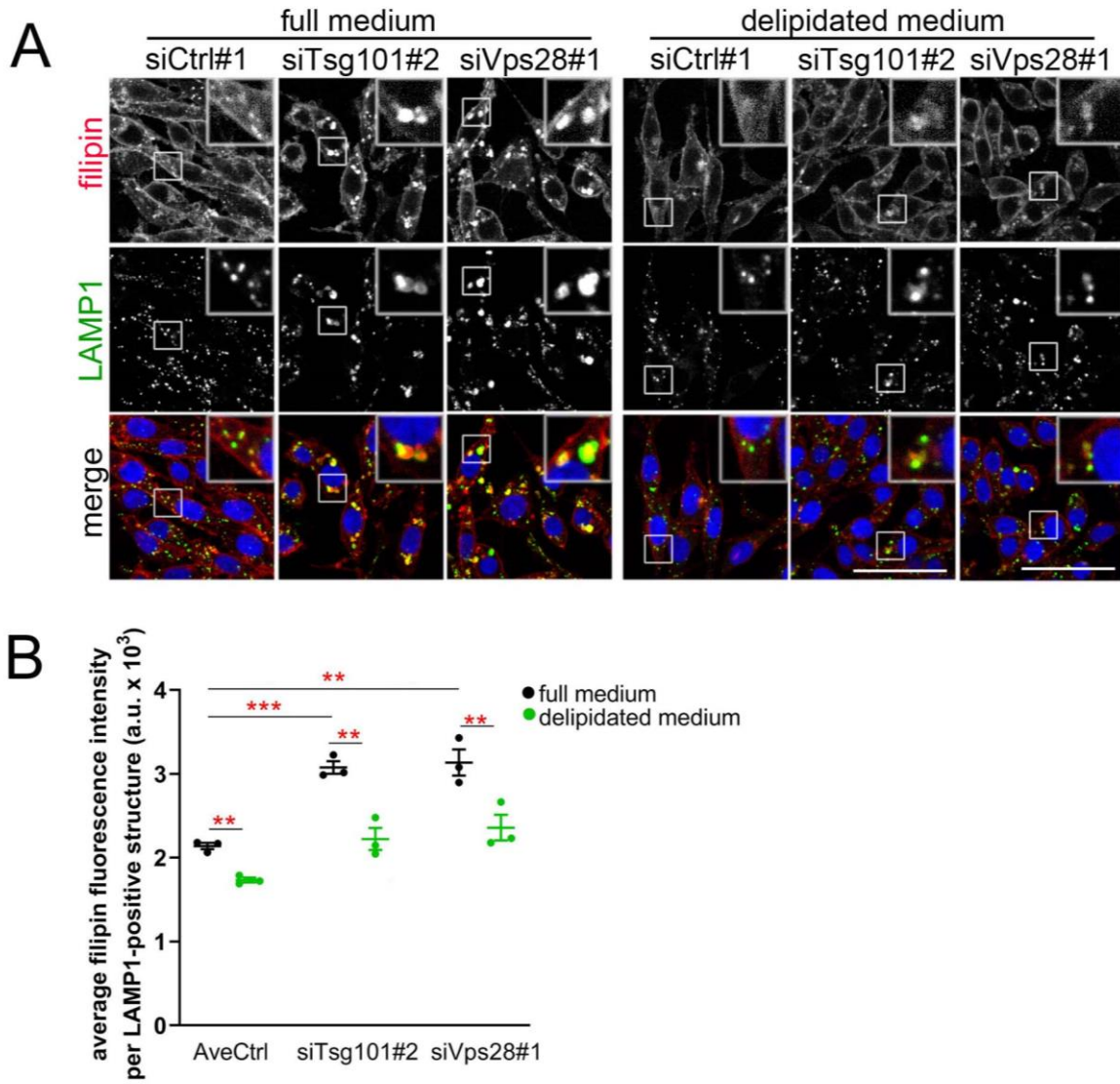


Figure 4.14. Endocytosed cholesterol accumulates on late endosomes/lysosomes upon ESCRT-I depletion. (A) Representative maximum intensity projection confocal images of fixed RKO cells cultured in full or delipidated medium showing the effect of ESCRT-I depletion on the intracellular distribution of free cholesterol marked with filipin dye (red) and LAMP1 protein (green) 48 h post transfection. ESCRT-I subunits were depleted using siTsg101#2 or siVps28#1 siRNAs. Control cells were transfected with non-targeting siCtrl#1 siRNA. Cell nuclei marked with DRAQ7 stain (blue). Scale bar, 50 μ m. (B) Quantitative analysis of microscopic images showing the average filipin fluorescence intensity per LAMP1-positive structure (arbitrary units, a.u.) in control cells (siCtrl#1) or cells with ESCRT-I depletion (siTsg101#2 or siVps28#1) cultured in full or delipidated medium. Values derived from independent experiments (dots) and their means ($n=3 \pm$ SEM) are presented. Paired two-tailed t test to averaged values measured for control cells transfected with non-targeting siCtrl#1 or #2 siRNAs (AveCtrl) was applied, ** $P < 0.01$, *** $P < 0.001$.

Because impaired lipid trafficking was associated with TFEB activation [294], the contribution of cholesterol accumulated in late endosomal/lysosomal structures to MiT-TFE activation upon ESCRT-I depletion was tested. To prevent the abnormal cholesterol accumulation, ESCRT-I-depleted RKO cells were cultured in delipidated medium. The quantitative confocal microscopy image analysis showed that an inhibited supply of exogenous lipids, including cholesterol, decreased the percentage of control cells with TFEB (Fig. 4.15A-B) and TFE3 (Fig. 4.16A-B) in the nucleus, indicating that basal levels of MiT-TFE activation depend on lipid availability. Nevertheless, reducing the accumulation of cholesterol by culturing cells in delipidated medium did not prevent the increase in percentage of cells with TFEB (Fig. 4.15A-B) and TFE3 (Fig. 4.16A-B) in the nucleus upon Tsg101 depletion.

Collectively, abnormal cholesterol accumulation in late endosomes/lysosomes did not contribute to the activation of TFEB or TFE3 in ESCRT-I-depleted cells. Thus, other molecular mechanisms underlying MiT-TFE activation upon ESCRT-I deficiency were subsequently examined.

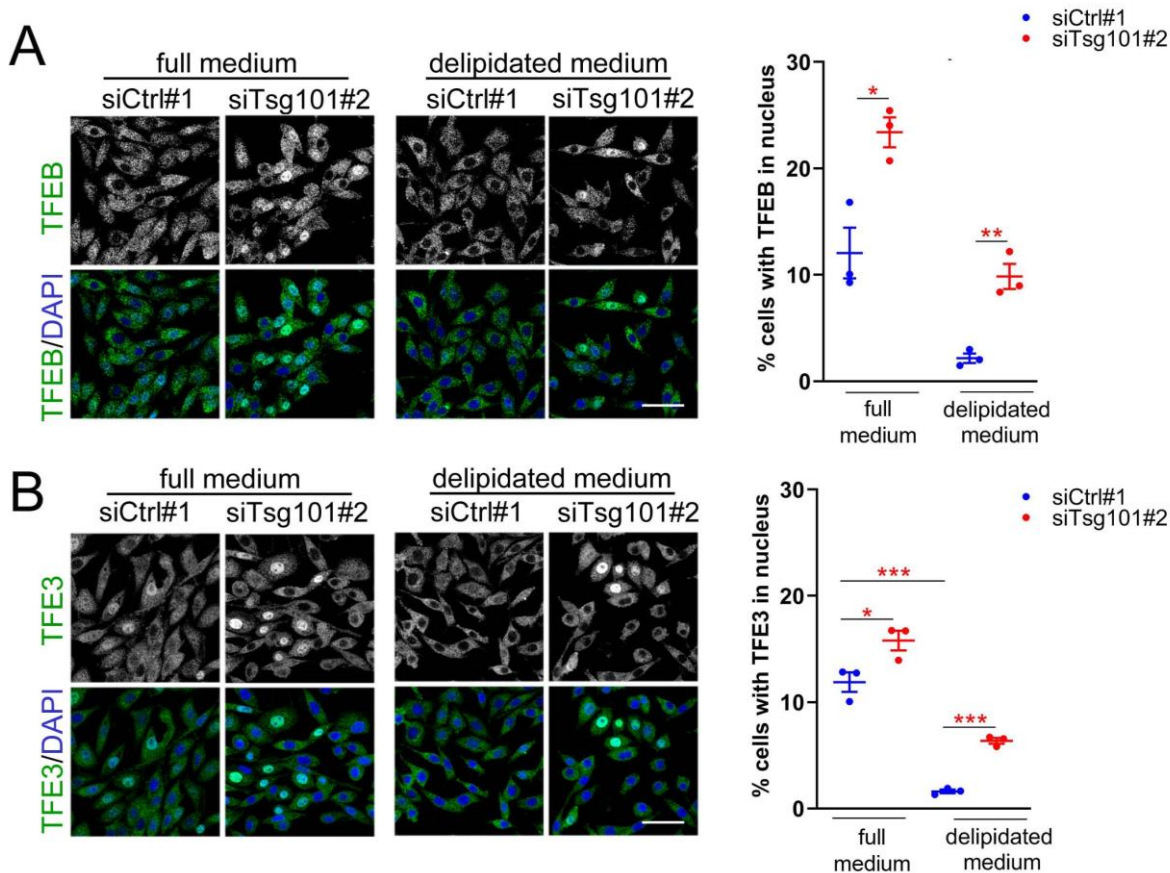


Figure 4.15. Cholesterol accumulation in endosomes and/or lysosomes does not contribute to the nuclear accumulation of TFEB and TFE3 factors upon Tsg101 depletion. (A-B) Representative maximum intensity projection images from confocal microscopy of fixed RKO cells showing the effect of Tsg101 depletion upon culture in full or delipidated medium on the intracellular distribution of TFEB (in A) or TFE3 (in B) 48 h post transfection. Control cells were transfected with non-targeting siCtrl#1 siRNA. Cell nuclei marked with DAPI stain (blue). Scale bar, 50 μ m. Graphs on the right present quantitative analysis of microscopic images showing percentage of cells with TFEB (in A) or TFE3 (in B) in the nucleus 48 h post transfection in control or Tsg101-depleted cells cultured in full or delipidated medium. Values derived from independent experiments (dots) and their means ($n=3 \pm$ SEM) are presented. Unpaired two-tailed t test to siCtrl#1 was applied, * $P < 0.05$, ** $P < 0.01$, *** $P < 0.001$.

4.5. The involvement of Ca^{2+} mediated signaling in the MiT-TFE activation upon ESCRT-I depletion

Because lack of ESCRT-I induced activation of MiT-TFE factors and impaired degradation of Ca^{2+} channel MCOLN1, the role of calcium- and MCOLN1-dependent signaling in the activation of MiT-TFE was investigated. To this end, BAPTA-AM, a chelator of intracellular pool of Ca^{2+} [46], or ML-SI1, an inhibitor of MCOLN1 activity [77, 295] were used to inhibit calcium-

or MCOLN1-regulated nuclear translocation of MiT-TFE. In control cells, treatment with chemical modulators of Ca^{2+} signaling did not reduce the basal percentage of cells with TFEB (Fig. 4.16A) or TFE3 in the nucleus (Fig. 4.16B), but rather upregulated the nuclear translocation of these proteins as compared to vehicle-treated cells. However, BAPTA-AM or ML-S11 treatment inhibited the nuclear accumulation of TFEB and TFE3 upon Tsg101 depletion (Fig. 4.16A-B).

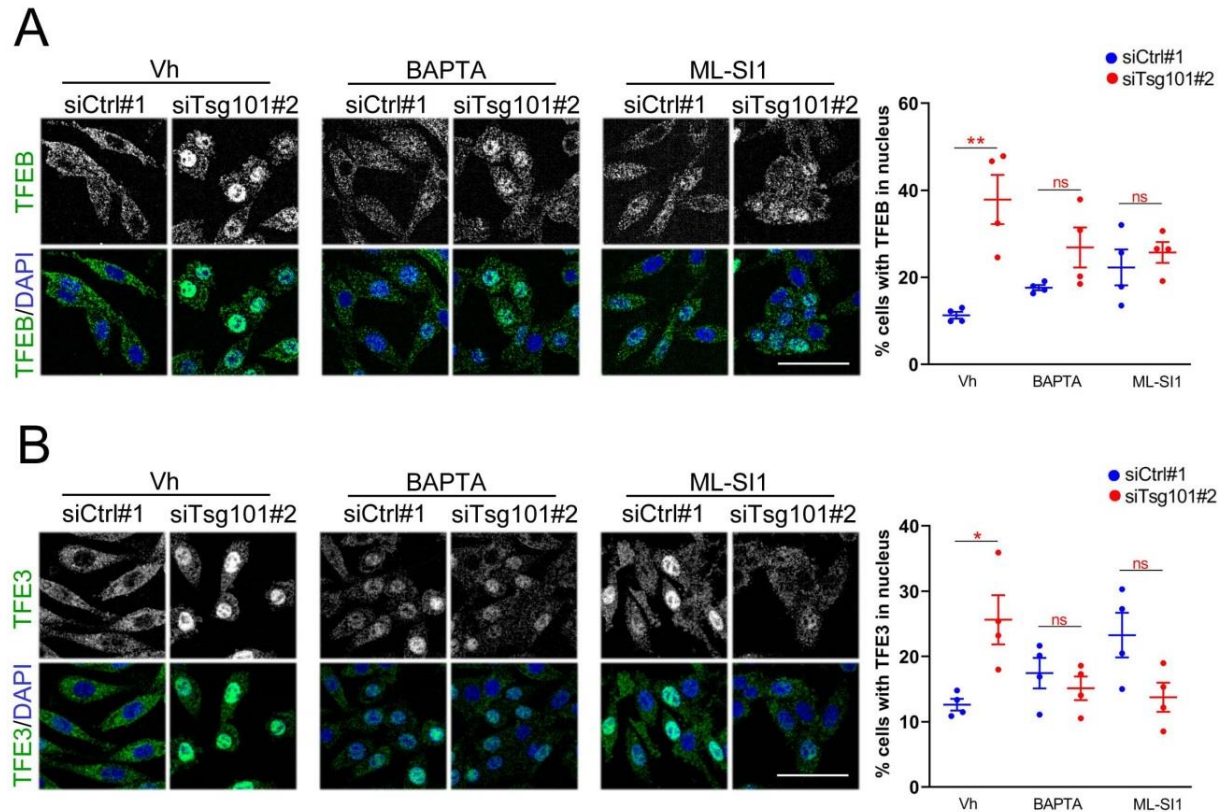


Figure 4.16. Chelation of intracellular pool of Ca^{2+} and inhibition of MCOLN1 channel activity reduce nuclear abundance of TFEB and TFE3 factors upon Tsg101 depletion. (A-B) Representative maximum intensity projection images from confocal microscopy of fixed RKO cells showing the effect of Tsg101 depletion and/or 2 h treatment with Vh (vehicle, DMSO), 2 h BAPTA-AM or 2 h ML-S11 on the intracellular distribution of TFEB (in A) or TFE3 (in B) 48 h post transfection. Tsg101 was depleted using siTsg101#2 siRNA. Control cells were transfected with non-targeting siCtrl#1 siRNA. Cell nuclei marked with DAPI stain (blue). Scale bar, 50 μm . Graphs on the right present quantitative analysis of microscopic images showing the percentage of cells with TFEB (in A) or TFE3 (in B) in the nucleus in control or Tsg101-depleted cells treated or not with BAPTA-AM or ML-S11. Values derived from independent experiments (dots) and their means ($n=4 \pm$ SEM) are presented. Unpaired two-tailed t test to siCtrl#1 was applied, $P \geq 0.05$ marked as “ns” - non-significant, * $P < 0.05$, ** $P < 0.01$.

MiT-TFE nuclear translocation may be promoted by Ca^{2+} -dependent phosphatase, calcineurin (CaN) [46, 54, 55]. Thus, the involvement of this protein in MiT-TFE activation upon ESCRT-I depletion was tested. To this end, cyclosporin A (CsA) was used to inhibit CaN activity [296]. Similarly to BAPTA-AM and ML-SI1, CsA treatment exhibited a tendency to increase basal nuclear levels of TFEB (Fig. 4.17A) or TFE3 (Fig. 4.17B) in control cells. Additionally, CsA treatment inhibited the accumulation of TFEB or TFE3 in the nuclei of Tsg101-deficient cells as compared to control cells (Fig. 4.17A-B). Consistent with this, the Laboratory of Cell Biology at IIMCB showed that depletion of Tsg101 decreased TFEB phosphorylation at S122 and S211 [293]. Nevertheless, inhibition of MCOLN1- Ca^{2+} -CaN signaling did not restore the reduced phosphorylation of TFEB [293]. Collectively, although calcium-mediated signaling affected the nuclear accumulation of TFEB and TFE3 induced upon Tsg101 depletion, this mechanism was not due to canonical CaN-dependent dephosphorylation of these transcription factors. Therefore, further investigation of the mechanism underlying MiT-TFE activation was needed.

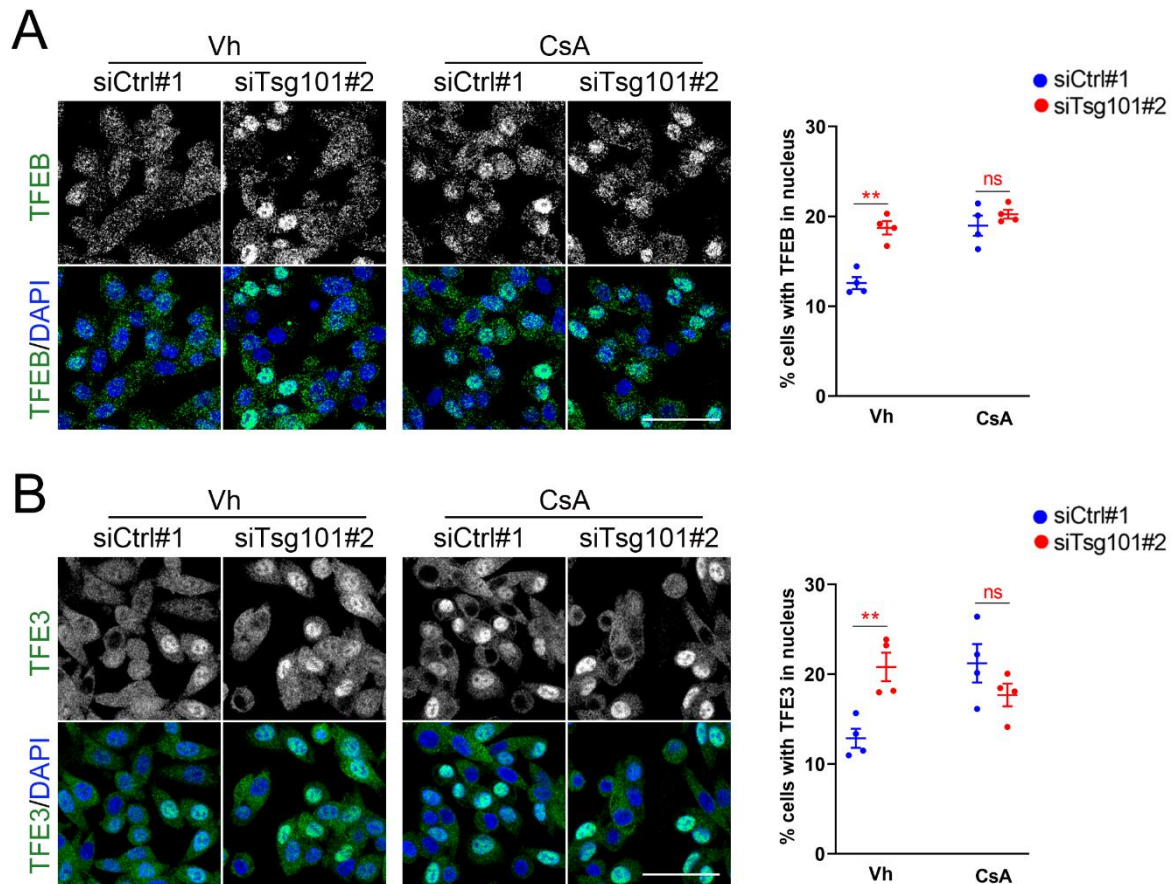


Figure 4.17. Inhibition of CaN does not reduce nuclear abundance of TFEB and TFE3 factors upon Tsg101 depletion. (A-B) Representative maximum intensity projection images from confocal microscopy of fixed RKO cells showing the effect of Tsg101 depletion and/or 2 h treatment with Vh (vehicle, DMSO) or CsA on the intracellular distribution of TFEB (in A) or TFE3 (in B) 48 h post transfection. Tsg101 was depleted using siTsg101#2 siRNA. Control cells were transfected with non-targeting siCtrl#1 siRNA. Cell nuclei marked with DAPI stain (blue). Scale bar, 50 μ m. Graphs on the right present quantitative analysis of microscopic images showing percentage of cells with TFEB (in A) or TFE3 (in B) in the nucleus in control or Tsg101-depleted cells and/or 2 h CsA treatment. Values derived from independent experiments (dots) and their means ($n=4 \pm$ SEM) are presented. Unpaired two-tailed t test to siCtrl#1 was applied, $P \geq 0.05$ marked as “ns” - non-significant, $**P < 0.01$.

4.6. The status of mTORC1 activation upon ESCRT-I depletion and its contribution to the MiT-TFE activation

Because lack of Tsg101 decreased the levels of TFEB phosphorylation at S122 [293], that was reported as direct mTORC1 target [151], the activity of mTORC1 in ESCRT-I-depleted RKO cells was verified. To this end, the phosphorylation states of mTORC1 canonical substrates [78], namely Ulk1 (S757), 4E-BP1 (T37/46) and S6K1 (S240/244), were examined together with TFEB S122 by western blotting. In order to inhibit mTORC1 activity, cells were cultured under nutrient-deficient (EBSS medium) conditions and compared to those cultivated under regular (EMEM full medium) conditions. In control cells, deprivation of nutrients abolished phosphorylation of all tested mTORC1 substrates, indicating their constitutive phosphorylation in RKO cells under normal growth conditions. Lack of Tsg101 or Vps28 reduced the phosphorylation of TFEB to the same levels as observed in EBSS medium. However, phosphorylations of canonical mTORC1 targets (Fig. 4.18A-B) were not affected by ESCRT-I depletion. This pointed to specific regulation of mTORC1-dependent TFEB phosphorylation.

Since signaling by mTORC1 is regulated by its intracellular distribution [78], the consequences of Tsg101 deficiency on the localization of mTOR were verified by confocal microscopy. Consistent with studies showing that active mTORC1 associates with lysosomes [102, 297], mTOR localized to LAMP1-positive structures in control cells (Fig. 4.19A) and dissociated from them upon nutrient deficiency (EBSS medium, Fig. 4.19A-B). However, lack of Tsg101 did not affect the lysosomal association of mTOR either under regular growth conditions or upon nutrient deficiency in comparison to control cells. This was in accordance with the biochemical results on mTORC1 signaling showing no changes in phosphorylation of canonical mTORC1 substrates upon Tsg101 deficiency (Fig. 4.18).

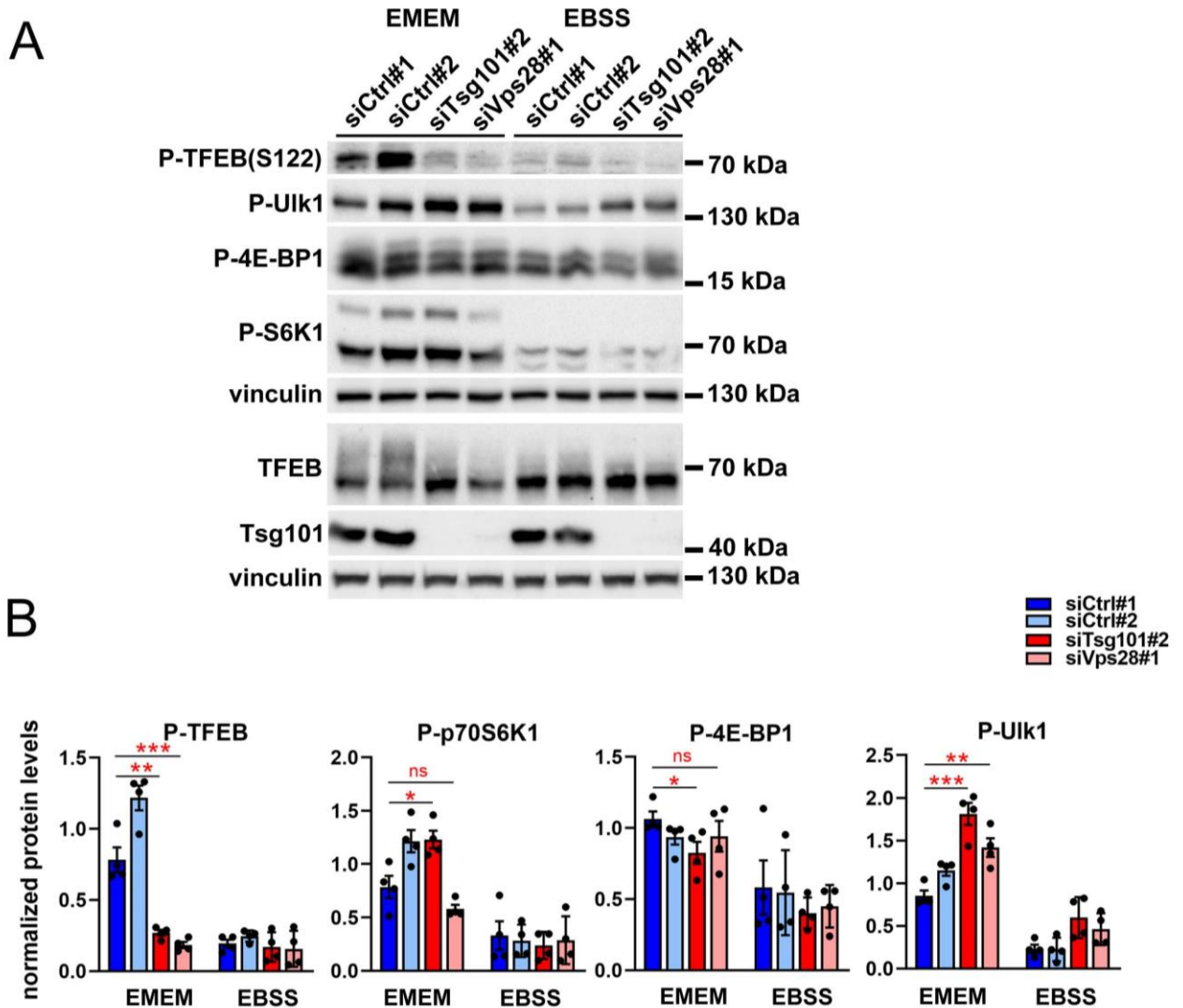


Figure 4.18. Depletion of ESCRT-I inhibits specific mTORC1 activity towards TFEB S122.

(A) Representative western blots showing the effect of ESCRT-I depletion in RKO cells cultured under regular (EMEM medium) or nutrient-deprived (EBSS medium) conditions on the phosphorylation of mTORC1 downstream targets. Two components of ESCRT-I, Tsg101 and Vps28, were depleted using single siRNAs (siTsg101#2 and siVps28#1). Control cells were transfected with non-targeting siRNAs (siCtrl#1 or #2). 2 h before collecting the cells, their medium was exchanged to fresh EMEM or EBSS medium. 48 h post transfection cells were lysed and immunoblotted with antibodies recognizing the indicated mTORC1 targets. Vinculin was used as a loading control. (B) Densitometry analysis of western blotting bands showing the phosphorylation levels of the indicated mTORC1 substrates in control or ESCRT-I-depleted cells presented as fold changes to averaged values measured for control cells. Dots indicate values derived from independent experiments. Bars represent the mean ($n=4 \pm$ SEM). Unpaired two-tailed t test to siCtrl#1 was applied. $P \geq 0.05$ marked as “ns”- non-significant, * $P < 0.05$, ** $P < 0.01$, *** $P < 0.001$.

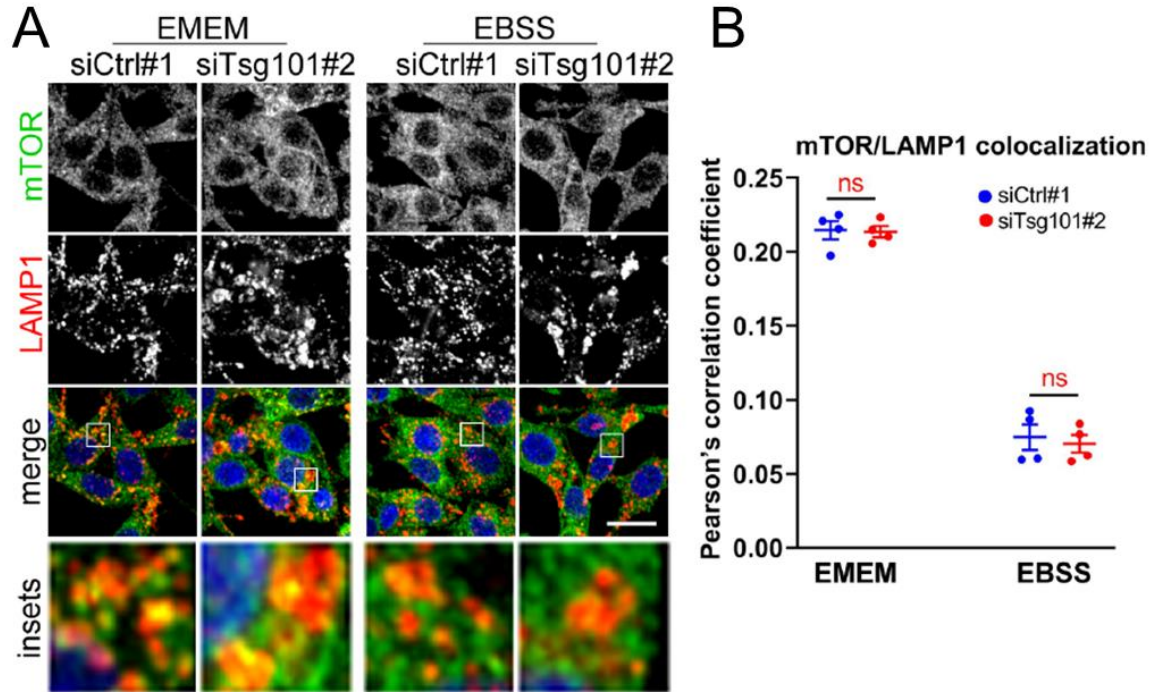


Figure 4.19. Tsg101 depletion does not affect mTOR association with late endosomes and/or lysosomes. (A) Representative single plane images from confocal microscopy of fixed RKO cells showing the effect of Tsg101 depletion in cells cultured under regular (EMEM medium) or nutrient-deprived (EBSS medium) conditions on the intracellular distribution of mTOR (green) and LAMP1 (red) 48 h post transfection. Control cells were transfected with non-targeting siCtrl#1 siRNA. 2 h before lysis, medium was exchanged to EMEM or EBSS medium. Cell nuclei marked with DAPI stain (blue). Scale bar, 20 μ m. (B) Quantitative analysis of microscopic images showing mTOR colocalization with LAMP1-positive structures expressed as Pearson's correlation coefficient in control or ESCRT-I-depleted cells. Values derived from independent experiments (dots) and their means (n=4 +/- SEM) are presented. Unpaired two-tailed *t* test to siCtrl#1 was applied, $P \geq 0.05$ marked as "ns"- non-significant.

Phosphorylation of TFEB and the resulting inhibition of its nuclear translocation are regulated via the activity of mTORC1 and the recruitment of TFEB to the lysosomal surface where phosphorylation occurs [107, 148, 152]. To verify whether ESCRT-I deficiency affected mTORC1-dependent nuclear accumulation and/or recruitment of MiT-TFE to the lysosomal surface, colocalization of TFEB or TFE3 with LAMP1-positive structures was measured by confocal microscopy upon inhibition of mTORC1 kinase activity. To this end, the second generation mTOR inhibitor, INK128, was used [298]. As anticipated, in control RKO cells, inhibition of mTORC1 activity promoted TFEB nuclear translocation (Fig. 4.20A-B) as well as its

colocalization with LAMP1-positive structures (Fig. 4.20A, C). Tsg101 deficiency modestly elevated TFEB nuclear translocation in INK128-treated cells (Fig. 4.20A-B) but did not promote TFEB colocalization with LAMP1-positive structures. In turn, depletion of Tsg101 diminished TFEB-LAMP1 colocalization induced by INK128 treatment (Fig. 4.20A, C).

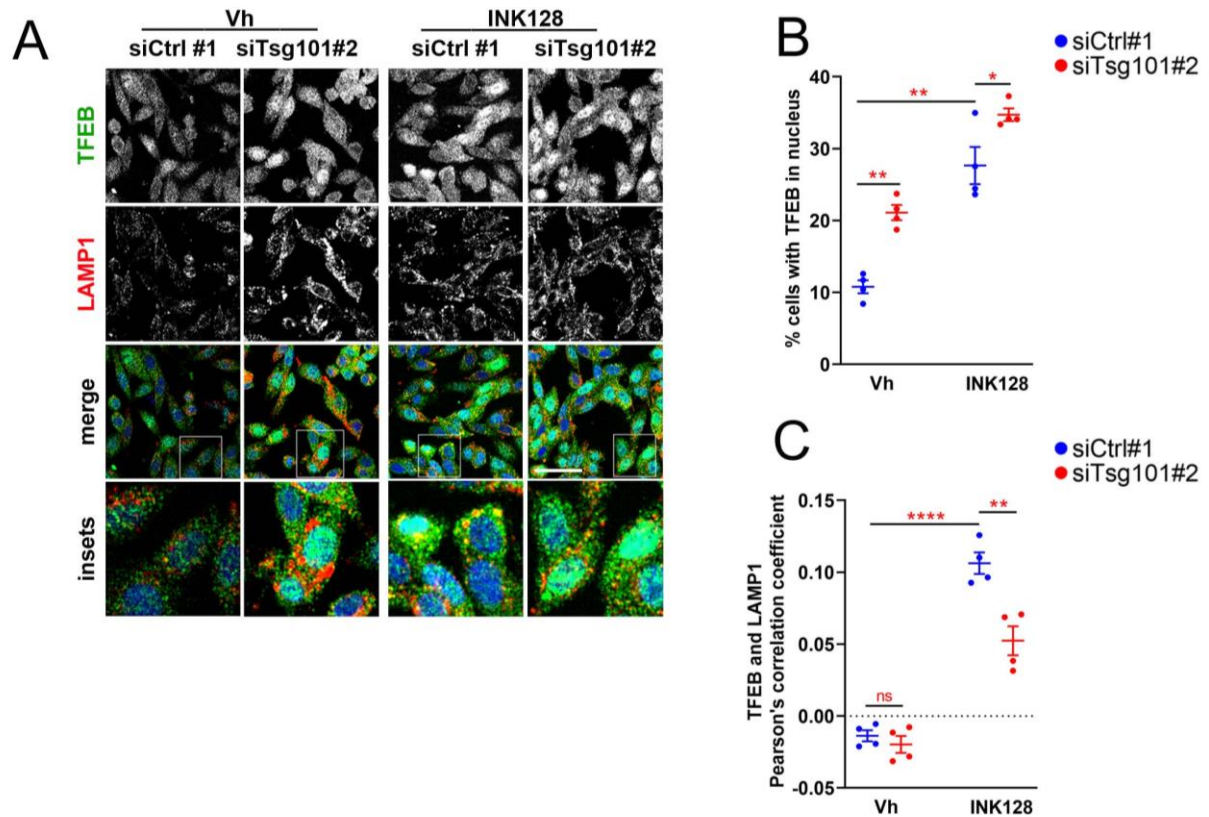


Figure 4.20. Tsg101 depletion reduces TFEB association with late endosomes and/or lysosomes upon mTORC1 inhibitor treatment. (A) Representative single plane images from confocal microscopy of fixed RKO cells showing the effect of Tsg101 depletion and/or 2 h vehicle (Vh, DMSO) and/or INK128 treatment on the intracellular distribution of TFEB (green) and LAMP1 (red) 48 h post transfection. Control cells were transfected with non-targeting siCtrl#1 siRNA. Cell nuclei marked with DAPI stain (blue). Scale bar, 100 μ m. (B-C) Quantitative analysis of microscopic images showing percentage of cells with TFEB in the nucleus (B) and TFEB colocalization with LAMP1-positive structures expressed as Pearson's correlation coefficient (C) in control or ESCRT-I-depleted cells. Values derived from independent experiments (dots) and their means ($n=4 \pm$ SEM) are presented. Unpaired (in B) and paired (in C) two-tailed t test to siCtrl#1 was applied, $P \geq 0.05$ marked as "ns"- non-significant, * $P < 0.05$, ** $P < 0.01$, **** $P < 0.0001$.

Similar to the results regarding the distribution of TFEB, mTORC1 inhibition increased TFE3 abundance in the nucleus (Fig. 4.21A-B) and enhanced TFE3 colocalization with LAMP1-

positive structures (Fig. 4.21C) in control RKO cells. However, in INK128-treated cells, Tsg101 depletion did not further potentiate TFE3 nuclear accumulation as it was observed for TFEB. Importantly, as in the case of TFEB, TFE3 colocalization with LAMP1-positive structures was reduced upon Tsg101 depletion (Fig. 4.21C).

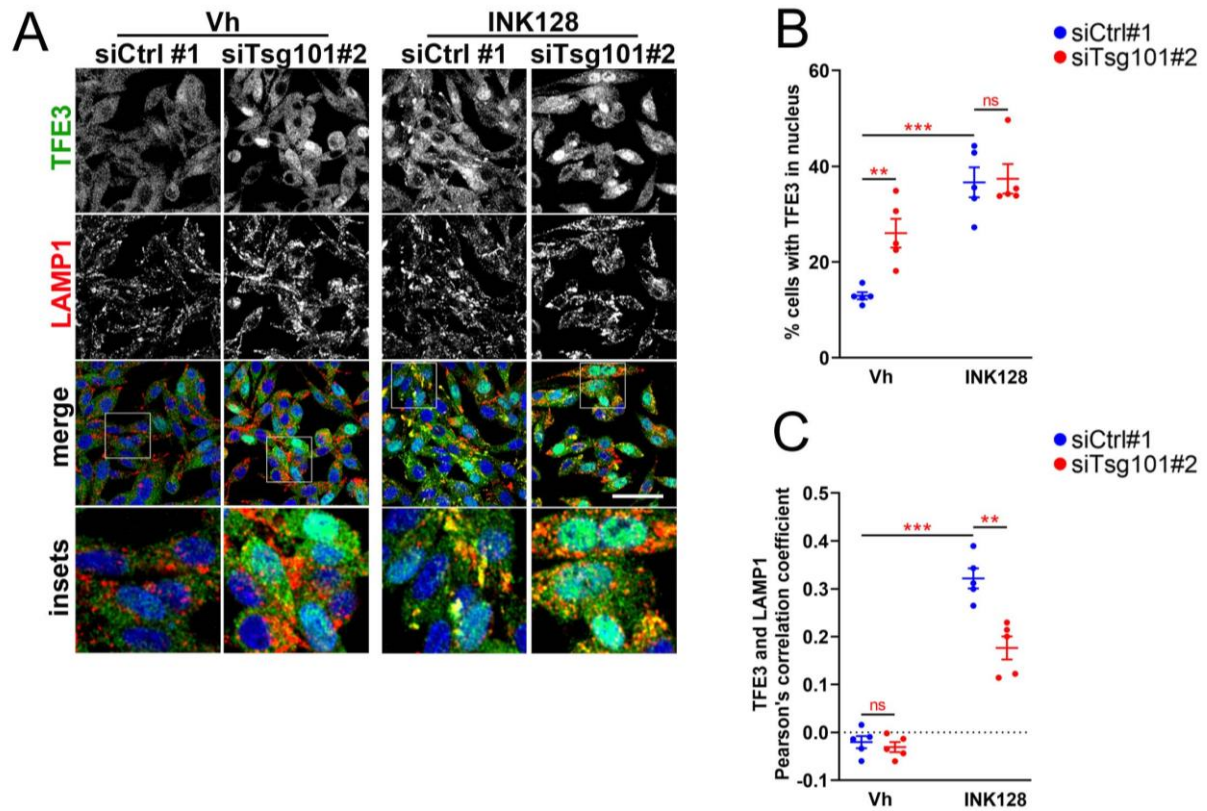


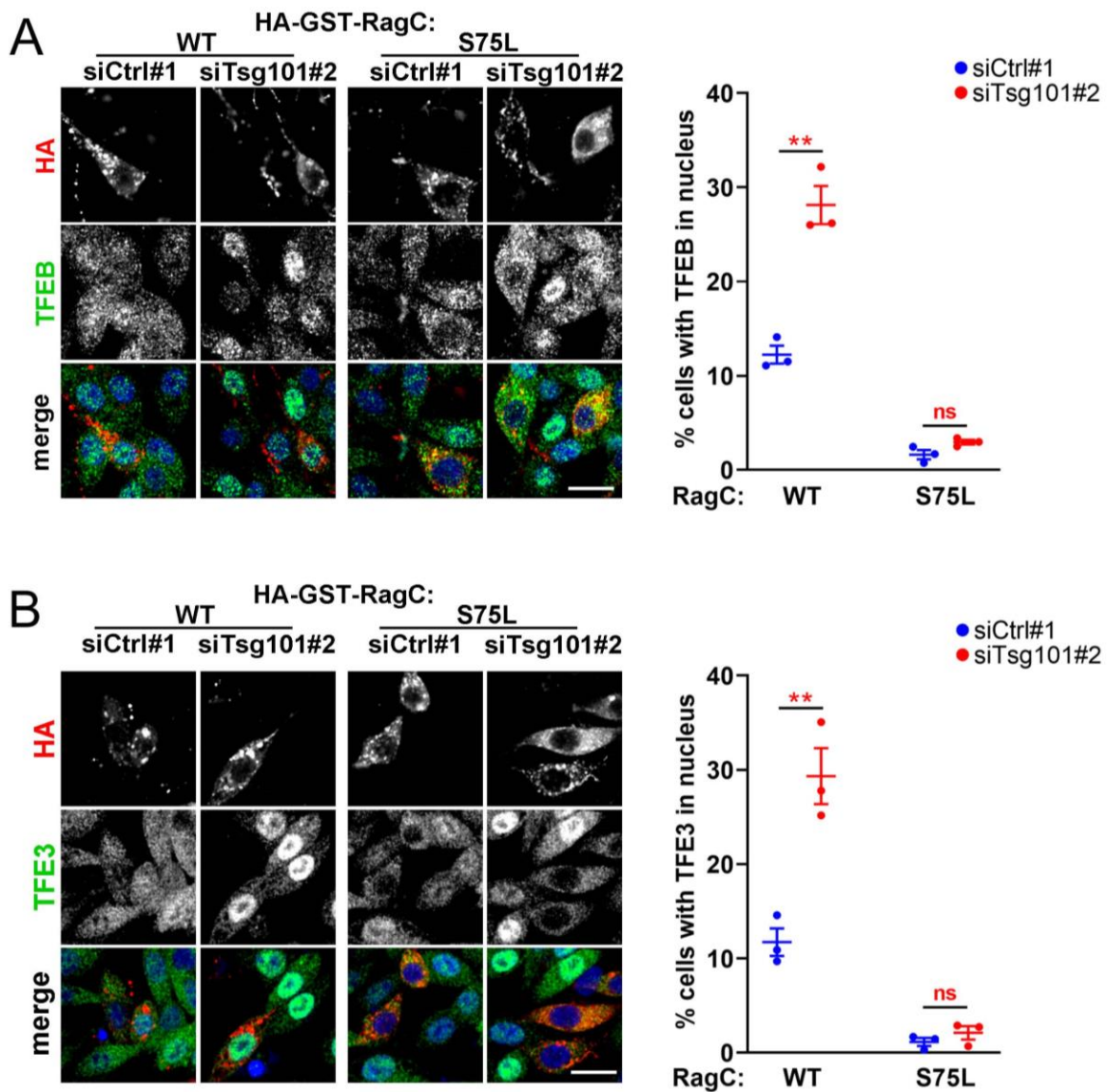
Figure 4.21. Tsg101 depletion reduces TFE3 association with late endosomes and/or lysosomes upon mTORC1 inhibitor treatment. (A) Representative single plane images from confocal microscopy of fixed RKO cells showing the effect of Tsg101 depletion and/or 2 h vehicle (Vh, DMSO) and/or INK128 treatment on the intracellular distribution of TFE3 (green) and LAMP1 (red) 48 h post transfection. Control cells were transfected with non-targeting siCtrl#1 siRNA. Cell nuclei marked with DAPI stain (blue). Scale bar, 100 μ m. (B-C) Quantitative analysis of microscopic images showing percentage of cells with TFE3 in the nucleus (B) and TFE3 colocalization with LAMP1-positive structures expressed as Pearson's correlation coefficient (C) in control or ESCRT-I-depleted cells. Values derived from independent experiments (dots) and their means ($n=4 \pm$ SEM) are presented. Unpaired (in B) and paired (in C) two-tailed t test to siCtrl#1 was applied, $P \geq 0.05$ marked as "ns"- non-significant, $**P < 0.01$, $***P < 0.001$.

Collectively, ESCRT-I depletion reduces MiT-TFE colocalization with LAMP1-positive structures in INK128-treated cells, pointing to the regulation via a specific mechanism, other than

the general inhibition of mTORC1 activity. Therefore, the mechanism underlying this specific response to ESCRT-I depletion was subsequently investigated.

4.7. The contribution of Rag GTPase complex to the activation of MiT-TFE signaling upon ESCRT-I depletion

Under nutrient-rich conditions, mTORC1-dependent phosphorylation of TFEB is mediated via active Rag GTPase complex [107, 148, 152]. Rag GTPase complex also promotes recruitment of MiT-TFE factors to lysosomes even upon pharmacological inhibition of mTOR activity [107, 148, 152]. To verify the effect of Rag GTPase-dependent activation on MiT-TFE signaling induced upon ESCRT-I depletion, constitutively active RagC mutant (S75L) was overexpressed. First, the nuclear accumulation of TFEB (Fig. 4.22A) and TFE3 (Fig. 4.22B) was analyzed by confocal microscopy. Control cells overexpressing wild-type RagC (WT) showed the expected basal nuclear localization of TFEB and TFE3 (around 10% of cells) that increased (to around 30%) due to Tsg101 depletion (Fig. 4.22A-B). In turn, overexpression of constitutively active RagC mutant S75L reduced the basal levels of TFEB and TFE3 in control cells and completely prevented their activation upon Tsg101 depletion (Fig. 4.22A-B).



Subsequently, the effect of activating Rag GTPase-dependent signaling on the phosphorylation levels of mTORC1 substrates upon ESCRT-I depletion was analyzed by western blotting (Fig. 4.23). The overexpression of WT RagC (used as a control) had no effect on phosphorylation of TFEB at S122 upon Tsg101 depletion. The overexpression of active RagC mutant (S75L) induced TFEB phosphorylation at S122 in control cells and prevented its dephosphorylation upon Tsg101 depletion. Of note, the phosphorylation levels of other mTORC1 targets, S6K1 or Ulk1, remained unaffected by active RagC mutant overexpression (Fig. 4.23A), showing the involvement of RagC in the regulation of substrate-specific mTORC1 signaling.

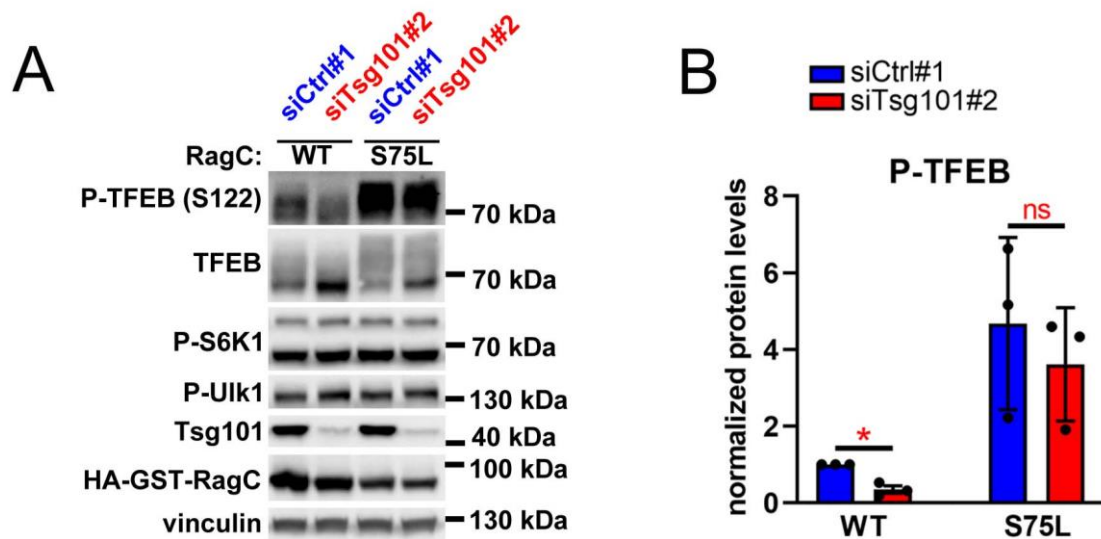


Figure 4.23. Constitutively active RagC mutant (S75L) prevents dephosphorylation of S122 of TFEB upon ESCRT-I depletion (A) Representative western blots showing the effect of Tsg101 depletion on phosphorylation levels of TFEB (S122), S6K1 and Ulk1 as well as total protein levels of TFEB, Tsg101, and HA-GST-RagC in RKO cells expressing wild-type (WT) or constitutively active RagC (S75L) 48 h post transfection. Vinculin was used as a loading control. (B) Densitometry analysis of western blotting bands showing the phosphorylation levels of S122 of TFEB in control or ESCRT-I depleted cells presented as a fold change to control cells. Dots indicate values derived from independent experiments. Bars represent the mean (n=3 +/- SEM). Unpaired two-tailed *t* test to siCtrl#1 was applied. $P \geq 0.05$ marked as “ns”- non-significant, $*P < 0.05$.

Taken together, the presented data unveiled that the activation of MiT-TFE factors upon ESCRT-I deficiency occurs due to the inactivation of Rag GTPase complex and the resulting inhibition of mTORC1 kinase activity specific towards MiT-TFE factors.

5. Discussion

Based on the results presented in this thesis, a model is proposed that illustrates the role of ESCRT-I in the regulation of lysosomal homeostasis and the consequences of ESCRT-I depletion on lysosomal morphology, function and signaling (Fig. 5.1). This model will be discussed below.

Collectively, the presented results show that mammalian ESCRT-I proteins maintain the turnover of lysosomal membrane proteins and thereby potentially restrict the size of lysosomes. The lysosomal membrane turnover is yet another source, in addition to endosomal sorting and autophagosome formation [186], from which ESCRT-I provides cargo for lysosomal degradation. Owing to the engagement of ESCRT-I in cargo delivery for lysosomal degradation from various sources, ESCRT-I restricts activation of MiT-TFE transcription factors by inducing their phosphorylation via the Rag GTPase-mTORC1 pathway. Moreover, ESCRT-I is required for proper cholesterol trafficking within the endolysosomal pathway. Because the cellular functions of ESCRT-I are crucial for providing cells with lysosome-derived metabolites, lack of ESCRT-I induces lysosomal nutrient starvation, i.e. impaired supply of nutrients derived from lysosomal degradation.

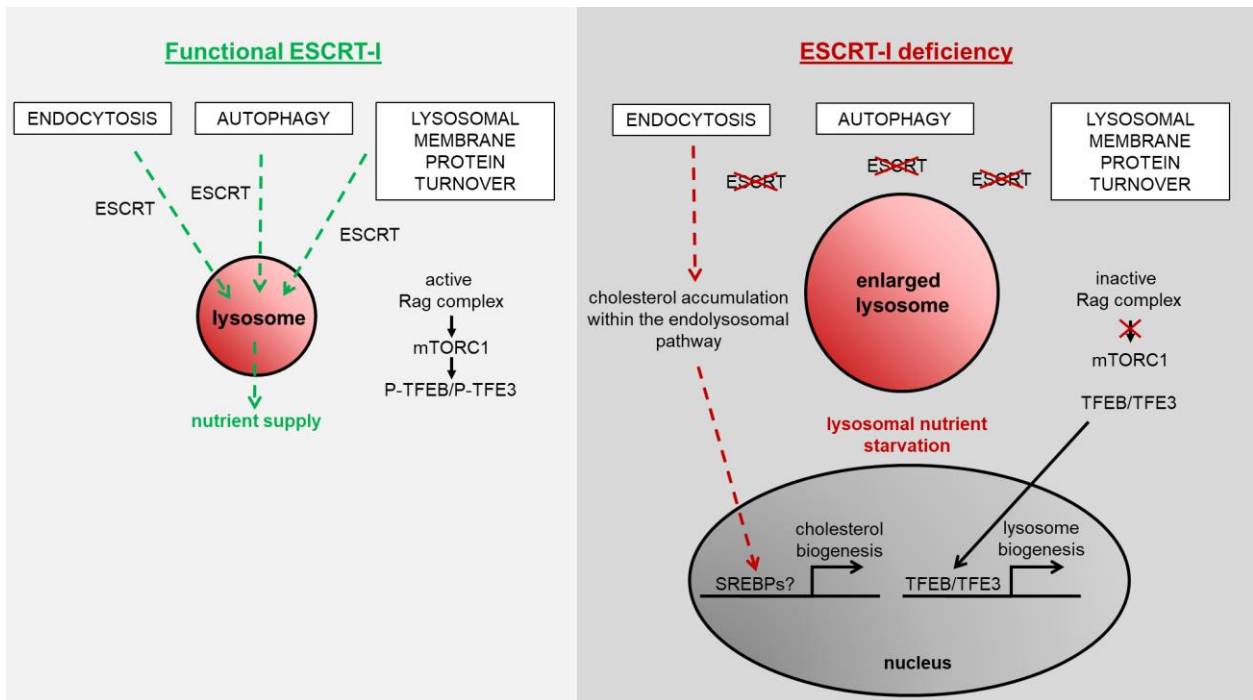


Figure 5.1. Model of the consequences of ESCRT-I depletion for lysosomal homeostasis.

Functional ESCRT-I enables cargo delivery to lysosomes from endocytosis, autophagy and lysosomal membrane protein turnover that allows proper supply of cells with nutrients from lysosomal degradation (left panel).

Lack of ESCRT-I inhibits turnover of lysosomal membrane proteins resulting in enlargement of lysosomes. Impaired cargo delivery to lysosomes from multiple delivery routes, such as cholesterol from endolysosomal trafficking, causes lysosomal nutrient starvation indicated by induction of starvation-like transcriptional responses related to cholesterol biosynthesis and lysosomal biogenesis. In part, these transcriptional changes are regulated via Rag GTPase-mTORC1-dependent TFEB/TFE3 activation (right panel).

5.1. ESCRT-I maintains lysosomal membrane protein turnover potentially thereby restricting size of lysosomes

The discovery presented in this thesis that ESCRT-I is involved in lysosomal membrane turnover was also reported in parallel in a recent publication by Zhang et al. [205]. Together these two studies show that the role of ESCRT components in lysosomal homeostasis goes beyond repairing lysosomal membranes in response to damage [49, 198, 299]. Moreover, the data presented here and by Zhang et al. are consistent with findings describing the role of ESCRT subunits in remodeling of the vacuolar membrane in yeast [200-203, 271]. This indicates that the role of ESCRT proteins in downregulating vacuolar/lysosomal membrane proteins is evolutionary

conserved in yeast and human cells. However, whether this occurs in all animals or in plants remains to be addressed.

The study of Zhang et al. showed that ESCRT components regulate turnover of LAMP1 and RNF152 lysosomal membrane proteins [205]. This thesis describes another target subjected to this mechanism, namely lysosomal Ca^{2+} channel, MCOLN1. Although it is a late endosomal/lysosomal membrane protein [58], GFP-MCOLN1 ectopically expressed in RKO cells was not particularly enriched on its target compartment (Fig. 4.8). Only weak GFP intensity was observed on LAMP1-positive structures and it was similar to that observed on the Golgi apparatus or endosomes, organelles involved in trafficking of newly synthesized membrane proteins to lysosomes [18, 26-29]. Lack of ESCRT-I leads to a marked, three-fold increase of GFP-MCOLN1 intensity on LAMP1-positive structures (Fig. 4.8) and a similarly strong accumulation of this protein was observed in whole cell lysates (Fig. 4.7). Importantly, experiments using BafA1 confirmed that this strong accumulation is due to inhibited lysosomal degradation of the protein (Fig. 4.8). Hence, in control RKO cells, the ectopically expressed GFP-MCOLN1 is very robustly degraded by ESCRT-I-dependent lysosomal membrane turnover. It remains to be verified whether degradation of endogenous MCOLN1 channel is also so fast, however up to date no reliable antibodies are available that would specifically recognize this protein.

The impaired turnover of lysosomal membrane proteins may be the reason for the enlargement of lysosomes upon ESCRT-I depletion. Supporting this notion, Lee et al. discovered that a mechanism of turnover of lysosomal membrane proteins involves invagination of the lysosomal limiting membrane and formation of luminal vesicles, thus regulating lysosomal size [286]. The observed increase in size of LAMP1-positive structures in cells lacking ESCRT-I (Fig. 4.2) is in agreement with previous reports [179, 236, 300]. However, the data presented in this thesis now clarify that the enlarged LAMP1-positive structures include lysosomes as many of these structures are positive for the LysoTracker dye (Fig. 4.3-4.4).

In addition to lack of membrane protein turnover, other intracellular events could potentially also account for lysosomal enlargement in cells lacking ESCRT-I. It may occur due to formation of hybrid endolysosomal organelles, not followed by lysosomal reformation, or as a consequence of increased lipid transfer from the ER that can happen via ER-lysosome contact sites [301, 302].

Enlarged lysosomes can be associated with nutrient starvation [17] or lysosomal dysfunction [303, 304]. Under nutrient-rich conditions, lysosome size may vary from around 0.1 μm to $>1 \mu\text{m}$

in diameter [305]. Serum and glutamine starvation leads to almost doubling of the lysosomal diameter in rat kidney cells [306]. Various types of lysosomal dysfunction may also cause lysosomal enlargement, however accompanied by increased lysosomal pH [304], observed as a lower or a lack of LysoTracker staining intensity. Stronger LysoTracker staining of cells lacking ESCRT-I described here (Fig. 4.3-4.4) shows that the pH of lysosomes is not increased but rather decreased. Moreover, strong LysoTracker staining of enlarged lysosomes upon ESCRT-I deficiency (Fig. 4.3-4.4) indicates that they preserve their integrity, as damaged lysosomes would not maintain their acidic pH [49, 198, 199]. Thus, lysosomal morphology in ESCRT-I-depleted cells exhibits features pointing to the deficiency of nutrients rather than lysosomal dysfunction or damage.

5.2. Delivery of luminal cargo to lysosomes, such as cathepsin D, seems to be not impaired upon ESCRT-I depletion

Detection of active cathepsin D in enlarged LAMP1-positive structures (Fig. 4.5) suggests that lysosomes of ESCRT-I-depleted cells could preserve their ability to degrade cargo. Thus, massive accumulation of ubiquitinated cargo within the endolysosomal pathway (Fig. 4.6) is likely a result of impaired intracellular trafficking of membrane proteins to the lysosomal lumen, rather than inability of lysosomes to degrade cargo. Intriguingly, ESCRT-I depletion was shown to inhibit a correct delivery of carboxypeptidase S to the vacuole in yeast and of cathepsin D to lysosomes in mouse fibroblasts [190]. The discrepancy between the findings presented here regarding cathepsin D trafficking and observations of others may be due to cell-type specific differences in transport of hydrolases. Nevertheless, further investigation needs to be carried out to clarify the actual involvement of ESCRT-I in this process.

As cathepsins are delivered to lysosomes upon their initial transport from the Golgi to late endosomes [6], it is possible that lack of ESCRT-I does not impair the transport of luminal content from late endosomes to lysosomes. This notion is reinforced by the accumulation of exogenous cholesterol in LAMP1-positive compartment observed here (Fig. 4.14). As essentially all enlarged LAMP1-positive structures contained cholesterol it indicates that exogenous cholesterol is able to reach the enlarged lysosomes via endolysosomal trafficking in cells lacking ESCRT-I. Hence, the data presented in this thesis suggest that ESCRT-I depletion inhibits delivery to the lysosomal lumen of cargo from endolysosomal membrane turnover but not of cargo transported inside the

lumen of endosomes. The delivery of luminal cargo into the enlarged lysosomes could occur as a consequence of transient (kiss-and-run) contacts between late endosomes and lysosomes or as a result of fusion between these organelles. Further investigation should address whether any of these events may occur in the absence of ESCRT-I. Nevertheless, these results do not rule out the possibility that luminal cargo, such as hydrolases or cholesterol, could be delivered to the enlarged lysosomes not directly from late endosomes but from other cellular compartments. For instance, cholesterol can be delivered to lysosomes from the ER via ER-lysosome contact sites [302, 307, 308]. However, such an alternative mechanism of lysosomal delivery has not been so far proposed for transport of hydrolases that are believed to reach lysosomes from late endosomes [309].

5.3. ESCRT-I depletion evokes a cholesterol starvation response due to the inhibited efflux of luminal cholesterol from enlarged lysosomes

Depletion of selected components of ESCRT was shown in two studies to cause accumulation of cholesterol on LAMP1-positive structures [300, 310]. The authors of these studies concluded that Hrs (ESCRT-0) and Vps4A/B, but not Tsg101, EAP20 (ESCRT-II) or CHMP6 (ESCRT-III), are specifically involved in cholesterol transport from the endolysosomal pathway, arguing that involvement of Hrs or Vps4A/B in this process is independent of other ESCRT. In contrast to these studies that used HeLa cells, the results presented here show that depletion of Tsg101 or Vps28 subunits in RKO cells leads to accumulation of cholesterol in LAMP1-positive structures. This points out that proper export of cholesterol from the endolysosomal pathway requires functional ESCRT-I proteins. Possibly, the discrepancy between the published data [300] and the results presented here concerning the effect of Tsg101 depletion may be caused by cell type-specific effects.

Upregulated expression of genes related to cholesterol biosynthesis (Fig. 4.9) and enrichment of SREBP target genes among them (Fig. 4.10) support the hypothesis that lack of ESCRT-I inhibits cholesterol efflux from lysosomes, causing a shortage of lysosome-derived cholesterol. Moreover, as reported by the Laboratory of Cell Biology at IIMCB [225], supplementation of ESCRT-I-depleted RKO cells with soluble cholesterol, which bypasses the endolysosomal pathway, prevented the induced expression of cholesterol biosynthesis genes. This confirms the notion that ESCRT-I deficiency impairs cholesterol accumulation at the ER due to impaired cholesterol export from lysosomes, leading to the activation of a „cholesterol starvation”

transcriptional response. However, how exactly ESCRT-I contributes to cholesterol efflux from lysosomes requires further investigation.

5.4. Activation of TFEB and TFE3 factors by Rag GTPase inhibition is likely a hallmark of lysosomal nutrient starvation due to lack of ESCRT-I

The activation of MiT-TFE transcription factor signaling observed in cells lacking ESCRT-I (Fig. 4.9-4.12) is consistent with the reasoning that ESCRT-I depletion leads to the deficiency of nutrients, as nuclear translocation of TFEB or TFE3 was shown to occur upon amino acid starvation and the resulting mTORC1 inhibition [148]. Accordingly, nuclear translocation of these transcription factors in cells lacking ESCRT-I (Fig. 4.11, 4.13) coincides with reduced phosphorylation of TFEB at S122 (Fig. 4.18), that is a target of mTORC1 [148-151]. Moreover, activation of MiT-TFE signaling in these cells occurs due to the inhibition of the Rag GTPase complex (Fig. 4.22, 4.23), that is known to take place upon reduced delivery of amino acids from lysosomes [152].

A specific downregulation of mTORC1 activity towards MiT-TFE factors but not towards its canonical targets upon ESCRT-I depletion (Fig. 4.18) is consistent with studies showing the involvement of Rag GTPase in the substrate-selective regulation of mTORC1 activity [311-314]. This substrate-specific effect could be explained by the mechanism of recruitment of mTOR targets to mTORC1. Structural analysis of S6K and 4E-BP1 revealed that these proteins can interact directly with the Raptor subunit of mTORC1 via a five amino acid region, called the TOR signaling (TOS) motif [79, 315, 316]. In turn, TFEB and TFE3 factors contain a Rag-binding site in their N-terminal regions, but not a TOS motif [152]. Thus, their association with mTORC1 is possible via the interaction with the Rag complex [152]. Of note, TFEB and TFE3 recognition and binding occur only with the active RagA/B^{GTP} and RagC/D^{GDP} state [313]. This could explain the regulation of TFEB phosphorylation via factors modulating the Rag GTPase activity, such as lysosomal nutrient availability. The phosphorylation of canonical mTORC1 targets in cells lacking ESCRT-I is not decreased probably due to mTORC1 association with Rheb. ESCRT-I depletion leads to accumulation of receptors on endosomes and their increased signaling as described [179, 317]. Possibly, receptor-mediated activation of Rheb may promote canonical mTORC1 activation, independently from targeting Rag-binding substrates.

5.5. A potential mechanism underlying regulation of substrate-specific Rag GTPase-dependent mTORC1 signaling may involve several proteins

Differential phosphorylation of mTORC1 substrates raises a question concerning the mechanism that can regulate the specific mTORC1-Rag GTPase-TFEB/TFE3 axis upon ESCRT-I depletion. Amino acids emerge as an important player in the regulation of Rag activation [103, 152, 313]. So far, few proteins were shown to regulate the Rag GTPase activity in response to amino acid levels. For instance, under amino acid-rich conditions lysosomal transmembrane proteins, SLC38A9 and V-type ATPase, promote activation of RagA/B [24, 110-113, 318]. Under amino acid-depleted conditions RNF152-dependent ubiquitination of RagA promotes recruitment of GATOR1 to the Rag GTPase complex and thus its inactivation [319, 320]. Interestingly, lysosomal membrane proteins, including RNF152 [205] and presented in this thesis MCOLN1 (Fig. 4.7-8), were shown to be downregulated in an ESCRT-dependent manner. It is possible that impairment of ESCRT-I-dependent degradation of lysosomal membrane proteins promotes RNF152 accumulation on the lysosomal surface leading to the conversion of RagA into an inactive state, which mimics nutrient-deficient conditions. Additionally, another lysosomal membrane protein PAT1/ SLC36A1, an amino acid transporter, was shown to interact with Rag GTPases [321]. Its overexpression suppressed the activation of mTORC1 under amino acid-rich conditions, likely draining the lysosomal lumen of amino acids [113]. Thus, reduced mTORC1 activity towards MiT-TFE factors in cells lacking ESCRT-I could be potentially caused by lysosomal accumulation of PAT1 or other proteins that can inhibit mTORC1. Under amino acid-rich conditions Rag GTPase is also activated via FLCN and its binding partner FNIP, which convert inactive RagC/D^{GTP} to the active RagC/D^{GDP} state [107, 108]. Given that loss of FLCN function leads to RagC/D inactivation and reduced activity of mTORC1 towards MiT-TFE factors [311-313, 322], it is possible that ESCRT-I depletion inhibits FLCN and/or FNIP function and thus inactivates Rag GTPase dependent-mTORC1 signaling in response to lysosomal nutrient starvation.

In addition to amino acids, Rag GTPase activity can also be modulated by cholesterol. SLC38A9 protein binds lysosomal cholesterol and stimulates Rag GTPase activation in response to cholesterol availability [297]. On the other hand, SLC38A9 also can interact with NPC1 protein and reduce mTORC1 activation upon deficiency of LDL-derived cholesterol. Thus, lysosomal cholesterol can regulate mTORC1 activity via the combined action of a positive regulator,

SLC38A9, and a negative regulator, NPC1. It is possible that lack of ESCRT-I leads to accumulation and increased interaction of SLC38A9 and NPC1 resulting in inactivation of the Rag GTPase-mTORC1-MiT-TFE axis. However, the cholesterol sensing mechanism underlying the control of the GTP/GDP-loading state of the Rag GTPase requires further investigation.

Specific mTORC1 activity towards TFEB, but not the TOS motif-containing substrates S6K and 4E-BP1, was reported in the literature for several pathological conditions. In Birt–Hogg–Dubé syndrome, a genetic disorder caused by loss-of-function mutations in gene encoding FLCN, a GAP for RagC/D, mTORC1 is hyperactivated towards S6K1 and 4E-BP1, but not TFEB [313]. As a result of FLCN depletion, RagC/D is kept inactive (as RagC/D^{GTP}), which leads to reduced MiT-TFE phosphorylation by mTORC1 [313]. Active MiT-TFE factors induce a transcriptional response, including increased expression of the gene encoding RagD, which in turn further promotes mTORC1 activity [323]. Similar dysregulation of mTORC1 substrate activity was reported in TSC disorder, caused by loss-of-function mutations in genes encoding TSC1 or TSC2 [314]. Moreover, mutations in subunits of the homotypic fusion and vacuole protein sorting (HOPS) complex identified in patients with a neurodegenerative phenotype result in the inhibition of mTORC1-dependent phosphorylation of TFE3 and TFEB, and do not reduce phosphorylation of S6K1, 4E-BP1 and Ulk1 [324]. Similarly to ESCRT-I deficiency, mutations in HOPS subunits lead to TFE3 nuclear accumulation, reduced phosphorylation of TFEB, and insufficient cargo delivery to lysosomes manifested by induced expression of MiT-TFE targets, but do not impair lysosomal acidification and activity of lysosomal hydrolases [324]. Collectively, dysregulation of substrate-specific mTORC1 signalling was reported as a hallmark of several human diseases. Because mTORC1 regulates essential biological processes, development of new therapeutic approaches that would affect mTORC1 activity towards selected substrates seems to be needed. Collectively, the data presented here and recent reports point out that ESCRT components and/or Rag GTPase complex and/or its regulators, such as FLCN, may constitute promising targets to selectively modulate mTORC1 function. However, whether selective mTORC1 activity can be druggable requires further investigation. Additional studies are also needed to identify novel mechanisms of recruiting substrates to mTORC1.

In addition to mediating mTORC1 association with lysosomes under nutrient-rich conditions, active Rag GTPase complex promotes recruitment of MiT-TFE factors to lysosomes [152]. The results presented here (Fig. 4.20-4.21) are consistent with the reports showing that

pharmacological inhibition of mTORC1 activity, but not of Rag GTPase, increases association of MiT-TFE factors with lysosomes [150, 152]. Similarly to reduced Rag GTPase-dependent recruitment of MiT-TFE to lysosomes upon starvation [152], lack of ESCRT-I partially prevents TFEB and TFE3 accumulation on lysosomes upon mTORC1 pharmacological inhibition (Fig. 4.20-4.21), likely due to inactivation of Rag GTPase caused by lysosomal nutrient starvation. Of note, the mechanism of Rag GTPase-dependent lysosomal accumulation of TFEB and TFE3 upon mTORC1 inhibition remains poorly described. However, it is possible that mTORC1 inhibition stabilizes Rag-TFEB and Rag-TFE3 interactions and thus slows down TFEB and TFE3 detachment from lysosomes. mTORC1-dependent phosphorylation of TFEB and TFE3 may also be required for destabilization of Rag-TFEB and Rag-TFE3 binding.

Overexpression of constitutively active RagC is sufficient to relocalize TFEB and TFE3 from the nucleus to the cytoplasm in control cells as well as upon ESCRT-I depletion (Fig. 4.22). Similarly, in TSC-deficient cells overexpression of RagC is sufficient to prevent nuclear accumulation of TFEB [314]. This suggests that modulation of the activity of RagC may constitute a promising target to affect MiT-TFE-specific mTORC1 activity in response to trafficking defects and/or impaired integration of signals from the extracellular environment.

5.6. Altered calcineurin activity or cholesterol-induced lysosomal stress are not causative factors of TFEB and TFE3 activation upon lysosomal nutrient starvation

In addition to the regulation by Rag GTPase-dependent mTORC1 signaling, TFEB can be activated via multiple upstream events that modulate its subcellular localization. For example, activation of MCOLN1 Ca^{2+} channel was shown to promote CaN-dependent activation of TFEB and TFE3 factors [46, 54]. In line with this, lysosomal accumulation of MCOLN1 (Fig. 4.8) is associated with nuclear accumulation of TFEB and TFE3 (Fig. 4.11, 4.13) upon ESCRT-I depletion. However, although Ca^{2+} -dependent signaling is required for activation of TFEB and TFE3 upon ESCRT-I depletion (Fig. 4.16-4.17), inhibition of this signaling does not preclude TFEB dephosphorylation at S122 (as presented in the study from the Laboratory of Cell Biology at IIMCB, [293]). This suggests existence of a mechanism other than CaN-dependent dephosphorylation of S122 of TFEB, which regulates its nuclear translocation. For example, a possible mechanism involved in regulation of shuttling of transcription factors between the cytoplasm and the nucleus could involve calcium ions [325, 326]. On the other hand, Ca^{2+} -dependent signaling affects also mTORC1 signaling. As reported by Li et al., lysosomal Ca^{2+}

release via MCOLN1 is required for mTORC1 activation [327]. Thus, inhibition of Ca^{2+} -dependent signaling may at the same time inhibit CaN-dependent dephosphorylation and mTORC1-dependent phosphorylation of TFEB. It is also possible that upon ESCRT-I depletion, TFEB and TFE3 can be dephosphorylated by other phosphatases, such as protein phosphatase 2A (PP2A) and/or protein phosphatase 1 (PPP1) [159]. Some studies reported that inactivation of mTOR leads to an increase in PP2A activity [328-330]. Finally, lack of ESCRT-I reduced the mTORC1-dependent phosphorylation of TFEB to the level comparable to the one observed upon starvation (Fig. 4.18). In ESCRT-I-depleted cells inhibition of Ca^{2+} -dependent signaling might not compensate impaired delivery of nutrients from lysosomal degradation, thus mTORC1 activity towards TFEB cannot be restored. Nevertheless, the exact mechanism of Ca^{2+} -dependent, but CaN-independent, regulation of MiT-TFE activation upon ESCRT-I depletion still remains to be addressed.

Phosphorylation of TFEB not only determines its subcellular localization but can also affect its stability. For instance, TFEB phosphorylation at S142 and S211, that sequesters it in the cytoplasm, was also shown to promote its proteasomal degradation [331, 332]. Hence, increased levels of TFEB and TFE3 proteins (Fig. 4.11) could result from their stabilization due to decreased phosphorylation. As the mRNA levels of TFEB and TFE3 upon ESCRT-I depletion are not significantly increased (Fig. 4.12 and not presented transcriptomic data), the observed elevated protein levels of these transcription factors are unlikely to be caused by a positive autoregulatory feedback loop.

In contrast to the implication of Ca^{2+} -dependent signaling in MiT-TFE activation, the involvement of lipids is less known. Boutry et al. reported that cholesterol accumulation in severe form of hereditary spastic paraplegia caused by the loss of spatacsin function promotes nuclear translocation of TFEB [294]. However, inhibition of endocytic uptake of exogenous cholesterol reduces cholesterol accumulation in cells lacking ESCRT-I (Fig. 4.14) but does not prevent MiT-TFE activation (Fig. 4.15). This suggests that abnormal cholesterol accumulation is not a causative factor for MiT-TFE nuclear translocation upon ESCRT-I depletion.

Cholesterol accumulation within the endolysosomal pathway is also a characteristic feature of NPC disease. In a cellular model of this lysosomal storage disease, mTORC1 was shown to be hyperactivated [333]. Castellano et al. proposed that cholesterol stimulates mTORC1 activity via lysosomal amino acid permease SLC38A9 [297]. They showed that sterol depletion, which may

resemble “cholesterol starvation” observed upon ESCRT-I depletion, promoted mTORC1 inactivation and nuclear accumulation of TFEB [297]. Thus inaccessibility of lysosome-derived cholesterol may constitute a common feature of ESCRT-I-depleted cells and NPC disease. However, how supplementation of cells with soluble cholesterol affects TFEB and TFE3 activation upon ESCRT-I depletion remains to be addressed.

Lack of ESCRT-I leads to massive intracellular accumulation of cargoes, such as ubiquitinated proteins and cholesterol (Fig. 4.6, 4.14). Despite the availability of amino acids and lipids in culture medium and unperturbed canonical mTORC1 activity (Fig. 4.18), ESCRT-I-depleted cells induce transcriptional responses characteristic of nutrient-depleted conditions (Fig. 4.9). This indicates that ESCRT-I-dependent delivery of nutrients and their efflux from lysosomes may be sensed via a specific mechanism, which is independent from the canonical mTORC1 activity.

5.7. Regulation of basal MiT-TFE signalling in cancer cells relies on Rag GTPase activity and availability of exogenous lipids

The obtained results showed that the regulation of MiT-TFE signaling is context-dependent and that different mechanisms underlie its activation in cells with functional ESCRT-I as compared to ESCRT-I-deficient conditions. The data presented here demonstrate that the availability of exogenous lipids is a crucial factor for basal TFEB and TFE3 activation (Fig. 4.15). Additionally, constitutive activation of RagC strongly induces phosphorylation of TFEB at S122 (Fig. 4.23) and completely prevents TFEB and TFE3 nuclear localization under all tested conditions (Fig. 4.22). In turn, inhibition of Ca^{2+} dependent signaling does not reduce the basal TFEB and TFE3 activation (Fig. 4.16-4.17). This suggests that in cancer cells, basal activation of TFEB and TFE3 is not regulated by Ca^{2+} . It is possible that an oncogenic mechanism which regulates their basal accumulation in the nucleus utilizes exogenous lipids and the activity of the mTORC1-Rag GTPase pathway.

The involvement of Ca^{2+} -CaN-dependent signaling in the activation of MiT-TFE was previously reported in the context of stress-induced responses, such as oxidative stress or integrated stress response [54, 55]. However, in the experiments shown here, chelation of an intracellular pool of Ca^{2+} and inhibition of CaN and MCOLN1 activity do not reduce but instead promote TFEB and TFE3 nuclear translocation under basal conditions (Fig. 4.16-4.17). Moreover, as reported by the Laboratory of Cell Biology at IIMCB, these conditions reduce TFEB

phosphorylation at S122, which could not be explained by inhibiting phosphatase activity [293]. Instead, Li et al. reported that Ca^{2+} -dependent signaling is required for the mTORC1 activity, showing another local function of Ca^{2+} [327]. The fact that neither in control nor ESCRT-I-depleted cells is calcineurin involved in TFEB phosphorylation at S122 [293] and MiT-TFE activation (Fig. 4.17), suggests an involvement of another regulatory mechanism, such as Ca^{2+} -dependent regulation of mTORC1 activity.

6. Future prospects

The data presented in this thesis describe a new role of ESCRT-I proteins in maintaining lysosomal homeostasis and show consequences of ESCRT-I depletion for lysosome-related signaling. These findings pose several questions that should be addressed to understand their further relevance and mechanistic details.

The results demonstrated in this thesis provide insights into a homeostatic response induced upon ESCRT-I deficiency, including MiT-TFE signaling. In many types of cancer, downregulation of ESCRT proteins correlates with poor patient prognosis [221]. Thus, it is possible that deficiency of ESCRT components may support cancer growth and spreading via promoting lysosomal biogenesis and autophagy. But, it is also plausible that targeting ESCRT-I function may particularly impair growth of cancer cells that strongly rely on their lysosomal function. Individual and/or concurrent inhibition of ESCRT function and MiT-TFE signaling via chemical or genetic approaches may induce cell death that could be tested using cell viability assays.

So far, the role of ESCRT proteins in degradation of lysosomal membrane proteins was directly shown only for a limited number of such substrates[205, 293]. Thus, identifying the subset of lysosomal membrane proteins regulated by ESCRT components could shed new light on signaling cascades and/or processes regulated by endocytic proteins. Such identification could be achieved by mass spectrometry analysis of lysosomes isolated from ESCRT-I-depleted cells using for example the Lyso-IP method [334].

The data presented here also show that in cells lacking ESCRT-I, luminal cargo, such as cholesterol, may reach lysosomes but cannot be released to other cellular destinations. But how ESCRT-I mediates cholesterol efflux from lysosomes remains unanswered. It is possible that components of ESCRT-I enable cholesterol transport between ER and lysosomes by inducing the formation of contact sites between these organelles [301]. To verify this possibility, confocal microscopy analysis of recruitment of ER markers (e.g. GFP-tagged VAPA protein) to lysosomes and/or imaging of lysosome-ER contact sites by electron microscopy upon ESCRT-I depletion should be considered.

Another important area for further studies concerns the mechanism of lysosomal nutrient starvation. It remains vague which proteins sense lysosomal nutrient starvation. Based on literature data, a likely candidate involved in the regulation of mTORC1 activity specific towards MiT-TFE

factors seems to be FLCN and/or its interacting partner FNIP [313, 335]. However, the role of other proteins cannot be excluded.

Addressing the issues described above will increase our understanding of mechanical basics of ESCRT-dependent regulation of lysosomal homeostasis and may point to potential strategies for targeting such regulations for therapeutic purposes.

7. Summary and conclusions

The data presented in this dissertation provide insights into the involvement of ESCRT-I proteins in maintenance of lysosomal homeostasis and characterize the consequences of ESCRT-I depletion on lysosomal morphology and function, as well as lysosome-related signalling. Specifically, the results indicate that:

- 1) ESCRT-I restricts the size of lysosomes.
- 2) ESCRT-I is involved in selective degradation of lysosomal membrane proteins, including MCOLN1 Ca²⁺ channel.
- 3) In ESCRT-I-depleted cells lysosomes are likely functional and luminal cargoes, such as cathepsin D or cholesterol, are delivered into lysosomes.
- 4) Depletion of ESCRT-I leads to increased nuclear accumulation of MiT-TFE transcription factors (TFEB and TFE3) and elevated expression of their target genes involved in lysosomal biogenesis and autophagy.
- 5) Depletion of ESCRT-I causes massive accumulation of cholesterol within the endolysosomal pathway and induces expression of cholesterol biosynthesis genes.
- 6) Abnormal accumulation of endocytosed cholesterol is not a causative factor for the activation of MiT-TFE transcription factors upon ESCRT-I depletion.
- 7) Ca²⁺-dependent signaling, but not CaN-dependent dephosphorylation, is required for activation of TFEB and TFE3 upon ESCRT-I depletion.
- 8) Lack of ESCRT-I does not affect the general mTORC1 activity.
- 9) ESCRT-I restricts nuclear translocation of TFEB and TFE3 factors by maintaining the activation of the non-canonical Rag GTPase-dependent mTORC1 pathway.

Based on the results presented in this thesis, it is proposed that ESCRT-I is required for proper delivery of nutrients derived from lysosomal degradation to restrict activation of MiT-TFE factors via the Rag GTPase-mTORC1 signaling pathway.

8. Literature

1. Sigismund S, Confalonieri S, Ciliberto A, Polo S, Scita G, Di Fiore PP: Endocytosis and signaling: cell logistics shape the eukaryotic cell plan. *Physiological reviews* 2012, 92(1):273-366.
2. Huotari J, Helenius A: Endosome maturation. *EMBO J* 2011, 30(17):3481-3500.
3. Cullen PJ, Steinberg F: To degrade or not to degrade: mechanisms and significance of endocytic recycling. *Nat Rev Mol Cell Biol* 2018, 19(11):679-696.
4. Raiborg C, Stenmark H: The ESCRT machinery in endosomal sorting of ubiquitylated membrane proteins. *Nature* 2009, 458(7237):445-452.
5. Luzio JP, Pryor PR, Bright NA: Lysosomes: fusion and function. *Nat Rev Mol Cell Biol* 2007, 8(8):622-632.
6. Trivedi PC, Bartlett JJ, Pulinilkunnil T: Lysosomal Biology and Function: Modern View of Cellular Debris Bin. *Cells* 2020, 9(5).
7. Saffi GT, Botelho RJ: Lysosome Fission: Planning for an Exit. *Trends in cell biology* 2019, 29(8):635-646.
8. Langemeyer L, Frohlich F, Ungermann C: Rab GTPase Function in Endosome and Lysosome Biogenesis. *Trends in cell biology* 2018, 28(11):957-970.
9. Christoforidis S, McBride HM, Burgoyne RD, Zerial M: The Rab5 effector EEA1 is a core component of endosome docking. *Nature* 1999, 397(6720):621-625.
10. Wilson JM, de Hoop M, Zorzi N, Toh BH, Dotti CG, Parton RG: EEA1, a tethering protein of the early sorting endosome, shows a polarized distribution in hippocampal neurons, epithelial cells, and fibroblasts. *Molecular biology of the cell* 2000, 11(8):2657-2671.
11. Shin HW, Hayashi M, Christoforidis S, Lacas-Gervais S, Hoepfner S, Wenk MR, Modregger J, Uttenweiler-Joseph S, Wilm M, Nystuen A *et al*: An enzymatic cascade of Rab5 effectors regulates phosphoinositide turnover in the endocytic pathway. *J Cell Biol* 2005, 170(4):607-618.
12. Rink J, Ghigo E, Kalaidzidis Y, Zerial M: Rab conversion as a mechanism of progression from early to late endosomes. *Cell* 2005, 122(5):735-749.
13. Hu YB, Dammer EB, Ren RJ, Wang G: The endosomal-lysosomal system: from acidification and cargo sorting to neurodegeneration. *Translational neurodegeneration* 2015, 4:18.
14. Wallroth A, Haucke V: Phosphoinositide conversion in endocytosis and the endolysosomal system. *The Journal of biological chemistry* 2018, 293(5):1526-1535.
15. Barral DC, Staiano L, Guimas Almeida C, Cutler DF, Eden ER, Futter CE, Galione A, Marques ARA, Medina DL, Napolitano G *et al*: Current methods to analyze lysosome morphology, positioning, motility and function. *Traffic* 2022, 23(5):238-269.
16. Appelqvist H, Waster P, Kagedal K, Ollinger K: The lysosome: from waste bag to potential therapeutic target. *Journal of molecular cell biology* 2013, 5(4):214-226.
17. Xu H, Ren D: Lysosomal physiology. *Annual review of physiology* 2015, 77:57-80.

18. Saftig P, Klumperman J: Lysosome biogenesis and lysosomal membrane proteins: trafficking meets function. *Nat Rev Mol Cell Biol* 2009, 10(9):623-635.
19. Zaidi N, Maurer A, Nieke S, Kalbacher H: Cathepsin D: a cellular roadmap. *Biochemical and biophysical research communications* 2008, 376(1):5-9.
20. Bouhamdani N, Comeau D, Turcotte S: A Compendium of Information on the Lysosome. *Front Cell Dev Biol* 2021, 9:798262.
21. Kalatzis V, Cherqui S, Antignac C, Gasnier B: Cystinosis, the protein defective in cystinosis, is a H(+)-driven lysosomal cystine transporter. *EMBO J* 2001, 20(21):5940-5949.
22. Liu B, Du H, Rutkowski R, Gartner A, Wang X: LAAT-1 is the lysosomal lysine/arginine transporter that maintains amino acid homeostasis. *Science* 2012, 337(6092):351-354.
23. Sagne C, Agulhon C, Ravassard P, Darmon M, Hamon M, El Mestikawy S, Gasnier B, Giros B: Identification and characterization of a lysosomal transporter for small neutral amino acids. *Proc Natl Acad Sci U S A* 2001, 98(13):7206-7211.
24. Wang S, Tsun ZY, Wolfson RL, Shen K, Wyant GA, Plovovich ME, Yuan ED, Jones TD, Chantranupong L, Comb W *et al*: Metabolism. Lysosomal amino acid transporter SLC38A9 signals arginine sufficiency to mTORC1. *Science* 2015, 347(6218):188-194.
25. Verdon Q, Boonen M, Ribes C, Jadot M, Gasnier B, Sagne C: SNAT7 is the primary lysosomal glutamine exporter required for extracellular protein-dependent growth of cancer cells. *Proc Natl Acad Sci U S A* 2017, 114(18):E3602-E3611.
26. Janvier K, Bonifacino JS: Role of the endocytic machinery in the sorting of lysosome-associated membrane proteins. *Molecular biology of the cell* 2005, 16(9):4231-4242.
27. Pryor PR, Reimann F, Gribble FM, Luzio JP: Mucopolin-1 is a lysosomal membrane protein required for intracellular lactosylceramide traffic. *Traffic* 2006, 7(10):1388-1398.
28. Vergarajauregui S, Puertollano R: Two di-leucine motifs regulate trafficking of mucopolin-1 to lysosomes. *Traffic* 2006, 7(3):337-353.
29. Miedel MT, Weixel KM, Bruns JR, Traub LM, Weisz OA: Posttranslational cleavage and adaptor protein complex-dependent trafficking of mucopolin-1. *The Journal of biological chemistry* 2006, 281(18):12751-12759.
30. Mindell JA: Lysosomal acidification mechanisms. *Annual review of physiology* 2012, 74:69-86.
31. Khalkhali-Ellis Z, Hendrix MJ: Two Faces of Cathepsin D: Physiological Guardian Angel and Pathological Demon. *Biol Med (Aligarh)* 2014, 6(2).
32. Wang R, Wang J, Hassan A, Lee CH, Xie XS, Li X: Molecular basis of V-ATPase inhibition by bafilomycin A1. *Nat Commun* 2021, 12(1):1782.
33. Schwake M, Schroder B, Saftig P: Lysosomal membrane proteins and their central role in physiology. *Traffic* 2013, 14(7):739-748.
34. Ikonen E: Cellular cholesterol trafficking and compartmentalization. *Nat Rev Mol Cell Biol* 2008, 9(2):125-138.

35. Luo J, Yang H, Song BL: Mechanisms and regulation of cholesterol homeostasis. *Nat Rev Mol Cell Biol* 2020, 21(4):225-245.
36. Zhang H: Lysosomal acid lipase and lipid metabolism: new mechanisms, new questions, and new therapies. *Current opinion in lipidology* 2018, 29(3):218-223.
37. Meng Y, Heybrock S, Neculai D, Saftig P: Cholesterol Handling in Lysosomes and Beyond. *Trends in cell biology* 2020, 30(6):452-466.
38. Pfeffer SR: NPC intracellular cholesterol transporter 1 (NPC1)-mediated cholesterol export from lysosomes. *The Journal of biological chemistry* 2019, 294(5):1706-1709.
39. Li J, Pfeffer SR: Lysosomal membrane glycoproteins bind cholesterol and contribute to lysosomal cholesterol export. *Elife* 2016, 5.
40. Heybrock S, Kanerva K, Meng Y, Ing C, Liang A, Xiong ZJ, Weng X, Ah Kim Y, Collins R, Trimble W *et al*: Lysosomal integral membrane protein-2 (LIMP-2/SCARB2) is involved in lysosomal cholesterol export. *Nat Commun* 2019, 10(1):3521.
41. Luo J, Jiang LY, Yang H, Song BL: Intracellular Cholesterol Transport by Sterol Transfer Proteins at Membrane Contact Sites. *Trends Biochem Sci* 2019, 44(3):273-292.
42. Horton JD, Goldstein JL, Brown MS: SREBPs: activators of the complete program of cholesterol and fatty acid synthesis in the liver. *J Clin Invest* 2002, 109(9):1125-1131.
43. Yang J, Zhao Z, Gu M, Feng X, Xu H: Release and uptake mechanisms of vesicular Ca(2+) stores. *Protein & cell* 2019, 10(1):8-19.
44. Garrity AG, Wang W, Collier CM, Levey SA, Gao Q, Xu H: The endoplasmic reticulum, not the pH gradient, drives calcium refilling of lysosomes. *Elife* 2016, 5.
45. Carafoli E: Calcium signaling: a tale for all seasons. *Proc Natl Acad Sci U S A* 2002, 99(3):1115-1122.
46. Medina DL, Di Paola S, Peluso I, Armani A, De Stefani D, Venditti R, Montefusco S, Scotto-Rosato A, Prezioso C, Forrester A *et al*: Lysosomal calcium signalling regulates autophagy through calcineurin and TFEB. *Nature cell biology* 2015, 17(3):288-299.
47. Scotto Rosato A, Montefusco S, Soldati C, Di Paola S, Capuozzo A, Monfregola J, Polishchuk E, Amabile A, Grimm C, Lombardo A *et al*: TRPML1 links lysosomal calcium to autophagosome biogenesis through the activation of the CaMKKbeta/VPS34 pathway. *Nat Commun* 2019, 10(1):5630.
48. Li X, Rydzewski N, Hider A, Zhang X, Yang J, Wang W, Gao Q, Cheng X, Xu H: A molecular mechanism to regulate lysosome motility for lysosome positioning and tubulation. *Nature cell biology* 2016, 18(4):404-417.
49. Skowyra ML, Schlesinger PH, Naismith TV, Hanson PI: Triggered recruitment of ESCRT machinery promotes endolysosomal repair. *Science* 2018, 360(6384).
50. Pryor PR, Mullock BM, Bright NA, Gray SR, Luzio JP: The role of intraorganellar Ca(2+) in late endosome-lysosome heterotypic fusion and in the reformation of lysosomes from hybrid organelles. *J Cell Biol* 2000, 149(5):1053-1062.

51. Samie M, Wang X, Zhang X, Goschka A, Li X, Cheng X, Gregg E, Azar M, Zhuo Y, Garrity AG *et al*: A TRP channel in the lysosome regulates large particle phagocytosis via focal exocytosis. *Dev Cell* 2013, 26(5):511-524.
52. Melchionda M, Pittman JK, Mayor R, Patel S: Ca²⁺/H⁺ exchange by acidic organelles regulates cell migration in vivo. *J Cell Biol* 2016, 212(7):803-813.
53. Creamer TP: Calcineurin. *Cell communication and signaling : CCS* 2020, 18(1):137.
54. Zhang X, Cheng X, Yu L, Yang J, Calvo R, Patnaik S, Hu X, Gao Q, Yang M, Lawas M *et al*: MCOLN1 is a ROS sensor in lysosomes that regulates autophagy. *Nat Commun* 2016, 7:12109.
55. Martina JA, Diab HI, Brady OA, Puertollano R: TFEB and TFE3 are novel components of the integrated stress response. *EMBO J* 2016, 35(5):479-495.
56. Park K, Lim H, Kim J, Hwang Y, Lee YS, Bae SH, Kim H, Kang SW, Kim JY, Lee MS: Lysosomal Ca²⁺-mediated TFEB activation modulates mitophagy and functional adaptation of pancreatic beta-cells to metabolic stress. *Nat Commun* 2022, 13(1):1300.
57. Azzi JR, Sayegh MH, Mallat SG: Calcineurin inhibitors: 40 years later, can't live without. *J Immunol* 2013, 191(12):5785-5791.
58. Wang W, Zhang X, Gao Q, Xu H: TRPML1: an ion channel in the lysosome. *Handbook of experimental pharmacology* 2014, 222:631-645.
59. Dong XP, Cheng X, Mills E, Delling M, Wang F, Kurz T, Xu H: The type IV mucopolipidosis-associated protein TRPML1 is an endolysosomal iron release channel. *Nature* 2008, 455(7215):992-996.
60. Eichelsdoerfer JL, Evans JA, Slaugenhaupt SA, Cuajungco MP: Zinc dyshomeostasis is linked with the loss of mucopolipidosis IV-associated TRPML1 ion channel. *The Journal of biological chemistry* 2010, 285(45):34304-34308.
61. Dong XP, Wang X, Shen D, Chen S, Liu M, Wang Y, Mills E, Cheng X, Delling M, Xu H: Activating mutations of the TRPML1 channel revealed by proline-scanning mutagenesis. *The Journal of biological chemistry* 2009, 284(46):32040-32052.
62. LaPlante JM, Sun M, Falardeau J, Dai D, Brown EM, Slaugenhaupt SA, Vassilev PM: Lysosomal exocytosis is impaired in mucopolipidosis type IV. *Molecular genetics and metabolism* 2006, 89(4):339-348.
63. Medina DL, Fraldi A, Bouche V, Annunziata F, Mansueto G, Spanpanato C, Puri C, Pignata A, Martina JA, Sardiello M *et al*: Transcriptional activation of lysosomal exocytosis promotes cellular clearance. *Dev Cell* 2011, 21(3):421-430.
64. Vergarajauregui S, Connelly PS, Daniels MP, Puertollano R: Autophagic dysfunction in mucopolipidosis type IV patients. *Human molecular genetics* 2008, 17(17):2723-2737.
65. Curcio-Morelli C, Charles FA, Micsenyi MC, Cao Y, Venugopal B, Browning MF, Dobrenis K, Cotman SL, Walkley SU, Slaugenhaupt SA: Macroautophagy is defective in mucopolipin-1-deficient mouse neurons. *Neurobiology of disease* 2010, 40(2):370-377.
66. Chen CS, Bach G, Pagano RE: Abnormal transport along the lysosomal pathway in mucopolipidosis, type IV disease. *Proc Natl Acad Sci U S A* 1998, 95(11):6373-6378.

67. Shen D, Wang X, Li X, Zhang X, Yao Z, Dibble S, Dong XP, Yu T, Lieberman AP, Showalter HD *et al*: Lipid storage disorders block lysosomal trafficking by inhibiting a TRP channel and lysosomal calcium release. *Nat Commun* 2012, 3:731.
68. Bargal R, Avidan N, Ben-Asher E, Olender Z, Zeigler M, Frumkin A, Raas-Rothschild A, Glusman G, Lancet D, Bach G: Identification of the gene causing mucopolidosis type IV. *Nature genetics* 2000, 26(1):118-123.
69. Sun M, Goldin E, Stahl S, Falardeau JL, Kennedy JC, Acierno JS, Jr., Bove C, Kaneski CR, Nagle J, Bromley MC *et al*: Mucopolidosis type IV is caused by mutations in a gene encoding a novel transient receptor potential channel. *Human molecular genetics* 2000, 9(17):2471-2478.
70. Bassi MT, Manzoni M, Monti E, Pizzo MT, Ballabio A, Borsani G: Cloning of the gene encoding a novel integral membrane protein, mucopolidin-and identification of the two major founder mutations causing mucopolidosis type IV. *American journal of human genetics* 2000, 67(5):1110-1120.
71. Dong XP, Shen D, Wang X, Dawson T, Li X, Zhang Q, Cheng X, Zhang Y, Weisman LS, Delling M *et al*: PI(3,5)P(2) controls membrane trafficking by direct activation of mucolipin Ca(2+) release channels in the endolysosome. *Nat Commun* 2010, 1(4):38.
72. Zhang X, Li X, Xu H: Phosphoinositide isoforms determine compartment-specific ion channel activity. *Proc Natl Acad Sci U S A* 2012, 109(28):11384-11389.
73. Chen CC, Keller M, Hess M, Schiffmann R, Urban N, Wolfgardt A, Schaefer M, Bracher F, Biel M, Wahl-Schott C *et al*: A small molecule restores function to TRPML1 mutant isoforms responsible for mucopolidosis type IV. *Nat Commun* 2014, 5:4681.
74. Zhang X, Chen W, Gao Q, Yang J, Yan X, Zhao H, Su L, Yang M, Gao C, Yao Y *et al*: Rapamycin directly activates lysosomal mucolipin TRP channels independent of mTOR. *PLoS biology* 2019, 17(5):e3000252.
75. Plesch E, Chen CC, Butz E, Scotto Rosato A, Krogsaeter EK, Yinan H, Bartel K, Keller M, Robaa D, Teupser D *et al*: Selective agonist of TRPML2 reveals direct role in chemokine release from innate immune cells. *Elife* 2018, 7.
76. Grimm C, Jors S, Saldanha SA, Obukhov AG, Pan B, Oshima K, Cuajungco MP, Chase P, Hodder P, Heller S: Small molecule activators of TRPML3. *Chemistry & biology* 2010, 17(2):135-148.
77. Leser C, Keller M, Gerndt S, Urban N, Chen CC, Schaefer M, Grimm C, Bracher F: Chemical and pharmacological characterization of the TRPML calcium channel blockers ML-SI1 and ML-SI3. *European journal of medicinal chemistry* 2021, 210:112966.
78. Liu GY, Sabatini DM: mTOR at the nexus of nutrition, growth, ageing and disease. *Nat Rev Mol Cell Biol* 2020, 21(4):183-203.
79. Nojima H, Tokunaga C, Eguchi S, Oshiro N, Hidayat S, Yoshino K, Hara K, Tanaka N, Avruch J, Yonezawa K: The mammalian target of rapamycin (mTOR) partner, raptor, binds the mTOR substrates p70 S6 kinase and 4E-BP1 through their TOR signaling (TOS) motif. *The Journal of biological chemistry* 2003, 278(18):15461-15464.

80. Kim DH, Sarbassov DD, Ali SM, Latek RR, Guntur KV, Erdjument-Bromage H, Tempst P, Sabatini DM: GbetaL, a positive regulator of the rapamycin-sensitive pathway required for the nutrient-sensitive interaction between raptor and mTOR. *Molecular cell* 2003, 11(4):895-904.
81. Sancak Y, Thoreen CC, Peterson TR, Lindquist RA, Kang SA, Spooner E, Carr SA, Sabatini DM: PRAS40 is an insulin-regulated inhibitor of the mTORC1 protein kinase. *Molecular cell* 2007, 25(6):903-915.
82. Peterson TR, Laplante M, Thoreen CC, Sancak Y, Kang SA, Kuehl WM, Gray NS, Sabatini DM: DEPTOR is an mTOR inhibitor frequently overexpressed in multiple myeloma cells and required for their survival. *Cell* 2009, 137(5):873-886.
83. Choi J, Chen J, Schreiber SL, Clardy J: Structure of the FKBP12-rapamycin complex interacting with the binding domain of human FRAP. *Science* 1996, 273(5272):239-242.
84. Sarbassov DD, Ali SM, Sengupta S, Sheen JH, Hsu PP, Bagley AF, Markhard AL, Sabatini DM: Prolonged rapamycin treatment inhibits mTORC2 assembly and Akt/PKB. *Molecular cell* 2006, 22(2):159-168.
85. Zheng Y, Jiang Y: mTOR Inhibitors at a Glance. *Molecular and cellular pharmacology* 2015, 7(2):15-20.
86. Sabatini DM: Twenty-five years of mTOR: Uncovering the link from nutrients to growth. *Proc Natl Acad Sci U S A* 2017, 114(45):11818-11825.
87. Gingras AC, Gygi SP, Raught B, Polakiewicz RD, Abraham RT, Hoekstra MF, Aebersold R, Sonenberg N: Regulation of 4E-BP1 phosphorylation: a novel two-step mechanism. *Genes & development* 1999, 13(11):1422-1437.
88. Jefferies HB, Fumagalli S, Dennis PB, Reinhard C, Pearson RB, Thomas G: Rapamycin suppresses 5'TOP mRNA translation through inhibition of p70s6k. *EMBO J* 1997, 16(12):3693-3704.
89. Kim DH, Sarbassov DD, Ali SM, King JE, Latek RR, Erdjument-Bromage H, Tempst P, Sabatini DM: mTOR interacts with raptor to form a nutrient-sensitive complex that signals to the cell growth machinery. *Cell* 2002, 110(2):163-175.
90. Raught B, Peiretti F, Gingras AC, Livingstone M, Shahbazian D, Mayeur GL, Polakiewicz RD, Sonenberg N, Hershey JW: Phosphorylation of eucaryotic translation initiation factor 4B Ser422 is modulated by S6 kinases. *EMBO J* 2004, 23(8):1761-1769.
91. Shahbazian D, Roux PP, Mieulet V, Cohen MS, Raught B, Taunton J, Hershey JW, Blenis J, Pende M, Sonenberg N: The mTOR/PI3K and MAPK pathways converge on eIF4B to control its phosphorylation and activity. *EMBO J* 2006, 25(12):2781-2791.
92. Caron A, Richard D, Laplante M: The Roles of mTOR Complexes in Lipid Metabolism. *Annual review of nutrition* 2015, 35:321-348.
93. Peterson TR, Sengupta SS, Harris TE, Carmack AE, Kang SA, Balderas E, Guertin DA, Madden KL, Carpenter AE, Finck BN *et al*: mTOR complex 1 regulates lipin 1 localization to control the SREBP pathway. *Cell* 2011, 146(3):408-420.

94. Dodd KM, Yang J, Shen MH, Sampson JR, Tee AR: mTORC1 drives HIF-1alpha and VEGF-A signalling via multiple mechanisms involving 4E-BP1, S6K1 and STAT3. *Oncogene* 2015, 34(17):2239-2250.
95. Duvel K, Yecies JL, Menon S, Raman P, Lipovsky AI, Souza AL, Triantafellow E, Ma Q, Gorski R, Cleaver S *et al*: Activation of a metabolic gene regulatory network downstream of mTOR complex 1. *Molecular cell* 2010, 39(2):171-183.
96. de la Cruz Lopez KG, Toledo Guzman ME, Sanchez EO, Garcia Carranca A: mTORC1 as a Regulator of Mitochondrial Functions and a Therapeutic Target in Cancer. *Frontiers in oncology* 2019, 9:1373.
97. Puente C, Hendrickson RC, Jiang X: Nutrient-regulated Phosphorylation of ATG13 Inhibits Starvation-induced Autophagy. *The Journal of biological chemistry* 2016, 291(11):6026-6035.
98. Kim J, Kundu M, Viollet B, Guan KL: AMPK and mTOR regulate autophagy through direct phosphorylation of Ulk1. *Nature cell biology* 2011, 13(2):132-141.
99. Mizushima N, Yoshimori T, Levine B: Methods in mammalian autophagy research. *Cell* 2010, 140(3):313-326.
100. Kim J, Kim E: Rag GTPase in amino acid signaling. *Amino acids* 2016, 48(4):915-928.
101. Bar-Peled L, Schweitzer LD, Zoncu R, Sabatini DM: Ragulator is a GEF for the rag GTPases that signal amino acid levels to mTORC1. *Cell* 2012, 150(6):1196-1208.
102. Sancak Y, Bar-Peled L, Zoncu R, Markhard AL, Nada S, Sabatini DM: Ragulator-Rag complex targets mTORC1 to the lysosomal surface and is necessary for its activation by amino acids. *Cell* 2010, 141(2):290-303.
103. Sancak Y, Peterson TR, Shaul YD, Lindquist RA, Thoreen CC, Bar-Peled L, Sabatini DM: The Rag GTPases bind raptor and mediate amino acid signaling to mTORC1. *Science* 2008, 320(5882):1496-1501.
104. Kim E, Goraksha-Hicks P, Li L, Neufeld TP, Guan KL: Regulation of TORC1 by Rag GTPases in nutrient response. *Nature cell biology* 2008, 10(8):935-945.
105. Bar-Peled L, Chantranupong L, Cherniack AD, Chen WW, Ottina KA, Grabiner BC, Spear ED, Carter SL, Meyerson M, Sabatini DM: A Tumor suppressor complex with GAP activity for the Rag GTPases that signal amino acid sufficiency to mTORC1. *Science* 2013, 340(6136):1100-1106.
106. Panchaud N, Peli-Gulli MP, De Virgilio C: Amino acid deprivation inhibits TORC1 through a GTPase-activating protein complex for the Rag family GTPase Gtr1. *Sci Signal* 2013, 6(277):ra42.
107. Petit CS, Rocznik-Ferguson A, Ferguson SM: Recruitment of folliculin to lysosomes supports the amino acid-dependent activation of Rag GTPases. *J Cell Biol* 2013, 202(7):1107-1122.
108. Tsun ZY, Bar-Peled L, Chantranupong L, Zoncu R, Wang T, Kim C, Spooner E, Sabatini DM: The folliculin tumor suppressor is a GAP for the RagC/D GTPases that signal amino acid levels to mTORC1. *Molecular cell* 2013, 52(4):495-505.

109. Han JM, Jeong SJ, Park MC, Kim G, Kwon NH, Kim HK, Ha SH, Ryu SH, Kim S: Leucyl-tRNA synthetase is an intracellular leucine sensor for the mTORC1-signaling pathway. *Cell* 2012, 149(2):410-424.
110. Shen K, Sabatini DM: Ragulator and SLC38A9 activate the Rag GTPases through noncanonical GEF mechanisms. *Proc Natl Acad Sci U S A* 2018, 115(38):9545-9550.
111. Wyant GA, Abu-Remaileh M, Wolfson RL, Chen WW, Freinkman E, Danai LV, Vander Heiden MG, Sabatini DM: mTORC1 Activator SLC38A9 Is Required to Efflux Essential Amino Acids from Lysosomes and Use Protein as a Nutrient. *Cell* 2017, 171(3):642-654 e612.
112. Rebsamen M, Pochini L, Stasyk T, de Araujo ME, Galluccio M, Kandasamy RK, Snijder B, Fauster A, Rudashevskaya EL, Bruckner M *et al*: SLC38A9 is a component of the lysosomal amino acid sensing machinery that controls mTORC1. *Nature* 2015, 519(7544):477-481.
113. Zoncu R, Bar-Peled L, Efeyan A, Wang S, Sancak Y, Sabatini DM: mTORC1 senses lysosomal amino acids through an inside-out mechanism that requires the vacuolar H(+)-ATPase. *Science* 2011, 334(6056):678-683.
114. Inoki K, Li Y, Xu T, Guan KL: Rheb GTPase is a direct target of TSC2 GAP activity and regulates mTOR signaling. *Genes & development* 2003, 17(15):1829-1834.
115. Demetriades C, Doumpas N, Teleman AA: Regulation of TORC1 in response to amino acid starvation via lysosomal recruitment of TSC2. *Cell* 2014, 156(4):786-799.
116. Menon S, Dibble CC, Talbott G, Hoxhaj G, Valvezan AJ, Takahashi H, Cantley LC, Manning BD: Spatial control of the TSC complex integrates insulin and nutrient regulation of mTORC1 at the lysosome. *Cell* 2014, 156(4):771-785.
117. Harrington LS, Findlay GM, Gray A, Tolkacheva T, Wigfield S, Rebholz H, Barnett J, Leslie NR, Cheng S, Shepherd PR *et al*: The TSC1-2 tumor suppressor controls insulin-PI3K signaling via regulation of IRS proteins. *J Cell Biol* 2004, 166(2):213-223.
118. Ma L, Chen Z, Erdjument-Bromage H, Tempst P, Pandolfi PP: Phosphorylation and functional inactivation of TSC2 by Erk implications for tuberous sclerosis and cancer pathogenesis. *Cell* 2005, 121(2):179-193.
119. Inoki K, Ouyang H, Zhu T, Lindvall C, Wang Y, Zhang X, Yang Q, Bennett C, Harada Y, Stankunas K *et al*: TSC2 integrates Wnt and energy signals via a coordinated phosphorylation by AMPK and GSK3 to regulate cell growth. *Cell* 2006, 126(5):955-968.
120. Inoki K, Zhu T, Guan KL: TSC2 mediates cellular energy response to control cell growth and survival. *Cell* 2003, 115(5):577-590.
121. Perera RM, Zoncu R: The Lysosome as a Regulatory Hub. *Annu Rev Cell Dev Biol* 2016, 32:223-253.
122. Hesketh GG, Wartosch L, Davis LJ, Bright NA, Luzio JP: The Lysosome and Intracellular Signalling. *Progress in molecular and subcellular biology* 2018, 57:151-180.

123. La Spina M, Contreras PS, Rissone A, Meena NK, Jeong E, Martina JA: MiT/TFE Family of Transcription Factors: An Evolutionary Perspective. *Front Cell Dev Biol* 2020, 8:609683.
124. Zhao GQ, Zhao Q, Zhou X, Mattei MG, de Crombrughe B: TFEC, a basic helix-loop-helix protein, forms heterodimers with TFE3 and inhibits TFE3-dependent transcription activation. *Molecular and cellular biology* 1993, 13(8):4505-4512.
125. Sardiello M, Palmieri M, di Ronza A, Medina DL, Valenza M, Gennarino VA, Di Malta C, Donaudy F, Embrione V, Polishchuk RS *et al*: A gene network regulating lysosomal biogenesis and function. *Science* 2009, 325(5939):473-477.
126. Palmieri M, Impey S, Kang H, di Ronza A, Pelz C, Sardiello M, Ballabio A: Characterization of the CLEAR network reveals an integrated control of cellular clearance pathways. *Human molecular genetics* 2011, 20(19):3852-3866.
127. Puertollano R, Ferguson SM, Brugarolas J, Ballabio A: The complex relationship between TFEB transcription factor phosphorylation and subcellular localization. *EMBO J* 2018, 37(11).
128. Settembre C, Di Malta C, Polito VA, Garcia Arencibia M, Vetrini F, Erdin S, Erdin SU, Huynh T, Medina D, Colella P *et al*: TFEB links autophagy to lysosomal biogenesis. *Science* 2011, 332(6036):1429-1433.
129. Martina JA, Diab HI, Lishu L, Jeong AL, Patange S, Raben N, Puertollano R: The nutrient-responsive transcription factor TFE3 promotes autophagy, lysosomal biogenesis, and clearance of cellular debris. *Sci Signal* 2014, 7(309):ra9.
130. Settembre C, De Cegli R, Mansueto G, Saha PK, Vetrini F, Visvikis O, Huynh T, Carissimo A, Palmer D, Klisch TJ *et al*: TFEB controls cellular lipid metabolism through a starvation-induced autoregulatory loop. *Nature cell biology* 2013, 15(6):647-658.
131. Nezich CL, Wang C, Fogel AI, Youle RJ: MiT/TFE transcription factors are activated during mitophagy downstream of Parkin and Atg5. *J Cell Biol* 2015, 210(3):435-450.
132. Spanpanato C, Feeney E, Li L, Cardone M, Lim JA, Annunziata F, Zare H, Polishchuk R, Puertollano R, Parenti G *et al*: Transcription factor EB (TFEB) is a new therapeutic target for Pompe disease. *EMBO Mol Med* 2013, 5(5):691-706.
133. Song W, Wang F, Savini M, Ake A, di Ronza A, Sardiello M, Segatori L: TFEB regulates lysosomal proteostasis. *Human molecular genetics* 2013, 22(10):1994-2009.
134. Rega LR, Polishchuk E, Montefusco S, Napolitano G, Tozzi G, Zhang J, Bellomo F, Taranta A, Pastore A, Polishchuk R *et al*: Activation of the transcription factor EB rescues lysosomal abnormalities in cystinotic kidney cells. *Kidney international* 2016, 89(4):862-873.
135. Decressac M, Mattsson B, Weikop P, Lundblad M, Jakobsson J, Bjorklund A: TFEB-mediated autophagy rescues midbrain dopamine neurons from alpha-synuclein toxicity. *Proc Natl Acad Sci U S A* 2013, 110(19):E1817-1826.
136. Kilpatrick K, Zeng Y, Hancock T, Segatori L: Genetic and chemical activation of TFEB mediates clearance of aggregated alpha-synuclein. *PloS one* 2015, 10(3):e0120819.

137. Polito VA, Li H, Martini-Stoica H, Wang B, Yang L, Xu Y, Swartzlander DB, Palmieri M, di Ronza A, Lee VM *et al*: Selective clearance of aberrant tau proteins and rescue of neurotoxicity by transcription factor EB. *EMBO Mol Med* 2014, 6(9):1142-1160.
138. Xiao Q, Yan P, Ma X, Liu H, Perez R, Zhu A, Gonzales E, Burchett JM, Schuler DR, Cirrito JR *et al*: Enhancing astrocytic lysosome biogenesis facilitates Abeta clearance and attenuates amyloid plaque pathogenesis. *The Journal of neuroscience : the official journal of the Society for Neuroscience* 2014, 34(29):9607-9620.
139. He X, Xie Y, Zheng Q, Zhang Z, Ma S, Li J, Li M, Huang Q: TFE3-Mediated Autophagy is Involved in Dopaminergic Neurodegeneration in Parkinson's Disease. *Front Cell Dev Biol* 2021, 9:761773.
140. Visvikis O, Ihuegbu N, Labeed SA, Luhachack LG, Alves AF, Wollenberg AC, Stuart LM, Stormo GD, Irazoqui JE: Innate host defense requires TFEB-mediated transcription of cytoprotective and antimicrobial genes. *Immunity* 2014, 40(6):896-909.
141. Pastore N, Brady OA, Diab HI, Martina JA, Sun L, Huynh T, Lim JA, Zare H, Raben N, Ballabio A *et al*: TFEB and TFE3 cooperate in the regulation of the innate immune response in activated macrophages. *Autophagy* 2016, 12(8):1240-1258.
142. Steingrimsson E, Copeland NG, Jenkins NA: Melanocytes and the microphthalmia transcription factor network. *Annual review of genetics* 2004, 38:365-411.
143. Garraway LA, Widlund HR, Rubin MA, Getz G, Berger AJ, Ramaswamy S, Beroukhi R, Milner DA, Granter SR, Du J *et al*: Integrative genomic analyses identify MITF as a lineage survival oncogene amplified in malignant melanoma. *Nature* 2005, 436(7047):117-122.
144. Tassabehji M, Newton VE, Read AP: Waardenburg syndrome type 2 caused by mutations in the human microphthalmia (MITF) gene. *Nature genetics* 1994, 8(3):251-255.
145. Dephoure N, Zhou C, Villen J, Beausoleil SA, Bakalarski CE, Elledge SJ, Gygi SP: A quantitative atlas of mitotic phosphorylation. *Proc Natl Acad Sci U S A* 2008, 105(31):10762-10767.
146. Mayya V, Lundgren DH, Hwang SI, Rezaul K, Wu L, Eng JK, Rodionov V, Han DK: Quantitative phosphoproteomic analysis of T cell receptor signaling reveals system-wide modulation of protein-protein interactions. *Sci Signal* 2009, 2(84):ra46.
147. Olsen JV, Vermeulen M, Santamaria A, Kumar C, Miller ML, Jensen LJ, Gnad F, Cox J, Jensen TS, Nigg EA *et al*: Quantitative phosphoproteomics reveals widespread full phosphorylation site occupancy during mitosis. *Sci Signal* 2010, 3(104):ra3.
148. Settembre C, Zoncu R, Medina DL, Vetrini F, Erdin S, Huynh T, Ferron M, Karsenty G, Vellard MC, Facchinetti V *et al*: A lysosome-to-nucleus signalling mechanism senses and regulates the lysosome via mTOR and TFEB. *EMBO J* 2012, 31(5):1095-1108.
149. Martina JA, Chen Y, Gucek M, Puertollano R: MTORC1 functions as a transcriptional regulator of autophagy by preventing nuclear transport of TFEB. *Autophagy* 2012, 8(6):903-914.

150. Rocznik-Ferguson A, Petit CS, Froehlich F, Qian S, Ky J, Angarola B, Walther TC, Ferguson SM: The transcription factor TFEB links mTORC1 signaling to transcriptional control of lysosome homeostasis. *Sci Signal* 2012, 5(228):ra42.
151. Vega-Rubin-de-Celis S, Pena-Llopis S, Konda M, Brugarolas J: Multistep regulation of TFEB by MTORC1. *Autophagy* 2017, 13(3):464-472.
152. Martina JA, Puertollano R: Rag GTPases mediate amino acid-dependent recruitment of TFEB and MITF to lysosomes. *J Cell Biol* 2013, 200(4):475-491.
153. Bronisz A, Sharma SM, Hu R, Godlewski J, Tzivion G, Mansky KC, Ostrowski MC: Microphthalmia-associated transcription factor interactions with 14-3-3 modulate differentiation of committed myeloid precursors. *Molecular biology of the cell* 2006, 17(9):3897-3906.
154. Jin J, Smith FD, Stark C, Wells CD, Fawcett JP, Kulkarni S, Metalnikov P, O'Donnell P, Taylor P, Taylor L *et al*: Proteomic, functional, and domain-based analysis of in vivo 14-3-3 binding proteins involved in cytoskeletal regulation and cellular organization. *Curr Biol* 2004, 14(16):1436-1450.
155. Li Y, Xu M, Ding X, Yan C, Song Z, Chen L, Huang X, Wang X, Jian Y, Tang G *et al*: Protein kinase C controls lysosome biogenesis independently of mTORC1. *Nature cell biology* 2016, 18(10):1065-1077.
156. Palmieri M, Pal R, Nelvagal HR, Lotfi P, Stinnett GR, Seymour ML, Chaudhury A, Bajaj L, Bondar VV, Bremner L *et al*: mTORC1-independent TFEB activation via Akt inhibition promotes cellular clearance in neurodegenerative storage diseases. *Nat Commun* 2017, 8:14338.
157. Glykofridis IE, Henneman AA, Balk JA, Goeij-de Haas R, Westland D, Piersma SR, Knol JC, Pham TV, Boekhout M, Zwartkruis FJT *et al*: Phosphoproteomic Analysis of FLCN Inactivation Highlights Differential Kinase Pathways and Regulatory TFEB Phosphoserines. *Molecular & cellular proteomics : MCP* 2022, 21(9):100263.
158. Hasegawa J, Tokuda E, Yao Y, Sasaki T, Inoki K, Weisman LS: PP2A-dependent TFEB activation is blocked by PIKfyve-induced mTORC1 activity. *Molecular biology of the cell* 2022, 33(3):ar26.
159. Martina JA, Puertollano R: Protein phosphatase 2A stimulates activation of TFEB and TFE3 transcription factors in response to oxidative stress. *The Journal of biological chemistry* 2018, 293(32):12525-12534.
160. Astanina E, Bussolino F, Doronzo G: Multifaceted activities of transcription factor EB in cancer onset and progression. *Molecular oncology* 2021, 15(2):327-346.
161. Schoneberg J, Lee IH, Iwasa JH, Hurley JH: Reverse-topology membrane scission by the ESCRT proteins. *Nat Rev Mol Cell Biol* 2017, 18(1):5-17.
162. Bache KG, Brech A, Mehlum A, Stenmark H: Hrs regulates multivesicular body formation via ESCRT recruitment to endosomes. *J Cell Biol* 2003, 162(3):435-442.

163. Raiborg C, Bache KG, Gillooly DJ, Madshus IH, Stang E, Stenmark H: Hrs sorts ubiquitinated proteins into clathrin-coated microdomains of early endosomes. *Nature cell biology* 2002, 4(5):394-398.
164. Raiborg C, Bache KG, Mehlum A, Stang E, Stenmark H: Hrs recruits clathrin to early endosomes. *EMBO J* 2001, 20(17):5008-5021.
165. Mayers JR, Fyfe I, Schuh AL, Chapman ER, Edwardson JM, Audhya A: ESCRT-0 assembles as a heterotetrameric complex on membranes and binds multiple ubiquitylated cargoes simultaneously. *The Journal of biological chemistry* 2011, 286(11):9636-9645.
166. Katzmann DJ, Babst M, Emr SD: Ubiquitin-dependent sorting into the multivesicular body pathway requires the function of a conserved endosomal protein sorting complex, ESCRT-I. *Cell* 2001, 106(2):145-155.
167. Lu Q, Hope LW, Brasch M, Reinhard C, Cohen SN: TSG101 interaction with HRS mediates endosomal trafficking and receptor down-regulation. *Proc Natl Acad Sci U S A* 2003, 100(13):7626-7631.
168. Teo H, Gill DJ, Sun J, Perisic O, Veprintsev DB, Vallis Y, Emr SD, Williams RL: ESCRT-I core and ESCRT-II GLUE domain structures reveal role for GLUE in linking to ESCRT-I and membranes. *Cell* 2006, 125(1):99-111.
169. Hierro A, Sun J, Rusnak AS, Kim J, Prag G, Emr SD, Hurley JH: Structure of the ESCRT-II endosomal trafficking complex. *Nature* 2004, 431(7005):221-225.
170. Schmidt O, Teis D: The ESCRT machinery. *Curr Biol* 2012, 22(4):R116-120.
171. Im YJ, Wollert T, Boura E, Hurley JH: Structure and function of the ESCRT-II-III interface in multivesicular body biogenesis. *Dev Cell* 2009, 17(2):234-243.
172. Adell MA, Vogel GF, Pakdel M, Muller M, Lindner H, Hess MW, Teis D: Coordinated binding of Vps4 to ESCRT-III drives membrane neck constriction during MVB vesicle formation. *J Cell Biol* 2014, 205(1):33-49.
173. Schoneberg J, Pavlin MR, Yan S, Righini M, Lee IH, Carlson LA, Bahrami AH, Goldman DH, Ren X, Hummer G *et al*: ATP-dependent force generation and membrane scission by ESCRT-III and Vps4. *Science* 2018, 362(6421):1423-1428.
174. Pfitzner AK, Mercier V, Jiang X, Moser von Filseck J, Baum B, Saric A, Roux A: An ESCRT-III Polymerization Sequence Drives Membrane Deformation and Fission. *Cell* 2020, 182(5):1140-1155 e1118.
175. Babst M, Wendland B, Estepa EJ, Emr SD: The Vps4p AAA ATPase regulates membrane association of a Vps protein complex required for normal endosome function. *EMBO J* 1998, 17(11):2982-2993.
176. Yang B, Stjepanovic G, Shen Q, Martin A, Hurley JH: Vps4 disassembles an ESCRT-III filament by global unfolding and processive translocation. *Nature structural & molecular biology* 2015, 22(6):492-498.
177. van Niel G, D'Angelo G, Raposo G: Shedding light on the cell biology of extracellular vesicles. *Nat Rev Mol Cell Biol* 2018, 19(4):213-228.

178. Razi M, Futter CE: Distinct roles for Tsg101 and Hrs in multivesicular body formation and inward vesiculation. *Molecular biology of the cell* 2006, 17(8):3469-3483.
179. Doyotte A, Russell MR, Hopkins CR, Woodman PG: Depletion of TSG101 forms a mammalian "Class E" compartment: a multicisternal early endosome with multiple sorting defects. *Journal of cell science* 2005, 118(Pt 14):3003-3017.
180. Brankatschk B, Wichert SP, Johnson SD, Schaad O, Rossner MJ, Gruenberg J: Regulation of the EGF transcriptional response by endocytic sorting. *Sci Signal* 2012, 5(215):ra21.
181. Dikic I, Elazar Z: Mechanism and medical implications of mammalian autophagy. *Nat Rev Mol Cell Biol* 2018, 19(6):349-364.
182. Filimonenko M, Stuffers S, Raiborg C, Yamamoto A, Malerod L, Fisher EM, Isaacs A, Brech A, Stenmark H, Simonsen A: Functional multivesicular bodies are required for autophagic clearance of protein aggregates associated with neurodegenerative disease. *J Cell Biol* 2007, 179(3):485-500.
183. Rusten TE, Vaccari T, Lindmo K, Rodahl LM, Nezis IP, Sem-Jacobsen C, Wendler F, Vincent JP, Brech A, Bilder D *et al*: ESCRTs and Fab1 regulate distinct steps of autophagy. *Curr Biol* 2007, 17(20):1817-1825.
184. Takahashi Y, Liang X, Hattori T, Tang Z, He H, Chen H, Liu X, Abraham T, Imamura-Kawasawa Y, Buchkovich NJ *et al*: VPS37A directs ESCRT recruitment for phagophore closure. *J Cell Biol* 2019, 218(10):3336-3354.
185. Takahashi Y, He H, Tang Z, Hattori T, Liu Y, Young MM, Serfass JM, Chen L, Gebru M, Chen C *et al*: An autophagy assay reveals the ESCRT-III component CHMP2A as a regulator of phagophore closure. *Nat Commun* 2018, 9(1):2855.
186. Vietri M, Radulovic M, Stenmark H: The many functions of ESCRTs. *Nat Rev Mol Cell Biol* 2020, 21(1):25-42.
187. Szymanska E, Budick-Harmelin N, Miaczynska M: Endosomal "sort" of signaling control: The role of ESCRT machinery in regulation of receptor-mediated signaling pathways. *Semin Cell Dev Biol* 2017, 74:11-20.
188. Cendrowski J, Maminska A, Miaczynska M: Endocytic regulation of cytokine receptor signaling. *Cytokine & growth factor reviews* 2016, 32:63-73.
189. Lloyd TE, Atkinson R, Wu MN, Zhou Y, Pennetta G, Bellen HJ: Hrs regulates endosome membrane invagination and tyrosine kinase receptor signaling in *Drosophila*. *Cell* 2002, 108(2):261-269.
190. Babst M, Odorizzi G, Estepa EJ, Emr SD: Mammalian tumor susceptibility gene 101 (TSG101) and the yeast homologue, Vps23p, both function in late endosomal trafficking. *Traffic* 2000, 1(3):248-258.
191. Hammond DE, Carter S, McCullough J, Urbe S, Vande Woude G, Clague MJ: Endosomal dynamics of Met determine signaling output. *Molecular biology of the cell* 2003, 14(4):1346-1354.

192. Malerod L, Stuffers S, Brech A, Stenmark H: Vps22/EAP30 in ESCRT-II mediates endosomal sorting of growth factor and chemokine receptors destined for lysosomal degradation. *Traffic* 2007, 8(11):1617-1629.
193. Banach-Orlowska M, Jastrzebski K, Cendrowski J, Maksymowicz M, Wojciechowska K, Korostynski M, Moreau D, Gruenberg J, Miaczynska M: The topology of the lymphotoxin beta receptor that accumulates upon endolysosomal dysfunction dictates the NF-kappaB signaling outcome. *Journal of cell science* 2018, 131(22).
194. Maminska A, Bartosik A, Banach-Orlowska M, Pilecka I, Jastrzebski K, Zdzalik-Bielecka D, Castanon I, Poulain M, Neyen C, Wolinska-Niziol L *et al*: ESCRT proteins restrict constitutive NF-kappaB signaling by trafficking cytokine receptors. *Sci Signal* 2016, 9(411):ra8.
195. Maejima I, Takahashi A, Omori H, Kimura T, Takabatake Y, Saitoh T, Yamamoto A, Hamasaki M, Noda T, Isaka Y *et al*: Autophagy sequesters damaged lysosomes to control lysosomal biogenesis and kidney injury. *EMBO J* 2013, 32(17):2336-2347.
196. Boya P, Kroemer G: Lysosomal membrane permeabilization in cell death. *Oncogene* 2008, 27(50):6434-6451.
197. Aits S, Jaattela M: Lysosomal cell death at a glance. *Journal of cell science* 2013, 126(Pt 9):1905-1912.
198. Radulovic M, Schink KO, Wenzel EM, Nahse V, Bongiovanni A, Lafont F, Stenmark H: ESCRT-mediated lysosome repair precedes lysophagy and promotes cell survival. *EMBO J* 2018, 37(21).
199. Lopez-Jimenez AT, Cardenal-Munoz E, Leuba F, Gerstenmaier L, Barisch C, Hagedorn M, King JS, Soldati T: The ESCRT and autophagy machineries cooperate to repair ESX-1-dependent damage at the Mycobacterium-containing vacuole but have opposite impact on containing the infection. *PLoS pathogens* 2018, 14(12):e1007501.
200. Zhu L, Jorgensen JR, Li M, Chuang YS, Emr SD: ESCRTs function directly on the lysosome membrane to downregulate ubiquitinated lysosomal membrane proteins. *Elife* 2017, 6.
201. Morshed S, Sharmin T, Ushimaru T: TORC1 regulates ESCRT-0 complex formation on the vacuolar membrane and microautophagy induction in yeast. *Biochemical and biophysical research communications* 2020, 522(1):88-94.
202. Yang X, Zhang W, Wen X, Bulinski PJ, Chomchai DA, Arines FM, Liu YY, Sprenger S, Teis D, Klionsky DJ *et al*: TORC1 regulates vacuole membrane composition through ubiquitin- and ESCRT-dependent microautophagy. *J Cell Biol* 2020, 219(3).
203. Yang X, Reist L, Chomchai DA, Chen L, Arines FM, Li M: ESCRT, not intraluminal fragments, sorts ubiquitinated vacuole membrane proteins for degradation. *J Cell Biol* 2021, 220(8).
204. Li SC, Kane PM: The yeast lysosome-like vacuole: endpoint and crossroads. *Biochimica et biophysica acta* 2009, 1793(4):650-663.

205. Zhang W, Yang X, Chen L, Liu YY, Venkatarangan V, Reist L, Hanson P, Xu H, Wang Y, Li M: A conserved ubiquitin- and ESCRT-dependent pathway internalizes human lysosomal membrane proteins for degradation. *PLoS biology* 2021, 19(7):e3001361.
206. Elia N, Sougrat R, Spurlin TA, Hurley JH, Lippincott-Schwartz J: Dynamics of endosomal sorting complex required for transport (ESCRT) machinery during cytokinesis and its role in abscission. *Proc Natl Acad Sci U S A* 2011, 108(12):4846-4851.
207. Connell JW, Lindon C, Luzio JP, Reid E: Spastin couples microtubule severing to membrane traffic in completion of cytokinesis and secretion. *Traffic* 2009, 10(1):42-56.
208. Votteler J, Sundquist WI: Virus budding and the ESCRT pathway. *Cell host & microbe* 2013, 14(3):232-241.
209. Jimenez AJ, Maiuri P, Lafaurie-Janvove J, Divoux S, Piel M, Perez F: ESCRT machinery is required for plasma membrane repair. *Science* 2014, 343(6174):1247136.
210. Scheffer LL, Sreetama SC, Sharma N, Medikayala S, Brown KJ, Defour A, Jaiswal JK: Mechanism of Ca²⁺(+)-triggered ESCRT assembly and regulation of cell membrane repair. *Nat Commun* 2014, 5:5646.
211. Katoh K, Suzuki H, Terasawa Y, Mizuno T, Yasuda J, Shibata H, Maki M: The penta-EF-hand protein ALG-2 interacts directly with the ESCRT-I component TSG101, and Ca²⁺-dependently co-localizes to aberrant endosomes with dominant-negative AAA ATPase SKD1/Vps4B. *The Biochemical journal* 2005, 391(Pt 3):677-685.
212. Ruhl S, Shkarina K, Demarco B, Heilig R, Santos JC, Broz P: ESCRT-dependent membrane repair negatively regulates pyroptosis downstream of GSDMD activation. *Science* 2018, 362(6417):956-960.
213. Raab M, Gentili M, de Belly H, Thiam HR, Vargas P, Jimenez AJ, Lautenschlaeger F, Voituriez R, Lennon-Dumenil AM, Manel N *et al*: ESCRT III repairs nuclear envelope ruptures during cell migration to limit DNA damage and cell death. *Science* 2016, 352(6283):359-362.
214. Denais CM, Gilbert RM, Isermann P, McGregor AL, te Lindert M, Weigelin B, Davidson PM, Friedl P, Wolf K, Lammerding J: Nuclear envelope rupture and repair during cancer cell migration. *Science* 2016, 352(6283):353-358.
215. Vietri M, Schink KO, Campsteijn C, Wegner CS, Schultz SW, Christ L, Thoresen SB, Brech A, Raiborg C, Stenmark H: Spastin and ESCRT-III coordinate mitotic spindle disassembly and nuclear envelope sealing. *Nature* 2015, 522(7555):231-235.
216. Migliano SM, Wenzel EM, Stenmark H: Biophysical and molecular mechanisms of ESCRT functions, and their implications for disease. *Current opinion in cell biology* 2022, 75:102062.
217. Li L, Cohen SN: Tsg101: a novel tumor susceptibility gene isolated by controlled homozygous functional knockout of allelic loci in mammalian cells. *Cell* 1996, 85(3):319-329.

218. Xu Z, Liang L, Wang H, Li T, Zhao M: HCRP1, a novel gene that is downregulated in hepatocellular carcinoma, encodes a growth-inhibitory protein. *Biochemical and biophysical research communications* 2003, 311(4):1057-1066.
219. Moberg KH, Schelble S, Burdick SK, Hariharan IK: Mutations in erupted, the Drosophila ortholog of mammalian tumor susceptibility gene 101, elicit non-cell-autonomous overgrowth. *Dev Cell* 2005, 9(5):699-710.
220. Broniarczyk J, Olejnik-Schmidt AK, Luczak MW, Schmidt MT, Dabrowski M, Jozefiak A, Kedzia W, Kwasniewska A, Gozdicka-Jozefiak A: Analysis of expression and structure of the TSG101 gene in cervical cancer cells. *International journal of molecular medicine* 2010, 25(5):777-783.
221. Miller DSJ, Bloxham RD, Jiang M, Gori I, Saunders RE, Das D, Chakravarty P, Howell M, Hill CS: The Dynamics of TGF-beta Signaling Are Dictated by Receptor Trafficking via the ESCRT Machinery. *Cell reports* 2018, 25(7):1841-1855 e1845.
222. Xu J, Yang W, Wang Q, Zhang Q, Li X, Lin X, Liu X, Qin Y: Decreased HCRP1 expression is associated with poor prognosis in breast cancer patients. *International journal of clinical and experimental pathology* 2014, 7(11):7915-7922.
223. Wittinger M, Vanhara P, El-Gazzar A, Savarese-Brenner B, Pils D, Anees M, Grunt TW, Sibilia M, Holcman M, Horvat R *et al*: hVps37A Status affects prognosis and cetuximab sensitivity in ovarian cancer. *Clinical cancer research : an official journal of the American Association for Cancer Research* 2011, 17(24):7816-7827.
224. Chen F, Deng J, Liu X, Li W, Zheng J: Corrigendum: HCRP-1 regulates cell migration and invasion via EGFR-ERK mediated up-regulation of MMP-2 with prognostic significance in human renal cell carcinoma. *Scientific reports* 2016, 6:19412.
225. Kolmus K, Erdenebat P, Szymanska E, Stewig B, Goryca K, Derezinska-Wolek E, Szumera-Cieckiewicz A, Brewinska-Olchowik M, Piwocka K, Prochorec-Sobieszek M *et al*: Concurrent depletion of Vps37 proteins evokes ESCRT-I destabilization and profound cellular stress responses. *Journal of cell science* 2021, 134(1).
226. Yang W, Wang JG, Xu J, Zhou D, Ren K, Hou C, Chen L, Liu X: HCRP1 inhibits TGF-beta induced epithelial-mesenchymal transition in hepatocellular carcinoma. *International journal of oncology* 2017, 50(4):1233-1240.
227. Chen F, Zhang L, Wu J, Huo F, Ren X, Zheng J, Pei D: HCRP-1 regulates EGFR-AKT-BIM-mediated anoikis resistance and serves as a prognostic marker in human colon cancer. *Cell death & disease* 2018, 9(12):1176.
228. Xu CY, Li ZJ, Hu WZ: Up-regulation of HCRP1 inhibits proliferation and invasion in glioma cells via suppressing the ERK and AKT signaling pathways. *Biomedicine & pharmacotherapy = Biomedecine & pharmacotherapie* 2017, 95:31-36.
229. Tomasich E, Topakian T, Heller G, Udovica S, Krainer M, Marhold M: Loss of HCRP1 leads to upregulation of PD-L1 via STAT3 activation and is of prognostic significance in EGFR-dependent cancer. *Translational research : the journal of laboratory and clinical medicine* 2021, 230:21-33.

230. Liu DC, Yang ZL, Jiang S: Identification of PEG10 and TSG101 as carcinogenesis, progression, and poor-prognosis related biomarkers for gallbladder adenocarcinoma. *Pathology oncology research : POR* 2011, 17(4):859-866.
231. Young TW, Rosen DG, Mei FC, Li N, Liu J, Wang XF, Cheng X: Up-regulation of tumor susceptibility gene 101 conveys poor prognosis through suppression of p21 expression in ovarian cancer. *Clinical cancer research : an official journal of the American Association for Cancer Research* 2007, 13(13):3848-3854.
232. Ferraiuolo RM, Manthey KC, Stanton MJ, Triplett AA, Wagner KU: The Multifaceted Roles of the Tumor Susceptibility Gene 101 (TSG101) in Normal Development and Disease. *Cancers* 2020, 12(2).
233. Toyoshima M, Tanaka N, Aoki J, Tanaka Y, Murata K, Kyuuma M, Kobayashi H, Ishii N, Yaegashi N, Sugamura K: Inhibition of tumor growth and metastasis by depletion of vesicular sorting protein Hrs: its regulatory role on E-cadherin and beta-catenin. *Cancer research* 2007, 67(11):5162-5171.
234. Li J, Belogortseva N, Porter D, Park M: Chmp1A functions as a novel tumor suppressor gene in human embryonic kidney and ductal pancreatic tumor cells. *Cell Cycle* 2008, 7(18):2886-2893.
235. You Z, Xin Y, Liu Y, Sun J, Zhou G, Gao H, Xu P, Chen Y, Chen G, Zhang L *et al*: Chmp1A acts as a tumor suppressor gene that inhibits proliferation of renal cell carcinoma. *Cancer letters* 2012, 319(2):190-196.
236. Szymanska E, Nowak P, Kolmus K, Cybulska M, Goryca K, Derezinska-Wolek E, Szumera-Cieckiewicz A, Brewinska-Olchowik M, Grochowska A, Piwocka K *et al*: Synthetic lethality between VPS4A and VPS4B triggers an inflammatory response in colorectal cancer. *EMBO Mol Med* 2020, 12(2):e10812.
237. Hu B, Jiang D, Chen Y, Wei L, Zhang S, Zhao F, Ni R, Lu C, Wan C: High CHMP4B expression is associated with accelerated cell proliferation and resistance to doxorubicin in hepatocellular carcinoma. *Tumour biology : the journal of the International Society for Oncodevelopmental Biology and Medicine* 2015, 36(4):2569-2581.
238. Li K, Liu J, Tian M, Gao G, Qi X, Pan Y, Ruan J, Liu C, Su X: CHMP4C Disruption Sensitizes the Human Lung Cancer Cells to Irradiation. *International journal of molecular sciences* 2015, 17(1).
239. Chen VY, Posada MM, Blazer LL, Zhao T, Rosania GR: The role of the VPS4A-exosome pathway in the intrinsic egress route of a DNA-binding anticancer drug. *Pharmaceutical research* 2006, 23(8):1687-1695.
240. Safaei R, Larson BJ, Cheng TC, Gibson MA, Otani S, Naerdemann W, Howell SB: Abnormal lysosomal trafficking and enhanced exosomal export of cisplatin in drug-resistant human ovarian carcinoma cells. *Molecular cancer therapeutics* 2005, 4(10):1595-1604.

241. Ritter AT, Shtengel G, Xu CS, Weigel A, Hoffman DP, Freeman M, Iyer N, Alivodej N, Ackerman D, Voskoboinik I *et al*: ESCRT-mediated membrane repair protects tumor-derived cells against T cell attack. *Science* 2022, 376(6591):377-382.
242. Wang J, Hou Y, Qi L, Zhai S, Zheng L, Han L, Guo Y, Zhang B, Miao P, Lou Y *et al*: Autosomal dominant hereditary spastic paraplegia caused by mutation of UBAP1. *Neurogenetics* 2020, 21(3):169-177.
243. Li P, Huang X, Chai S, Zhu D, Huang H, Ma F, Zhang S, Xie X: A novel mutation in the UBAP1 gene causing hereditary spastic paraplegia: A case report and overview of the genotype-phenotype correlation. *Frontiers in genetics* 2022, 13:936292.
244. Bourinaris T, Smedley D, Cipriani V, Sheikh I, Athanasiou-Fragkouli A, Chinnery P, Morris H, Real R, Harrison V, Reid E *et al*: Identification of UBAP1 mutations in juvenile hereditary spastic paraplegia in the 100,000 Genomes Project. *European journal of human genetics : EJHG* 2020, 28(12):1763-1768.
245. Farazi Fard MA, Rebelo AP, Buglo E, Nemati H, Dastsooz H, Gehweiler I, Reich S, Reichbauer J, Quintans B, Ordonez-Ugalde A *et al*: Truncating Mutations in UBAP1 Cause Hereditary Spastic Paraplegia. *American journal of human genetics* 2019, 104(4):767-773.
246. Isaacs AM, Johannsen P, Holm I, Nielsen JE: Frontotemporal dementia caused by CHMP2B mutations. *Current Alzheimer research* 2011, 8(3):246-251.
247. Cox LE, Ferraiuolo L, Goodall EF, Heath PR, Higginbottom A, Mortiboys H, Hollinger HC, Hartley JA, Brockington A, Burness CE *et al*: Mutations in CHMP2B in lower motor neuron predominant amyotrophic lateral sclerosis (ALS). *PloS one* 2010, 5(3):e9872.
248. Parkinson N, Ince PG, Smith MO, Highley R, Skibinski G, Andersen PM, Morrison KE, Pall HS, Hardiman O, Collinge J *et al*: ALS phenotypes with mutations in CHMP2B (charged multivesicular body protein 2B). *Neurology* 2006, 67(6):1074-1077.
249. Edgar JR, Willen K, Gouras GK, Futter CE: ESCRTs regulate amyloid precursor protein sorting in multivesicular bodies and intracellular amyloid-beta accumulation. *Journal of cell science* 2015, 128(14):2520-2528.
250. Spencer B, Emadi S, Desplats P, Eleuteri S, Michael S, Kosberg K, Shen J, Rockenstein E, Patrick C, Adame A *et al*: ESCRT-mediated uptake and degradation of brain-targeted alpha-synuclein single chain antibody attenuates neuronal degeneration in vivo. *Molecular therapy : the journal of the American Society of Gene Therapy* 2014, 22(10):1753-1767.
251. Ugbode C, West RJH: Lessons learned from CHMP2B, implications for frontotemporal dementia and amyotrophic lateral sclerosis. *Neurobiology of disease* 2021, 147:105144.
252. Seu KG, Trump LR, Emberesh S, Lorsbach RB, Johnson C, Mezmarich J, Underhill HR, Chou ST, Sakthivel H, Nassar NN *et al*: VPS4A Mutations in Humans Cause Syndromic Congenital Dyserythropoietic Anemia due to Cytokinesis and Trafficking Defects. *American journal of human genetics* 2020, 107(6):1149-1156.
253. Rodger C, Flex E, Allison RJ, Sanchis-Juan A, Hasenahuer MA, Cecchetti S, French CE, Edgar JR, Carpentieri G, Ciolfi A *et al*: De Novo VPS4A Mutations Cause Multisystem

- Disease with Abnormal Neurodevelopment. *American journal of human genetics* 2020, 107(6):1129-1148.
254. Bonam SR, Wang F, Muller S: Lysosomes as a therapeutic target. *Nature reviews Drug discovery* 2019, 18(12):923-948.
 255. Ballabio A, Gieselmann V: Lysosomal disorders: from storage to cellular damage. *Biochimica et biophysica acta* 2009, 1793(4):684-696.
 256. Udayar V, Chen Y, Sidransky E, Jagasia R: Lysosomal dysfunction in neurodegeneration: emerging concepts and methods. *Trends in neurosciences* 2022, 45(3):184-199.
 257. Root J, Merino P, Nuckols A, Johnson M, Kukar T: Lysosome dysfunction as a cause of neurodegenerative diseases: Lessons from frontotemporal dementia and amyotrophic lateral sclerosis. *Neurobiology of disease* 2021, 154:105360.
 258. Platt FM: Emptying the stores: lysosomal diseases and therapeutic strategies. *Nature reviews Drug discovery* 2018, 17(2):133-150.
 259. Fleming A, Noda T, Yoshimori T, Rubinsztein DC: Chemical modulators of autophagy as biological probes and potential therapeutics. *Nature chemical biology* 2011, 7(1):9-17.
 260. Xiao Q, Yan P, Ma X, Liu H, Perez R, Zhu A, Gonzales E, Tripoli DL, Czerniewski L, Ballabio A *et al*: Neuronal-Targeted TFEB Accelerates Lysosomal Degradation of APP, Reducing Abeta Generation and Amyloid Plaque Pathogenesis. *The Journal of neuroscience : the official journal of the Society for Neuroscience* 2015, 35(35):12137-12151.
 261. Torra A, Parent A, Cuadros T, Rodriguez-Galvan B, Ruiz-Bronchal E, Ballabio A, Bortolozzi A, Vila M, Bove J: Overexpression of TFEB Drives a Pleiotropic Neurotrophic Effect and Prevents Parkinson's Disease-Related Neurodegeneration. *Molecular therapy : the journal of the American Society of Gene Therapy* 2018, 26(6):1552-1567.
 262. Tsunemi T, Ashe TD, Morrison BE, Soriano KR, Au J, Roque RA, Lazarowski ER, Damian VA, Masliah E, La Spada AR: PGC-1alpha rescues Huntington's disease proteotoxicity by preventing oxidative stress and promoting TFEB function. *Science translational medicine* 2012, 4(142):142ra197.
 263. Machado ER, Annunziata I, van de Vlekkert D, Grosveld GC, d'Azzo A: Lysosomes and Cancer Progression: A Malignant Liaison. *Front Cell Dev Biol* 2021, 9:642494.
 264. Zhitomirsky B, Assaraf YG: Lysosomal sequestration of hydrophobic weak base chemotherapeutics triggers lysosomal biogenesis and lysosome-dependent cancer multidrug resistance. *Oncotarget* 2015, 6(2):1143-1156.
 265. Ballesteros-Alvarez J, Dilshat R, Fock V, Moller K, Karl L, Larue L, Ogmundsdottir MH, Steingrimsson E: MITF and TFEB cross-regulation in melanoma cells. *PloS one* 2020, 15(9):e0238546.
 266. Perera RM, Stoykova S, Nicolay BN, Ross KN, Fitamant J, Boukhali M, Lengrand J, Deshpande V, Selig MK, Ferrone CR *et al*: Transcriptional control of autophagy-lysosome function drives pancreatic cancer metabolism. *Nature* 2015, 524(7565):361-365.

267. Kauffman EC, Ricketts CJ, Rais-Bahrami S, Yang Y, Merino MJ, Bottaro DP, Srinivasan R, Linehan WM: Molecular genetics and cellular features of TFE3 and TFEB fusion kidney cancers. *Nature reviews Urology* 2014, 11(8):465-475.
268. Giatromanolaki A, Kalamida D, Sivridis E, Karagounis IV, Gatter KC, Harris AL, Koukourakis MI: Increased expression of transcription factor EB (TFEB) is associated with autophagy, migratory phenotype and poor prognosis in non-small cell lung cancer. *Lung Cancer* 2015, 90(1):98-105.
269. Liang J, Jia X, Wang K, Zhao N: High expression of TFEB is associated with aggressive clinical features in colorectal cancer. *OncoTargets and therapy* 2018, 11:8089-8098.
270. Cao M, Luo X, Wu K, He X: Targeting lysosomes in human disease: from basic research to clinical applications. *Signal transduction and targeted therapy* 2021, 6(1):379.
271. Morshed S, Tasnin MN, Ushimaru T: ESCRT machinery plays a role in microautophagy in yeast. *BMC Mol Cell Biol* 2020, 21(1):70.
272. Jia J, Claude-Taupin A, Gu Y, Choi SW, Peters R, Bissa B, Mudd MH, Allers L, Pallikkuth S, Lidke KA *et al*: Galectin-3 Coordinates a Cellular System for Lysosomal Repair and Removal. *Dev Cell* 2020, 52(1):69-87 e68.
273. Jeong JY, Yim HS, Ryu JY, Lee HS, Lee JH, Seen DS, Kang SG: One-step sequence- and ligation-independent cloning as a rapid and versatile cloning method for functional genomics studies. *Applied and environmental microbiology* 2012, 78(15):5440-5443.
274. Suzuki K, Bose P, Leong-Quong RY, Fujita DJ, Riabowol K: REAP: A two minute cell fractionation method. *BMC research notes* 2010, 3:294.
275. Hirst J, Edgar JR, Esteves T, Darios F, Madeo M, Chang J, Roda RH, Durr A, Anheim M, Gellera C *et al*: Loss of AP-5 results in accumulation of aberrant endolysosomes: defining a new type of lysosomal storage disease. *Human molecular genetics* 2015, 24(17):4984-4996.
276. Love MI, Huber W, Anders S: Moderated estimation of fold change and dispersion for RNA-seq data with DESeq2. *Genome biology* 2014, 15(12):550.
277. Aibar S, Gonzalez-Blas CB, Moerman T, Huynh-Thu VA, Imrichova H, Hulselmans G, Rambow F, Marine JC, Geurts P, Aerts J *et al*: SCENIC: single-cell regulatory network inference and clustering. *Nature methods* 2017, 14(11):1083-1086.
278. Bache KG, Slagsvold T, Cabezas A, Rosendal KR, Raiborg C, Stenmark H: The growth-regulatory protein HCRP1/hVps37A is a subunit of mammalian ESCRT-I and mediates receptor down-regulation. *Molecular biology of the cell* 2004, 15(9):4337-4346.
279. Stefani F, Zhang L, Taylor S, Donovan J, Rollinson S, Doyotte A, Brownhill K, Bennion J, Pickering-Brown S, Woodman P: UBAP1 is a component of an endosome-specific ESCRT-I complex that is essential for MVB sorting. *Curr Biol* 2011, 21(14):1245-1250.
280. Wunderley L, Brownhill K, Stefani F, Taberero L, Woodman P: The molecular basis for selective assembly of the UBAP1-containing endosome-specific ESCRT-I complex. *Journal of cell science* 2014, 127(Pt 3):663-672.

281. Kazmi F, Hensley T, Pope C, Funk RS, Loewen GJ, Buckley DB, Parkinson A: Lysosomal sequestration (trapping) of lipophilic amine (cationic amphiphilic) drugs in immortalized human hepatocytes (Fa2N-4 cells). *Drug metabolism and disposition: the biological fate of chemicals* 2013, 41(4):897-905.
282. Lemieux B, Percival MD, Falgoutyret JP: Quantitation of the lysosomotropic character of cationic amphiphilic drugs using the fluorescent basic amine Red DND-99. *Analytical biochemistry* 2004, 327(2):247-251.
283. Klionsky DJ, Abdelmohsen K, Abe A, Abedin MJ, Abeliovich H, Acevedo Arozena A, Adachi H, Adams CM, Adams PD, Adeli K *et al*: Guidelines for the use and interpretation of assays for monitoring autophagy (3rd edition). *Autophagy* 2016, 12(1):1-222.
284. Chazotte B: Labeling lysosomes in live cells with LysoTracker. *Cold Spring Harbor protocols* 2011, 2011(2):pdb prot5571.
285. Chen CS, Chen WN, Zhou M, Arttamangkul S, Haugland RP: Probing the cathepsin D using a BODIPY FL-pepstatin A: applications in fluorescence polarization and microscopy. *Journal of biochemical and biophysical methods* 2000, 42(3):137-151.
286. Lee C, Lamech L, Johns E, Overholtzer M: Selective Lysosome Membrane Turnover Is Induced by Nutrient Starvation. *Dev Cell* 2020, 55(3):289-297 e284.
287. Di Malta C, Cinque L, Settembre C: Transcriptional Regulation of Autophagy: Mechanisms and Diseases. *Front Cell Dev Biol* 2019, 7:114.
288. Zhao Q, Gao SM, Wang MC: Molecular Mechanisms of Lysosome and Nucleus Communication. *Trends Biochem Sci* 2020, 45(11):978-991.
289. Vance JE, Karten B: Niemann-Pick C disease and mobilization of lysosomal cholesterol by cyclodextrin. *Journal of lipid research* 2014, 55(8):1609-1621.
290. Eid W, Dauner K, Courtney KC, Gagnon A, Parks RJ, Sorisky A, Zha X: mTORC1 activates SREBP-2 by suppressing cholesterol trafficking to lysosomes in mammalian cells. *Proc Natl Acad Sci U S A* 2017, 114(30):7999-8004.
291. Kwiatkowska K, Marszalek-Sadowska E, Traczyk G, Koprowski P, Musielak M, Lugowska A, Kulma M, Grzelczyk A, Sobota A: Visualization of cholesterol deposits in lysosomes of Niemann-Pick type C fibroblasts using recombinant perfringolysin O. *Orphanet journal of rare diseases* 2014, 9:64.
292. Brovkovich V, Aldrich A, Li N, Atilla-Gokcumen GE, Frasor J: Removal of Serum Lipids and Lipid-Derived Metabolites to Investigate Breast Cancer Cell Biology. *Proteomics* 2019, 19(18):e1800370.
293. Wrobel M, Cendrowski J, Szymanska E, Grebowicz-Maciukiewicz M, Budick-Harmelin N, Macias M, Szybinska A, Mazur M, Kolmus K, Goryca K *et al*: ESCRT-I fuels lysosomal degradation to restrict TFEB/TFE3 signaling via the Rag-mTORC1 pathway. *Life science alliance* 2022, 5(7).
294. Boutry M, Pierga A, Matusiak R, Branchu J, Houllegatte M, Ibrahim Y, Balse E, El Hachimi KH, Brice A, Stevanin G *et al*: Loss of spatacsin impairs cholesterol trafficking and calcium homeostasis. *Commun Biol* 2019, 2:380.

295. Sun X, Yang Y, Zhong XZ, Cao Q, Zhu XH, Zhu X, Dong XP: A negative feedback regulation of mTORC1 activity by the lysosomal Ca²⁺ channel MCOLN1 (mucopolin 1) using a CALM (calmodulin)-dependent mechanism. *Autophagy* 2018, 14(1):38-52.
296. Liu J, Farmer JD, Jr., Lane WS, Friedman J, Weissman I, Schreiber SL: Calcineurin is a common target of cyclophilin-cyclosporin A and FKBP-FK506 complexes. *Cell* 1991, 66(4):807-815.
297. Castellano BM, Thelen AM, Moldavski O, Feltes M, van der Welle RE, Mydock-McGrane L, Jiang X, van Eijkeren RJ, Davis OB, Louie SM *et al*: Lysosomal cholesterol activates mTORC1 via an SLC38A9-Niemann-Pick C1 signaling complex. *Science* 2017, 355(6331):1306-1311.
298. Hsieh AC, Liu Y, Edlind MP, Ingolia NT, Janes MR, Sher A, Shi EY, Stumpf CR, Christensen C, Bonham MJ *et al*: The translational landscape of mTOR signalling steers cancer initiation and metastasis. *Nature* 2012, 485(7396):55-61.
299. Eriksson I, Waster P, Ollinger K: Restoration of lysosomal function after damage is accompanied by recycling of lysosomal membrane proteins. *Cell death & disease* 2020, 11(5):370.
300. Du X, Kazim AS, Brown AJ, Yang H: An essential role of Hrs/Vps27 in endosomal cholesterol trafficking. *Cell reports* 2012, 1(1):29-35.
301. Tan JX, Finkel T: A phosphoinositide signalling pathway mediates rapid lysosomal repair. *Nature* 2022, 609(7928):815-821.
302. Wilhelm LP, Wendling C, Védie B, Kobayashi T, Chenard MP, Tomasetto C, Drin G, Alpy F: STARD3 mediates endoplasmic reticulum-to-endosome cholesterol transport at membrane contact sites. *EMBO J* 2017, 36(10):1412-1433.
303. Platt FM, d'Azzo A, Davidson BL, Neufeld EF, Tiffit CJ: Lysosomal storage diseases. *Nature reviews Disease primers* 2018, 4(1):27.
304. Lakpa KL, Khan N, Afghah Z, Chen X, Geiger JD: Lysosomal Stress Response (LSR): Physiological Importance and Pathological Relevance. *Journal of neuroimmune pharmacology : the official journal of the Society on NeuroImmune Pharmacology* 2021, 16(2):219-237.
305. Zhou J, Tan SH, Nicolas V, Bauvy C, Yang ND, Zhang J, Xue Y, Codogno P, Shen HM: Activation of lysosomal function in the course of autophagy via mTORC1 suppression and autophagosome-lysosome fusion. *Cell research* 2013, 23(4):508-523.
306. Yu L, McPhee CK, Zheng L, Mardones GA, Rong Y, Peng J, Mi N, Zhao Y, Liu Z, Wan F *et al*: Termination of autophagy and reformation of lysosomes regulated by mTOR. *Nature* 2010, 465(7300):942-946.
307. Eden ER, Sanchez-Heras E, Tsapara A, Sobota A, Levine TP, Futter CE: Annexin A1 Tethers Membrane Contact Sites that Mediate ER to Endosome Cholesterol Transport. *Dev Cell* 2016, 37(5):473-483.
308. Lim CY, Davis OB, Shin HR, Zhang J, Berdan CA, Jiang X, Coughlin JL, Ory DS, Nomura DK, Zoncu R: ER-lysosome contacts enable cholesterol sensing by mTORC1 and

- drive aberrant growth signalling in Niemann-Pick type C. *Nature cell biology* 2019, 21(10):1206-1218.
309. Braulke T, Bonifacino JS: Sorting of lysosomal proteins. *Biochimica et biophysica acta* 2009, 1793(4):605-614.
310. Du X, Kazim AS, Dawes IW, Brown AJ, Yang H: The AAA ATPase VPS4/SKD1 regulates endosomal cholesterol trafficking independently of ESCRT-III. *Traffic* 2013, 14(1):107-119.
311. Li K, Wada S, Gosis BS, Thorsheim C, Loose P, Arany Z: Folliculin promotes substrate-selective mTORC1 activity by activating RagC to recruit TFE3. *PLoS biology* 2022, 20(3):e3001594.
312. Asrani K, Woo J, Mendes AA, Schaffer E, Vidotto T, Villanueva CR, Feng K, Oliveira L, Murali S, Liu HB *et al*: An mTORC1-mediated negative feedback loop constrains amino acid-induced FLCN-Rag activation in renal cells with TSC2 loss. *Nat Commun* 2022, 13(1):6808.
313. Napolitano G, Di Malta C, Esposito A, de Araujo MEG, Pece S, Bertalot G, Matarese M, Benedetti V, Zampelli A, Stasyk T *et al*: A substrate-specific mTORC1 pathway underlies Birt-Hogg-Dube syndrome. *Nature* 2020, 585(7826):597-602.
314. Alesi N, Akl EW, Khabibullin D, Liu HJ, Nidhiry AS, Garner ER, Filippakis H, Lam HC, Shi W, Viswanathan SR *et al*: TSC2 regulates lysosome biogenesis via a non-canonical RAGC and TFEB-dependent mechanism. *Nat Commun* 2021, 12(1):4245.
315. Yang H, Jiang X, Li B, Yang HJ, Miller M, Yang A, Dhar A, Pavletich NP: Mechanisms of mTORC1 activation by RHEB and inhibition by PRAS40. *Nature* 2017, 552(7685):368-373.
316. Schalm SS, Fingar DC, Sabatini DM, Blenis J: TOS motif-mediated raptor binding regulates 4E-BP1 multisite phosphorylation and function. *Curr Biol* 2003, 13(10):797-806.
317. Bache KG, Stuffers S, Malerod L, Slagsvold T, Raiborg C, Lechardeur D, Walchli S, Lukacs GL, Brech A, Stenmark H: The ESCRT-III subunit hVps24 is required for degradation but not silencing of the epidermal growth factor receptor. *Molecular biology of the cell* 2006, 17(6):2513-2523.
318. Jung J, Genau HM, Behrends C: Amino Acid-Dependent mTORC1 Regulation by the Lysosomal Membrane Protein SLC38A9. *Molecular and cellular biology* 2015, 35(14):2479-2494.
319. Deng L, Jiang C, Chen L, Jin J, Wei J, Zhao L, Chen M, Pan W, Xu Y, Chu H *et al*: The ubiquitination of rag A GTPase by RNF152 negatively regulates mTORC1 activation. *Molecular cell* 2015, 58(5):804-818.
320. Jin G, Lee SW, Zhang X, Cai Z, Gao Y, Chou PC, Rezaeian AH, Han F, Wang CY, Yao JC *et al*: Skp2-Mediated RagA Ubiquitination Elicits a Negative Feedback to Prevent Amino-Acid-Dependent mTORC1 Hyperactivation by Recruiting GATOR1. *Molecular cell* 2015, 58(6):989-1000.

321. Ogmundsdottir MH, Heublein S, Kazi S, Reynolds B, Visvalingam SM, Shaw MK, Goberdhan DC: Proton-assisted amino acid transporter PAT1 complexes with Rag GTPases and activates TORC1 on late endosomal and lysosomal membranes. *PloS one* 2012, 7(5):e36616.
322. Jansen RM, Peruzzo R, Fromm SA, Yokom AL, Zoncu R, Hurley JH: Structural basis for FLCN RagC GAP activation in MiT-TFE substrate-selective mTORC1 regulation. *Science advances* 2022, 8(37):eadd2926.
323. Di Malta C, Siciliano D, Calcagni A, Monfregola J, Punzi S, Pastore N, Eastes AN, Davis O, De Cegli R, Zampelli A *et al*: Transcriptional activation of RagD GTPase controls mTORC1 and promotes cancer growth. *Science* 2017, 356(6343):1188-1192.
324. van der Welle REN, Jobling R, Burns C, Sanza P, van der Beek JA, Fasano A, Chen L, Zwartkruis FJ, Zwakenberg S, Griffin EF *et al*: Neurodegenerative VPS41 variants inhibit HOPS function and mTORC1-dependent TFEB/TFE3 regulation. *EMBO Mol Med* 2021, 13(5):e13258.
325. Sweitzer TD, Hanover JA: Calmodulin activates nuclear protein import: a link between signal transduction and nuclear transport. *Proc Natl Acad Sci U S A* 1996, 93(25):14574-14579.
326. Holaska JM, Black BE, Rastinejad F, Paschal BM: Ca²⁺-dependent nuclear export mediated by calreticulin. *Molecular and cellular biology* 2002, 22(17):6286-6297.
327. Li RJ, Xu J, Fu C, Zhang J, Zheng YG, Jia H, Liu JO: Regulation of mTORC1 by lysosomal calcium and calmodulin. *Elife* 2016, 5.
328. Hartley D, Cooper GM: Role of mTOR in the degradation of IRS-1: regulation of PP2A activity. *Journal of cellular biochemistry* 2002, 85(2):304-314.
329. Di Conza G, Trusso Cafarello S, Lorocho S, Mennerich D, Deschoemaeker S, Di Matteo M, Ehling M, Gevaert K, Prenen H, Zahedi RP *et al*: The mTOR and PP2A Pathways Regulate PHD2 Phosphorylation to Fine-Tune HIF1alpha Levels and Colorectal Cancer Cell Survival under Hypoxia. *Cell reports* 2017, 18(7):1699-1712.
330. Cianfanelli V, Fuoco C, Lorente M, Salazar M, Quondamatteo F, Gherardini PF, De Zio D, Nazio F, Antonioli M, D'Orazio M *et al*: AMBRA1 links autophagy to cell proliferation and tumorigenesis by promoting c-Myc dephosphorylation and degradation. *Nature cell biology* 2015, 17(1):20-30.
331. Sha Y, Rao L, Settembre C, Ballabio A, Eissa NT: STUB1 regulates TFEB-induced autophagy-lysosome pathway. *EMBO J* 2017, 36(17):2544-2552.
332. Rao L, Sha Y, Eissa NT: The E3 ubiquitin ligase STUB1 regulates autophagy and mitochondrial biogenesis by modulating TFEB activity. *Molecular & cellular oncology* 2017, 4(6):e1372867.
333. Davis OB, Shin HR, Lim CY, Wu EY, Kukurugya M, Maher CF, Perera RM, Ordonez MP, Zoncu R: NPC1-mTORC1 Signaling Couples Cholesterol Sensing to Organelle Homeostasis and Is a Targetable Pathway in Niemann-Pick Type C. *Dev Cell* 2021, 56(3):260-276 e267.

334. Abu-Remaileh M, Wyant GA, Kim C, Laqtom NN, Abbasi M, Chan SH, Freinkman E, Sabatini DM: Lysosomal metabolomics reveals V-ATPase- and mTOR-dependent regulation of amino acid efflux from lysosomes. *Science* 2017, 358(6364):807-813.
335. Gosis BS, Wada S, Thorsheim C, Li K, Jung S, Rhoades JH, Yang Y, Brandimarto J, Li L, Uehara K *et al*: Inhibition of nonalcoholic fatty liver disease in mice by selective inhibition of mTORC1. *Science* 2022, 376(6590):eabf8271.

9. Publications by Marta Wróbel

1. Cendrowski, J., **Kaczmarek, M.**, Mazur, M., Kuzmich-Kowalska, K., Jastrzebski, K., Brewinska-Olchowik, M., Kominek, A., Piwocka, K., Miaczynska, M. Splicing variation of BMP2K balances abundance of COPII assemblies and autophagic degradation in erythroid cells. *Elife* 2020, 9.
2. **Wrobel M.**, Cendrowski J, Szymanska E, Grebowicz-Maciukiewicz M, Budick-Harmelin N, Macias M, Szybinska A, Mazur M, Kolmus K, Goryca K *et al*: ESCRT-I fuels lysosomal degradation to restrict TFEB/TFE3 signaling via the Rag-mTORC1 pathway. *Life science alliance* 2022, 5(7).

10. Supplementary materials

Table 1. List of upregulated genes upon depletion of Tsg101 (1166 genes) or Vps28 (601 genes)

Condition (siRNA- mediated depletion)	Gene symbols
siTsg101#2	<p>TNFRSF9, CXCL8, LINC00856, NEURL3, MMP10, CXCL3, HKDC1, TUSC3, GCNT3, TNFAIP6, SIGLEC15, TNIP3, SPINK1, CXCL1, CCL20, PLK2, IKBKG, PLEKHG4, KRTAP5-1, WNT7B, GK, CPAMD8, EID3, HMGCS1, MFAP2, IGFN1, SYNGR3, ODF3L2, CLDN1, SIGLEC9, RPLP0P2, ITGAX, BIRC3, FMO4, IL1A, MMP3, TNFAIP8, PI3, KRT15, FAM120AOS, CLIP4, GPR137C, EBI3, LIPG, CXCL2, KRT34, IFI44, BCAT1, LINC00520, C3, TANK, ZNF165, PIR, SRP14-AS1, IRAK2, ANKDD1A, DHCR7, MMP1, N4BP2, RCSD1, NFKBIA, MSMO1, OSGIN1, RPL31, B3GNT5, SLC7A11, TM4SF1, MET, CD82, MVP, MIR22HG, LOC100126784, SLC36A1, SFN, PTPMT1, FBXO32, GCLM, EPAS1, OARD1, PCSK9, NINJ1, TP53INP2, SQLE, FDFT1, ABCA5, HDAC9, IDI1, MFAP3L, USP53, TFRC, LACTB, NEK8, NQO1, TMEM102, NFKBIE, CBLB, TANGO2, AAK1, PDXDC1, BHLHE40, NTN1, NPC1, RPL13P5, DYNLT3, CEBPB, AP1G2, SAT1, SEMA3C, SOD2, SIK1, IL11, PDE4DIP, PFKFB2, LTB4R2, HSD17B7, PPP2R3A, STK17A, AHNAK2, NSDHL, SLC16A13, HSD17B14, ZNF354A, WDTC1, SLC41A2, IL6ST, RIOK3, RAB4B, N4BP3, TCP11L2, ARRDC4, GLA, C8orf31, ZC3H6, UBLCP1, RIT1, KDM6A, FAM102A, MAPKAP1, IL21R, KBTBD8, STX12, HMOX1, RELB, AMPD3, SOS2, ARL1, LACC1, IGSF8, ICAM1, PLEKHM1, CALU, MVK, OPTN, ZFAT, ESM1, AGPAT4, NRBF2, TM4SF19, ATP6V0A1, TRIQK, HSPA12A, IQCG, DUSP1, FAM49B, C6orf141, SMAP1, EPB41L1, PLK3, PJA2, TCF20, MARCKS, ACHE, FAM221A, C3orf58, KIF21A, NRP1, RALA, SPRY2, KLHL21, TSC22D2, XIAP, PRMT2, RETREG1, WSB1, CYLD, LRP8, MVD, MGST1, STXBP2, CSF1, BCL9, PLTP, ITPKC, DNAJB4, CTNS, RBAKDN, NFKBIZ, PRDM8, TYMP, KDM6B, SRXN1, ALG14, ACAT2, WWTR1, TUBB2A, UBXN8, DGKI, CD68, VAMP7, ZCWPW1, OCRL, ATP10D, GEM, PDIA4, FAM214B, PPFIBP1, UGCG, SLC46A3, INSIG1, ATP9A, TMEFF1, HMGCR, BCL10, CCSER2, ZDHHC1, TNIP1, TAPT1, CAMKMT, COA6, ZFHX2, C7orf13, KLF6, CUL9, CNDP2, TTL, IL32, ENTPD7, DUSP16, LINC00346, RPS6KL1, SELIL3, ERG28, GPRC5A, CLCN6, C9orf72, PPP2R5B, KMT5A, HM13, CDK20, MIB1, TMEM53, ACSL5, INSIG2, RNF6, SCARNA5, SPIRE1, PIP4K2A, MMAB, DYRK3, ZBTB46, CYP51A1, ZNF697, C1GALT1, TRPM4, STARD4, ZCCHC6, MAP3K14, SLC38A6, NEAT1, PLA2G12A, CRY1, AKTIP, AKT3, RASAL2, ME2, TNFAIP3, SLC38A7, ZCCHC2, DNAJB2, RND3, PRKCD, GALNT11, NUDT12, MMP25, TYW1, NA, RNF103, RBPI, MTMR9LP, ZNF621, RFK, GFPT2, GRB10, CREB3, AKAP13, PIK3CD, NRAS, MXD1, EFN2, NDUFB2-AS1, RPS6KC1, C3orf52, HERC2P7, UBE2I, FHIT, ADTRP, NEU1, ZDHHC9, GGPS1, SYT7, MYH14, MEST, ABL2, SEPSECS, MR1, WDR45, LRRC8E, UCHL3, LYST, NFKBIB, SNORA80B, ESYT2, ZNF217, IPP, CASTOR1, CETN2, DPH3, CDCP1, CCNG2, RNF213, EBLN3P, PDCD6, RRAS, TMEM65, SLC2A6, WDFY1, LINC00941, ARRDC3, NIT1, ASB7, RSPH3, PDK1, ZFAND2A, DNASE1L1, SEZ6L2, YWHAZ, C12orf49, NCOA3, AP1AR, POLR3F, GPCPD1, NFKB1, USP11, FAM24B, SERINC2, STOML1, MTRF1L, PITHD1, ERN1, DST, ACSL3, CPZ, CCNC, PCSK7, BACH1, NFE2L2, ZFYVE1, SELENOI, PGM1, FZD8, RABGGTB, RAB1A, SH3RF1, USP12, MTAP, PLEKHO2, STAG2, LOC642852, SQSTM1, SLC35D1, KCTD9, RAPGEF2, DNAJB5, PSMB8, SAT2, DCTN4, STARD3NL, STARD10, ATM, MCL1, PPP2R1B, CCNE1, TNFSF15, TNFSF9, RHBDF2, TATDN1, ANXA7, ZNF354B, SECISBP2L, PRKACA, KDM4C, ASAH1, ABCA1, TNC, FNIP2, FGFR4, SEC24A, CDKN1A, MLYCD, DYNC1H1, TMF1, CSPP1, LURAP1L, C18orf32, HELQ, BROX, PPP3CB, TP53INP1, SPAG9, JUNB, FSTL3, EIF2B2, SDSL, WDR1, GOPC, MBTPS1, TBC1D2B, CLIP2, LDLR, E2F5, G6PD, ARNTL, TSPAN3, GID4, PRELID3A, TAF13, GCLC, CAMSAP2, VPS41, FAR1, CYB5D1, BANF1, CDK19, TMEM159, TMCC1-AS1, TALDO1, CNOT7, FBXL12, WDR83, ATP6V1H, CD163L1, SOX4, TRIT1, GLMP, VPS13C, INO80B, ITGAV, GAB2, BOD1, VTI1A, PRKAB2, TSLP, YBX1, SDCBP, RELL2, FASN, LMAN1, CDK18, YTHDF3, NSMF, PELI1, MFSD11, PTPN14, SERTAD3, PDK3, NIPAL2, FTH1, PEX1, ORAI3, SEPT3, C11orf80, ZNF616, G3BP2, CLCN7, IL13RA2, ATG16L1, ZFR, SRGAP1, NRBP1, PLPP6, STK32C, DENND5A, TOM1, UBE4A, KATNAL1, ZNF816, U2SURP, GSE1, ZSWIM4, KCNC4, EEA1, ATP13A3, CNST, KAT5, DPYSL2, LZTS3, ZFAND3, RPS7, MCOLN1, SF1, PER3, GIPR, TMEM41B, NUP205, MAP4K4, DNAJB9, ZNF841, SLC9A8, RNF167, VEGFC,</p>

TTC37, RIPK2, BCAP31, LINC01278, NIT2, PDPK1, MTHFR, NPEPPS, TPD52L1, ACOX1, KLF11, RWDD2B, LINC00174, IFNGR2, NSRP1, SLC35D2, SRPRA, TMEM192, NHLRC2, SKAP2, STYXL1, ZNF720, TMEM35B, GOT1, HSPA13, CHKB, GPN2, SDC3, SLC26A11, LINC-PINT, INTS3, SIRT7, LMBRD2, TCEAL9, H6PD, COG6, TMTC3, ODC1, CMAS, LTBP1, CLDND1, PIK3C2A, ACACA, SLC7A2, ATP6V1B2, RIF1, TSPAN17, UHRF1BP1L, ZNHIT6, SLC29A2, JSRP1, ZNF622, YOD1, ATG12, C6orf62, CA5BP1, TMEM241, EIF4B, ERCC5, PLEKHA3, SCAF11, CBR1, HNF4G, HPS3, HGSNAT, RBMX2, TSEN15, GMDS, PSMG4, TMBIM1, MICA, SLK, CDC73, RAB7A, PPP2CA, SNHG16, NAA60, DAAMI, GNPTG, ZNF322, ISOC1, MCRS1, WDR3, ARFGAP3, BLVRA, TBC1D10A, COPS5, HDHD3, RNF144A, WASHC3, UAPI, RALBP1, ZMIZ1, ESCO1, SNX10, CTBS, GTF2E1, HSP90AA1, AFAP1, RNF146, LYPLAL1, HIVEP1, TNKS, CDK11B, TRAPPC4, ZNF263, WDR35, PKP2, ACTR3, VPS37A, OSBP, PCED1A, TSPAN31, FEM1C, GABARAP, CDK9, LRP1, ATP6V0A2, PITRM1, EPG5, EPB41L5, SELENOM, PNPLA8, PSAP, CREM, WFS1, TMEM14B, SPRTN, MCCC1, ATXN2, CCNL2, RCHY1, AK2, SMCR8, RAB18, MMADHC, TMEM131, TMEM251, SOX12, CCDC90B, ARPC1A, LMO4, TVP23B, PDGFA, CHSY1, FYTTD1, POMP, MRPS18C, GPR157, SYNJ2BP, PIKFYVE, PRKCSH, ZNF561, BORCS7, DMTF1, TRAPPC11, CREBL2, EIF3I, RRAGC, CPQ, ZNF644, SMARCAD1, RNF157, TTC23, TOMM20, RDH11, GOLGA2, APEX2, UPP1, PSMA1, FXN, SLC27A1, PRRC2C, C5orf51, AKAP12, HSD17B12, ZNF254, RB1CC1, MED7, KDM5C, GLIPR1, EIF3B, ZRANB2, ZNF800, ABHD5, KCTD13, USP46, SCAPER, MRPL34, THAP5, GLUL, FER, DERL2, CIRBP, WDR19, PHLDB3, FOSL2, NECAP2, COPB2, SGSH, PANX1, SNX12, S100A11, KDM3A, TTI2, ARNTL2, TUBB3, MAN1B1, GLTP, ZSCAN26, JOSD1, ZNF277, UGDH, UFL1, RER1, IFNGR1, CLIP1, OLMALINC, BRWD3, GORASP2, EIF1, SHTN1, NT5E, NA, TXNDC15, IAH1, PVRIG, CARNMT1, LRP12, PPP3R1, DNAJC24, FBXO38, THTPA, TMEM38B, TCEAL8, SNX3, COL4A3BP, WWP1, PDE6D, VPS35, ANKIB1, PKNOX1, FAF2, FAM160A2, GUK1, ANKRD44, RNF19B, SEC22B, BRPF1, DOCK7, ARFGEF3, NKIRAS1, SERPINB8, ATG7, BRMS1L, STAM, ZNF787, RGS19, PHKB, SCYL2, UNC50, GOLGA4, SCAF1, PGM2L1, TRAPPC3, MGRN1, CCDC82, ABCC4, PAPD4, RBSN, RHOB, H1FX, POLR1D, C3orf38, LOC652276, FNBP1L, TMEM231, CMBL, BLZF1, FBXO10, LINC-PINT, TTC5, TRIP10, TTC1, MDM4, PHYH, TMEM185B, RPL35A, FBXO8, PSD4, PIK3R2, CWC15, MSANTD4, HABP4, PSMC1, DDX19A, SLC25A16, APH1B, AP5Z1, MBD4, SETDB2, SENP6, PTGR1, NMI, ARSA, MED21, ID1, TRMO, MTG1, CTSL, USP40, TIGAR, UTP14A, ESD, TDRD3, UHMK1, LINC01347, GRINA, PSMA6, ELF1, VGF, RHPN1-AS1, SNX19, TRAPPC6B, ARVCF, MTRR, SRA1, UBE2B, POLK, TM9SF1, TMEM87B, SNRNP27, LINC01003, DCUN1D5, ZCCHC9, IREB2, ETF1, GALNT12, RBM26, TERF1, DCUN1D1, AGGF1, CANX, RPL39, SLC8B1, HLA-F, MRPL30, KLHL12, CARS, ANAPC4, UBA6, SUCO, COX7A2, EPCAM, FAM217B, FDPS, DAP3, UVRAG, SH3PXD2B, SMS, TEAD1, DDX52, PARD3, SPG21, VPS26A, HGS, NDFIP1, TRMT61B, JAK1, GRN, IP6K2, PITX1, RALGPS2, PTAR1, HGF, CCNH, VPS9D1-AS1, ZCRB1, FAM177A1, CCDC59, EMC2, PLBD1, P4HB, EHMT1, HSDL2, NBR2, CCDC102A, RBM42, SLC39A11, DARS2, UBE2A, EHD1, CAPN7, ZNF623, PLIN3, FARSB, TTC39C, ZC2HC1A, PPP1CC, ZNF462, NFYB, MICU2, ASF1A, ID3, PPP3CA, CLNS1A, PHKA2, NCL, PSMG2, SIL1, RPL8, PTPN21, WDR47, SIRT2, HMGA2, HOXC10, SART1, LARP7, RARS, FGD1, USP15, NAV1, NAF1, STRAP, LRRC41, FKBP8, LNPB, RAP1B, CSTF1, WRAP53, BACE2, CTU1, BET1L, FECH, LYRM1, MRPS30, TMUB1, SKIV2L, ARL6IP1, PLA2G4A, XYLB, PPIP5K2, AP3B1, QDPR, KRAS, DMXL1, M6PR, LAMTOR3, ACSL1, WDYHV1, MYADM, PPIL2, DDX47, FASTKD5, HINT3, EP300, C8orf37, XRN2, EXOC1, CFL2, ATF5, WDSUB1, ZDHHC2, TAF11, PLRG1, TMEM168, PLAG1, PRCP, ARID4B, HIST1H2BK, METTL14, RBL2, TFEB, RPL22L1, NKTR, SFSWAP, COMMD2, FASTKD1, SNORA27, ALG9, GK5, ZNF627, OSTM1, IL13RA1, GNL3L, LAMA1, SMAD1, TRAF5, ADAM10, MORF4L2, MRAS, UEVLD, DPH6, ORMDL1, NCKAP1, SKI, LAMP1, ZNF92, PEAK1, F8A1, AFF3, IDH3B, ZNF32, FRA10AC1, DUS4L, TYW3, SPRY4, ERP29, MRPS25, FUS, TMEM5, SLC19A1, MED13L, CAMK2D, CACUL1, ERFF1, MRPS36, DCUN1D4, NAPA, NIPA2, SPNS1, EXTL2, TFG, PON2, RPL24, FEM1A, ERCC8, EIF2S2, SUCLA2, C12orf4, ZNF10, PHF11, CHCHD7, SIRT5, GEN1, SZT2, MAP3K4, UGT8, MRPL35, ANXA2, C2orf69, HNRNPLL, AFG3L2, BTF3L4, SCRIN2, SNUPN, AP4M1, MED23, GGNBP2, GNAI1, TP53I11, NAP1L1, RNF170, PAXBP1, JAZF1, DOCK11, ATRX, ST6GALNAC6, GFPT1, ATP6AP2, POLR2I, LACTB2, SDC1, MAP2K3, PHIP, NELFB, CDC37L1, PARG, TYW5, DECR1, BTG3, MRPS35, RECQL, CLN3, PQBP1, PAQR3, PRPF40B, CHAC2, CHMP1A, MSX2, PPP1R35, TNFRSF1A, ASNS, MBD6, ZNF131, MTO1, SLC38A9, PTPRA, PKN3, TUSC2, COX8A, SECISBP2, PTP4A1, MTM1, HNRNPH3, STUB1, HSPB11, AKNA, HSBP1L1,

	<p>NUDCD1, NHEJ1, PIGP, ABRAXAS1, UTRN, TUBB4B, TPRKB, N6AMT1, NR4A1, SCR3, KDM1A, USP1, ACADM, SLC25A13, BCL3, PHKG2, SSB, SNORA14A, OXA1L, NHLRC3, HECTD2, MAK16, HOXA7, TNRC6B, REV1, ZNF275, GTPBP8, KDELC2, ANKRD49, E2F2, SRGAP2, MZT1, AKAP1, PM20D2, PRELID2, ASH2L, NEMP1, NDC80, KIF22, RFC5, IMP3, TTF1, KLF10, NOV, HIST1H2BF, MTCH1</p>
siVps28#2	<p>TNFRSF9, CXCL8, LINC00856, NEURL3, MMP10, CXCL3, HKDC1, TUSC3, GCNT3, TNFAIP6, F2RL2, SIGLEC15, TNIP3, SPINK1, CSF2, CXCL1, CCL20, PLK2, TREML3P, WNT7B, EID3, HMGC51, RPLP0P2, ITGAX, MMP19, BIRC3, MMP3, TNFAIP8, PI3, EBI3, LIPG, CXCL2, TNFRSF1B, SGSM1, IFI44, LINC00520, CYP4F11, ZNF165, PIR, IRAK2, SLC26A6, DHCR7, KIAA1217, MMP1, N4BP2, TMEM88, SH3TC2, NFKBIA, MSMO1, OSGIN1, B3GNT5, SLC7A11, TM4SF1, MET, CD82, MVP, MIR22HG, LOC100126784, SLC36A1, SFN, FOXL1, FBXO32, PLAU, GCLM, EPAS1, PCSK9, NINJ1, TP53INP2, SQLE, FDFT1, ABCA5, HDAC9, IDI1, USP53, TFRC, LACTB, NQO1, TMEM102, NFKBIE, PTK6, CBLB, TANGO2, BHLHE40, NPC1, DYNLT3, CEBPB, SAT1, PATJ, SOD2, SIK1, SLC2A3, PDE4DIP, PFKFB2, LTB4R2, HSD17B7, PI4KAP1, STK17A, NSDHL, SLC16A13, HSD17B14, ZNF354A, SLC41A2, IL6ST, RIOK3, RAB4B, N4BP3, GLA, RIT1, FAM102A, KIAA0319, KBTBD8, HBEGF, IL17RC, HMOX1, PISD, RELB, FLNB, AMPD3, TLE6, LACC1, ICAM1, PLEKHM1, MVK, OPTN, ESM1, TM4SF19, TRIQK, DUSP1, FAM49B, C6orf141, PLK3, MARCKS, ACHE, FAM221A, BCL2L2, C3orf58, KIF21A, RALA, SPRY2, KLHL21, PRMT2, SMIM3, LRP8, MVD, MGST1, STXBP2, CSF1, ITPKC, DNAJB4, CTNS, NFKBIZ, TYMP, B4GALT5, KDM6B, SRXN1, ACAT2, TUBB2A, DGKI, ITPR1, CD68, ZCWPW1, OCRL, ABHD4, KLC3, ATP10D, GEM, FAM214B, INSIG1, HMGCR, ALS2CL, SLC12A6, PLEKHN1, MAPKBP1, KCNAB3, CCSER2, ARHGEF26, TNIP1, ZFH2, KLF6, STAP2, CNDP2, IL32, ENTPD7, LINC00346, RPS6KL1, SEL1L3, ERG28, CLCN6, KLF5, C9orf72, PPP2R5B, CDK20, GPAT3, ACSL5, INSIG2, MBOAT2, MMAB, TRIB1, DYRK3, CYP51A1, ZNF697, C1GALT1, STARD4, ZCCHC6, MAP3K14, GABARAPL1, NR4A2, TMEM150A, SLC38A6, NEAT1, PLA2G12A, TNFAIP3, SLC38A7, ZCCHC2, ITGA2, RND3, PRKCD, SGK494, MAST4, ATXN7L1, GALNT11, CISH, MMP25, ACOT13, RNF103, MAN2B1, ALDOC, PIK3CD, CRIP2, ALOX12B, MXD1, EFNB2, RPS6KC1, C3orf52, FHIT, NEU1, ZDHHC9, IL12A, LOC90768, SYT7, MYH14, ABL2, BCAR3, LRRC8E, ELMSAN1, UCHL3, LYST, NFKBIB, MREG, ZNF217, PICK1, CETN2, TAB3, PFKFB4, CCNG2, RRAS, SLC2A6, ARRC3, NIT1, PDK1, DNASE1L1, TESK1, NCOA3, NFKB1, SERINC2, METTL27, PLEKHM3, PITHD1, STX11, ERN1, BACH1, GCH1, LOC642852, SQSTM1, PSMB8, BAIAP2L1, SAT2, ZC3H12A, REL, CCNE1, MYOF, TNFSF9, RHBDF2, LCP1, FNIP2, FGFR4, DYNC1H1, GSR, PELO, FAM117A, SPAG9, NIPAL1, RETSAT, JUNB, FSTL3, EIF2B2, PRSS22, CLDN12, LDLR, GABARAPL2, G6PD, GID4, STXBP1, FAM160A1, GCLC, SLC37A3, TMEM159, TMCC1-AS1, TALDO1, SLC35C2, GLMP, GAB2, TRAF3IP2, FIG4, ZNF267, LSR, RAB11FIP4, FASN, NSMF, USP43, ARSJ, CLN8, HLA-A, SGIP1, ZNF616, TBC1D17, CLCN7, NPLOC4, BBS12, SMURF1, SLC17A5, TM7SF2, RAP2B, KCNK1, IKZF3, DEXI, TMEM106A, LZTS3, MCOLN1, MAP4K4, DNAJB9, ZNF841, RIPK2, ZFAND5, UBL3, PGD, EML2, CDC42EP3, SRPRA, RTN4R, SKAP2, STYXL1, KHNYN, TIPRL, KCTD11, ZNFX1, DUSP18, SLC26A11, LINC-PINT, C1RL, STX4, GADD45A, MCF2L2, GDDP5, CMAS, CLDND1, C16orf72, SLC29A2, JSRP1, PSMA3, MT1X, BTBD11, EIF4B, CBR1, HNF4G, RHPN1, HPS3, FAM131A, MICA, ANKRD9, RAB7A, RRP12, DAAM1, GNPTG, CTSD, SNX29, SETD7, BLVRA, HDHD3, GSK3B, ZMIZ1, PTRH1, LPP, DESI1, ZNF474, PHYKPL, VPS37A, UBE2D1, MAP3K9, PITRM1, TMEM63B, FMNL3, SELENOM, USP2-AS1, TMEM14B, ZNF556, AK2, TMEM251, SYNGAP1, SCARNA17, SOX12, TDRKH, TPP1, TAP1, MRPS18C, RNF207, POLR3D, HTRA2, KCTD7, PSMA1, PVR, ATG2A, CHMP4C, SDC4, PLXND1, ZDHHC17, AKAP12, ZFYVE26, CTC1, GLIPR1, ABHD5, RTKN, NOCT, SIDT2, ASL, SAV1, FAM98B, DPP3, UBAP1, IRS2, PCYT2, GLTP, DOCK6, ACY1, SHTN1, MROH1, PVRIG, WBP1L, CYTOR, MFHAS1, ABCB6, STAT2, ATP6V1D, RNF19B, RYBP, STX3, USE1, ZHX2, CMIP, IRGQ, FAS, ABCC4, CHST15, BLZF1, FBXO10, MTURN, MYO5C, OGFOD2, CSNK1E, HOOK2, FBXO8, TIMM8A, LGALS8, PDCD2, CHCHD3, MYO18A, DDX60L, DRAM1, AKR1A1, SVIL, PPM1K, ARHGAP5, NLN, ESD, INF2, ATG9A, VAT1, PNKD, ADK, ZDHHC13, VARS, PIK3C3, GNE, ASS1, TNFRSF10A, FADS3, UBA6, SNCAIP, WBP2, FPGS, FBXL20, VPS26A, PRICKLE3, SKIL, TMC6, ITPR2, TFDP2, SPRYD3, SH2D3A, PPM1N, IP6K2, WDR81, GAA, TMEM132A, DHRS11, TOR1AIP1, C17orf49, IL15RA, RELB, ST13, BBS7, KCNQ4, NCL, CCNJ, GPC1, FAM83H, AAED1, MOB3A, FLII, SLC25A1, UAP1L1, SLC19A2, FSD1L, BACE2, DUSP22, LRRC1, MRPS30, OFD1, ERLIN1, TASP1, PCYOX1L, SLC15A4, EPHX2, STK3, ZNF567, INTS14, MT1L, ZFYVE27,</p>

HIST1H2BK, OS9, MT1E, ATP13A2, PIEZO1, MLLT6, HECTD3, LMLN, RHBDD3, MRM1, FTL, VPS26B, ETS2, MICAL2, MICB, SLC12A8, MAST2, ARG2, KLF15, ADA, SEC31A, CARS2, PTPN23, PORCN, HDAC10, ENTPD2, PIK3AP1, CIPC, XPR1, WDR18, PPM1H, MT2A, SFXN2, PPP6R2, MPRIP, VDR, DPH2, LDHA, DTNB, HES1, GSDMD, UNC93B1, TNFRSF21, NBEAL2, KREMEN2, YBX3, ETV6, GNAL, LIMS1, FDXR, HSPB1, EIF5A2
--

Table 2. List of commonly upregulated genes upon Tsg101 and Vps28 depletion (480 genes)

Gene symbols
ATM, LYST, FXN, GIPR, GLA, ICAM1, MET, NPC1, OCRL, G6PD, NEU1, PEX1, LDLR, IL1A, CXCL8, IL13RA2, BLVRA, CSF1, CYP51A1, GRINA, HMGCR, ITGAX, RPL8, RPL35A, RPL39, ZNF787, IP6K2, MAPKAP1, TCEAL8, SDCBP, EID3, CHAC2, KDM1A, PM20D2, RPS7, CHCHD7, FECH, IL32, CPZ, USP1, PIR, SOD2, WDR45, CTNS, CSTF1, TRAF5, FAM102A, GGPS1, CLDND1, PAQR3, TTC23, TUBB2A, MZT1, KDM6B, ZNF697, ZNF275, NAA60, ZNF621, HLA-F, TMEM251, RPL22L1, TTI2, MVK, TFRC, ORMDL1, UGT8, WDSUB1, LACC1, SMARCA1, TNIP3, RELL2, COL4A3BP, ZNF720, NEMP1, ZCCHC9, AFAP1, ZNF841, BCAP31, PDK3, MORF4L2, C6orf141, MYH14, FHIT, SLC26A11, SLC38A6, KIF21A, ARNTL, SF1, SECISBP2L, TFG, PDE4DIP, SNX10, CCNE1, CCNH, GUK1, CLCN7, CLNS1A, KLF6, DHCR7, EIF4B, GCLC, CXCL1, SLC29A2, TNFRSF9, IRAK2, AK2, ARVCF, CBR1, ESD, GFPT1, GCLM, CXCL2, CXCL3, HMGCS1, ID3, CD82, MARCKS, MXD1, ME2, MMP1, MMP3, MMP10, MTAP, MVD, NFKBIB, OSBP, PDK1, PI3, SERPINB8, PIK3C2A, PPP2CA, PSMA6, CLIP1, SAT1, ATXN2, SDC1, SPINK1, SQLE, SRPRA, TPD52L1, UVRAG, ZNF131, ZNF165, STAM, BLZF1, TNKS, TNFSF9, RIPK2, RIOK3, SUCLA2, AP1G2, SKAP2, MAP3K14, GPRC5A, NFKB1, ACOX1, PLK3, E2F2, EFNB2, NINJ1, RAB1A, TANK, SYT7, BCL9, CETN2, DUSP1, FDFT1, FGD1, IDI1, YBX1, CCL20, SMS, LRP8, RAB7A, HGS, DGKI, AP4M1, ETF1, GCNT3, UBE4A, PDIA4, PIK3CD, PRCP, AKAP12, SART1, ABL2, RND3, BCL3, CEBPB, FOSL2, NKTR, RALA, ABCA1, IFNGR2, INSIG1, LMAN1, TAF11, ZNF354A, EBI3, ABCC4, FSTL3, STUB1, ACAT2, MAP3K4, UCHL3, WFS1, LIPG, TP53I11, TNIP1, TUBB4B, SFN, PFKFB2, PHYH, POLR2I, RRAS, TNFAIP3, USP15, LRRC41, ARPC1A, RELB, ZNF217, PLK2, DNAJB2, MSMO1, TUSC3, LMO4, WDR3, RALBP1, AFG3L2, BTG3, GLIPR1, SNRNP27, HOXA7, SOS2, SOX12, STXBP2, SLC35D2, RER1, DNAJB4, TMF1, STRAP, TUSC2, GABARAP, KIF22, TTF1, RFC5, F8A1, FBXO10, FBXO8, FKBP8, HNRNP3, MLYCD, SIRT2, SIRT5, DNAJB9, PSD4, ATP6V0A2, PKN3, NRBP1, LRP12, ST6GALNAC6, OSTM1, CCDC59, TMEM5, PPIL2, MTCH1, TRAPPC3, SIGLEC9, APEX2, FAF2, RNF144A, TSC22D2, PLEKHM1, KLHL21, AP5Z1, JOSD1, UHRF1BP1L, CUL9, N4BP3, NUP205, ARL6IP1, MGRN1, SRGAP2, MED13L, TMEM131, NELFB, NSDHL, POMP, ATP6V1H, LACTB2, INSIG2, TRAPPC4, POLK, MAN1B1, ACSL5, HSD17B14, HSD17B7, ARID4B, GLTP, MRPL35, FAM49B, MRPS30, RWDD2B, SLC2A6, KCTD9, ZCCHC2, TRMT61B, CDC37L1, PHIP, GPN2, DARS2, N4BP2, UBA6, IMP3, C9orf72, DDX19A, YOD1, CMAS, FEM1A, ERRI1, CCSER2, GNL3L, PLEKHA3, PARD3, AGPAT4, MGST1, ARFGEF3, ENTPD7, PITHD1, C12orf4, TIGAR, KMT5A, TMEM159, ATP10D, NFKBIA, SRGAP1, FNIP2, METTL14, KRT34, KDM6A, IL21R, FASTKD5, TRAPPC11, LAMTOR3, OPTN, SEC24A, RBM26, TMEM168, MRPS25, USP46, MRPL34, PVRIG, SECISBP2, TMEM185B, ATP13A3, C3orf52, ZCCHC6, NHEJ1, CSPP1, SLC8B1, LRRC8E, HKDC1, FAM214B, NRBF2, ATG16L1, PLA2G12A, CCNL2, RNF170, HDHD3, NFKBIZ, NUDT12, B3GNT5, NSRP1, SLC41A2, FYTDD1, HPS3, KBTBD8, LACTB, ZFHX2, MMAB, MBD6, FBXO32, ZNF354B, WNT7B, SLC36A1, SELENOM, SRXN1, PTPRA, TTC5, MTG1, NAF1, HINT3, TBC1D2B, JSRP1, UBLCP1, MAP2K3, ZNF627, PSMB8, VPS37A, ZNF92, TANGO2, CBLB, RASAL2, ABCA5, NR4A1, SIK1, C3orf58, PGM2L1, PAPD4, PCSK9, C5orf51, C8orf37, ZNF616, SERINC2, DNAJC24, BIRC3, OSGIN1, ARRDC4, TMEM65, FAM120AOS, ZNF644, SLC16A13, ZNF254, PLPP6, FBXO38, SIGLEC15, AMPD3, GSR, CSF2, NQO1, PLEKHM3, ITPR1, TYMP, TM4SF19, CLCN6, ERN1, FLNB, HBEGF, HMOX1, IL6ST, JUNB, PGD, RAP2B, REL, DYRK3, BHLHE40, SQSTM1, F2RL2, FASN, NFKBIE, STK17A, ALDOC, GEM, IFI44, TALDO1, RIT1, SLC2A3, ESM1, TNFAIP6, IKZF3, TM4SF1, EIF2B2, SLC7A11, TNFAIP8, ACOT13, CLN8, KIAA1217, ZMIZ1, MCOLN1, TP53INP2, ABHD4, PRSS22, GID4, ZC3H12A, GABARAPL1, SMIM3, STARD4, TIPRL, TMEM88, PRKCD